

NGU



Norges geologiske
undersøkelse

Nr. 300

Bulletin 20



Universitetsforlaget 1973
Trondheim · Oslo · Bergen · Tromsø

554.81
NOR



NGU Norges geologiske undersøkelse

Geological Survey of Norway

Norges geologiske undersøkelse (Geological Survey of Norway), Leiv Eirikssons vei 39, Trondheim. Telephone: national (075) 20166, international +47 75 20166. Postal address: Box 3006, N-7001 Trondheim, Norway.

Managing Director: *Aslak Kvalheim*

Geological division: Director Dr. philos. *Peter Padget*

Geophysical division: Director *Inge Aalstad*

Chemical division: Director *Aslak Kvalheim*

The publications of *Norges geologiske undersøkelse* are issued as consecutively numbered volumes, and are subdivided into two series, Bulletin and Skrifter.

Bulletin comprise scientific contributions to the earth sciences of regional Norwegian, general, or specialist interest.

Skrifter comprise papers and reports of specialist or public interest of regional, technical, economic, environmental, and other aspects of applied earth sciences, issued in Norwegian, and with an Abstract in English.

EDITOR

Knut Am, Norges geologiske undersøkelse, P.O.Box 3006, N-7001 Trondheim, Norway.

PUBLISHER

Universitetsforlaget, P.O.Box 307, Blindern, Oslo 3, Norway. American Office: P.O.Box 142, Boston, Massachusetts 02113, U.S.A.

EARLIER PUBLICATIONS AND MAPS

A list of NGU publications and maps, 'Fortegnelse over publikasjoner og kart utgitt av Norges geologiske undersøkelse', is revised at irregular intervals. The last issue appeared in 1971 and copies can be obtained from the Publisher.

The most recent maps available from NGU are listed inside the back cover.

MANUSCRIPTS

Instructions to contributors to the NGU Series can be found in NGU Nr. 273, pp. 1-5.

554.81
NOR
20

m.l. eks.

7.24

geologic Profile
of the Continental Shelf and
Vøring Plateau¹

MARKVARD A. SELLEVOLL

UTGÅTT FRA
STAVANGER BIBLIOTEK

Sellevoll, M. A. 1973: A continuous seismic and magnetic profile across the Norwegian continental shelf and Vøring Plateau. *Norges geol. Unders.* 300, 1-10.

The upper part of the continental slope in the Storegga region dips at approximately 30° and from the foot of this feature an undulating surface continues to the base of the slope. In some places these undulations have a sinusoidal form which diminishes in amplitude with depth. The lower part of the continental slope consists of a convex front approximately 200 m high, which is thought to have developed along with the undulating surface by repeated slumping of unconsolidated material from the shelf edge. A very shallow crystalline basement exists on the outer part of the continental rise, while beneath the abyssal plain a layered structure is indicated. The south-western part of the Vøring Plateau is bounded by an escarpment. The plateau itself consists of layered sediments with an observed maximum thickness of 1.7 km and is assumed to be Cenozoic in age.

M. A. Sellevoll, *Universitetet i Bergen, Jordskjelvstasjonen, Villavei 9, N-5000 Bergen, Norway*

Introduction

The data presented in this paper are based on a continuous seismic profile between 63°12'N, 5°57'E on the continental shelf of Norway and the outer part of the Vøring Plateau. The route followed during the traverse is indicated in Fig. 1. It follows the continental shelf in the Møre region, across the slope and adjacent oceanic basin, to the slope and outer part of the Vøring Plateau. Magnetic measurements were also made along this traverse and are presented together with the continuous seismic profiling data, but the former observations are not discussed in detail here. The purpose of this paper is to discuss some of the major features found along the measured profile. This will be done in three sections as follows:

1. The continental shelf edge and slope
2. The continental rise and the ocean floor
3. The Vøring Plateau and its outer slope.

The continental shelf edge and slope

The continental shelf edge (the Storegga Region) and the continental slope were crossed three times during the survey (between 21.00 hours [22/8] and

¹ Publication No. 67 in The Norwegian Geotraverse Project
Publication No. 15 in The NTNF Continental Shelf Project

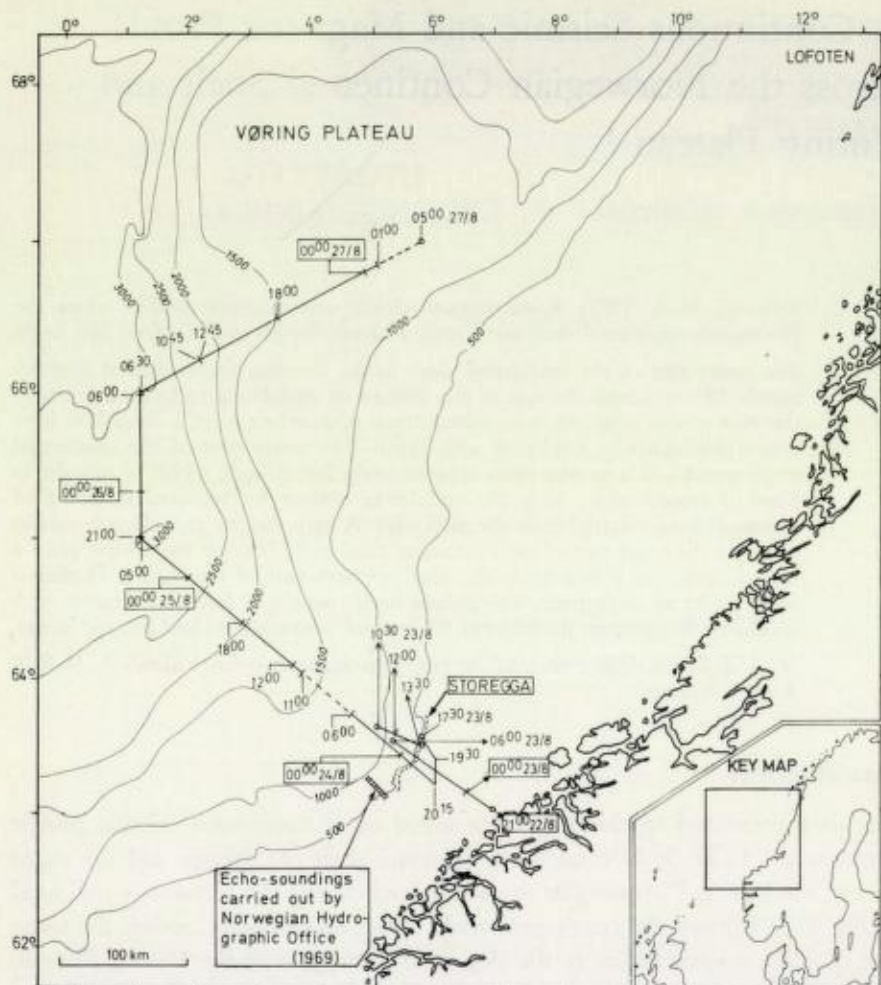


Fig. 1. Location map.

06.00 hours [24/8]) (Fig. 1). The Storegga region has formerly been studied in detail by Holtedahl (1955) by means of echo-soundings, dredging and coring. Holtedahl considered that the present shelf topography suggested a bottom consisting of consolidated rocks covered to a greater or lesser extent by sediments. On the basis of the submarine relief a former relative sea level at about 270 m was suggested, while another sea level 400–500 m below the present one was also tentatively proposed.

Recent geophysical and geological investigations have shown that the Norwegian Continental Shelf consists of large sequences of unconsolidated, semi-consolidated, and consolidated sediments of assumed Cenozoic and Mesozoic age, resting on a crystalline basement (Holtedahl & Sellevoll, 1971). A characteristic feature, almost everywhere in the shelf region, is that the sedimentary rock sequence is cut by an erosional surface on which unconsolidated deposits, presumably of Quaternary age, were deposited.

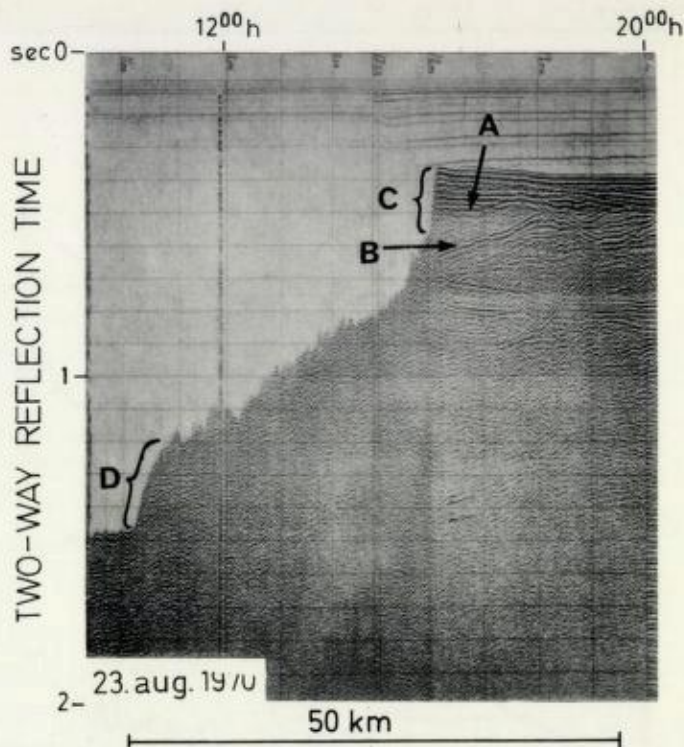


Fig. 2. Continuous seismic profile across the Shelf Edge and the Upper Continental Slope.

In Fig. 2, which represents a seismic profile across the shelf edge and slope, the A-horizon is assumed to be the discontinuity between horizontally layered Quaternary deposits and the pre-Quaternary sedimentary rocks beneath. The horizon named B is another interface of similar type to A but of unknown age. These two good reflecting horizons (A and B) presumably represent oversedimented former erosion surfaces, which are now strongly discordant to the present and upper slope. The shelf edge forms a pronounced physical feature, 150 m high, with a dip of 20° – 35° . Features such as those described above are often observed along the shelf edge, but are especially well developed in the Storegga region.

Fig. 2 also illustrates the fact that the greater part of the slope has a very uneven surface, though unfortunately the resolution used during this survey was too low for a detailed study of these slope features. On the basis of the echo-soundings presented by Holtedahl (1955) it seems likely that these same uneven bottom features also occur in other parts of the Storegga region. Four echo-sounding profiles from a region adjacent to that of our profile, run in 1969 by the Norwegian Hydrographic Office, illustrate in far greater detail than our recordings the form of this undulating slope surface (Fig. 3). These undulations vary from 30 m to a few meters in height and are between 100 and 250 m in breadth at their base in the downslope direction. The sounding data were studied and discussed by Holtedahl & Sellevoll (1971), who

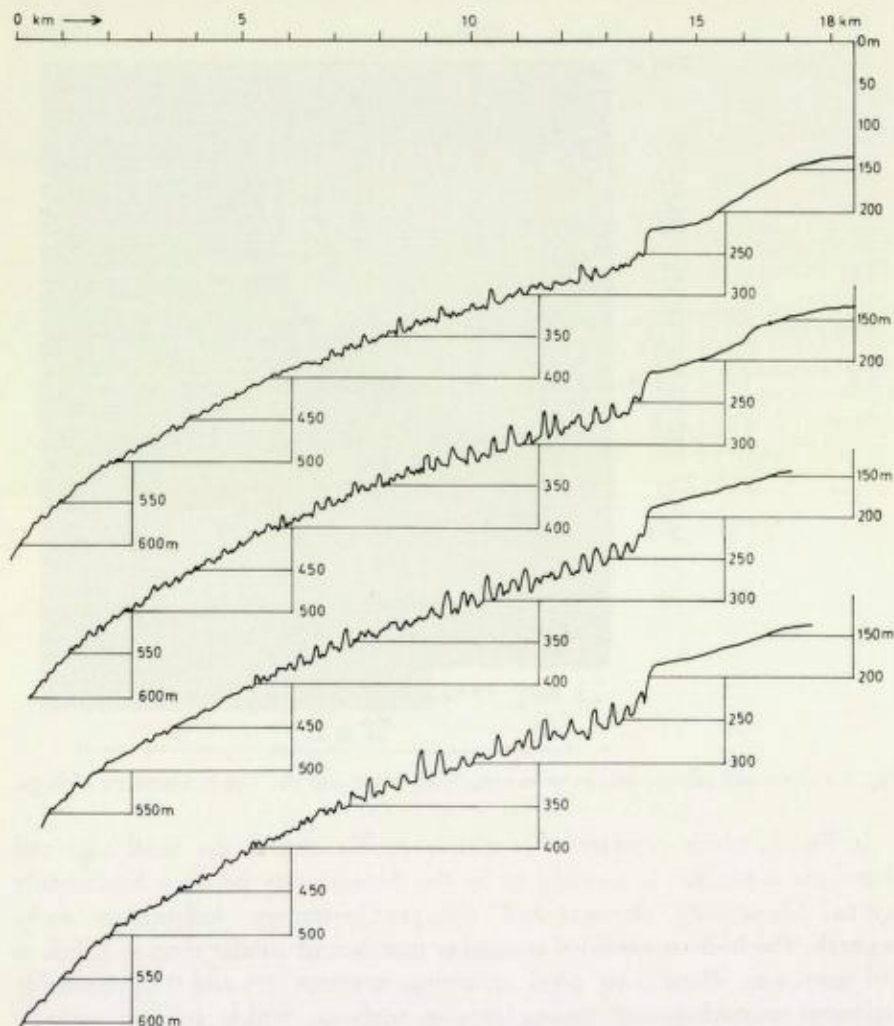
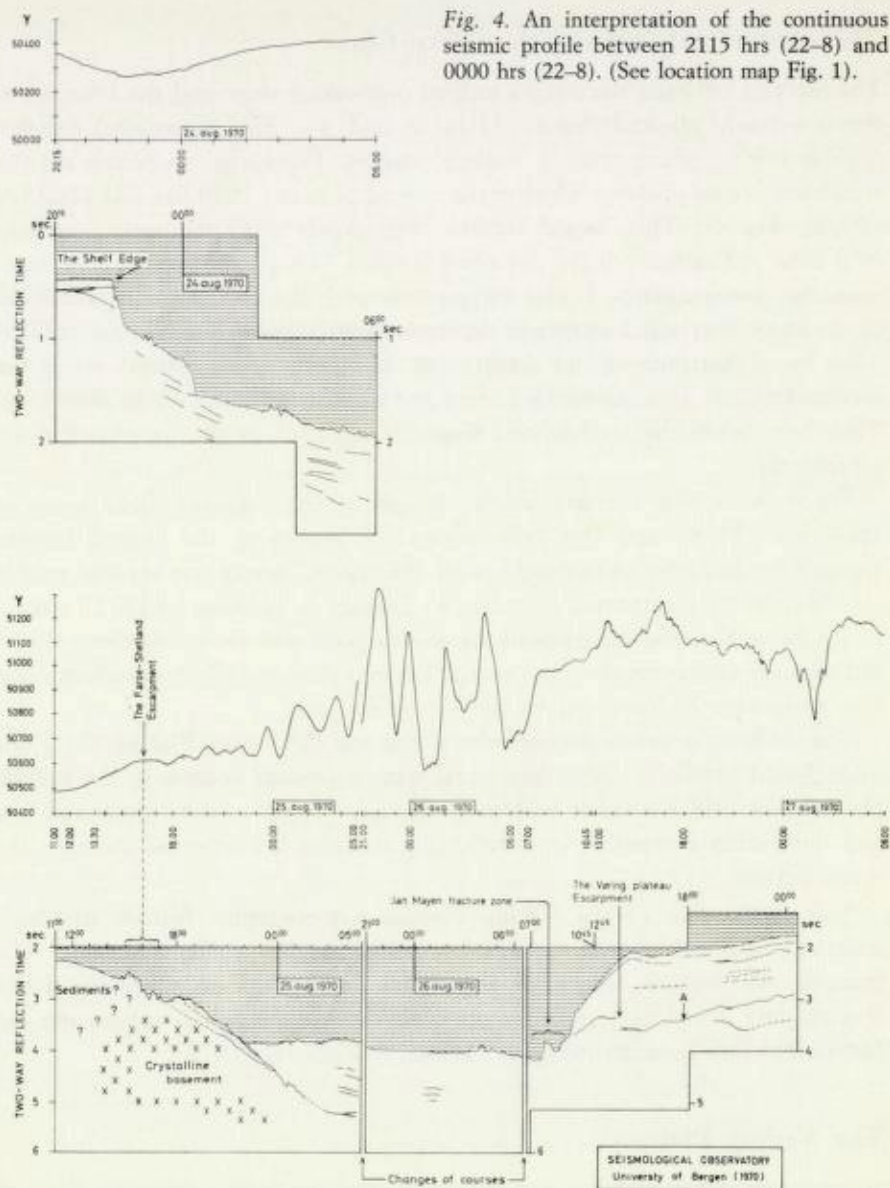


Fig. 3. Echosoundings carried out by the Hydrographical Survey of Norway in the region marked on Fig. 1.

suggested that the undulating surface features on the upper continental slope were ridges, most likely representing terminal moraines formed during the last glaciation. The undulations show a successively diminishing 'amplitude' from the steep upper slopes down to a water depth of 450 m, where they die out. This interpretation by Holtedahl & Sellevoll was made before any continuous seismic record was available showing the sub-bottom structure in this region.

Figs. 2 and 4 show that the lower part of the continental slope at a depth of 1000 m (1.4 sec two-way reflection time) has a convex shape. Such a feature is sometimes observed at the lower parts of continental slopes. The height of this convex front is approximately 200 m in the present case, and the front itself has a maximum dip of 10° . The formation of such a feature may be explained in several ways. One is that it has been built up during the slumping



of material from the shelf edge and upper continental slope, which moves progressively downslope towards the continental rise. Another possibility is that the front represents an escarpment developed by the modification of the slump front by bottom currents.

Even though the recordings are poor, slightly reflecting horizons are observed underneath the continental slope surface. (Fig. 4).

The continental rise and the ocean floor

The junction between the convex-formed continental slope and the continental rise is a clearly marked feature (Figs. 2 and 4). The continental rise is a slightly sloping plane with a uneven surface. Especially noticeable are the rough and jagged surfaces which were crossed between 1600 hrs and 1800 hrs (24/8 – Fig. 4). This jagged surface corresponds with the outer boundary of a large sedimentary basin described by Åm (1970) on the basis of aeromagnetic measurements. It also corresponds with the northward continuation of the Faroe-Shetland Escarpment determined by Talwani & Eldholm (1972). They found that there is no doubt that basement depth changes across the escarpment, but its exact configuration and location are difficult to determine. They have taken the well-defined magnetic lineation as the location for the escarpment.

Fig. 4 shows that a characteristic change in the magnetic field occurs at 1600 hrs (24/8) and this falls within the region of the jagged bottom topography and also corresponds with the region where our seismic profile should cross the escarpment according to Talwani & Eldholm's (1972) tracing of the Faroe-Shetland Escarpment. From this point and sea-wards there are no sedimentary structures observed except for two shallow reflectors, which form two wedges on the lower part of the continental rise.

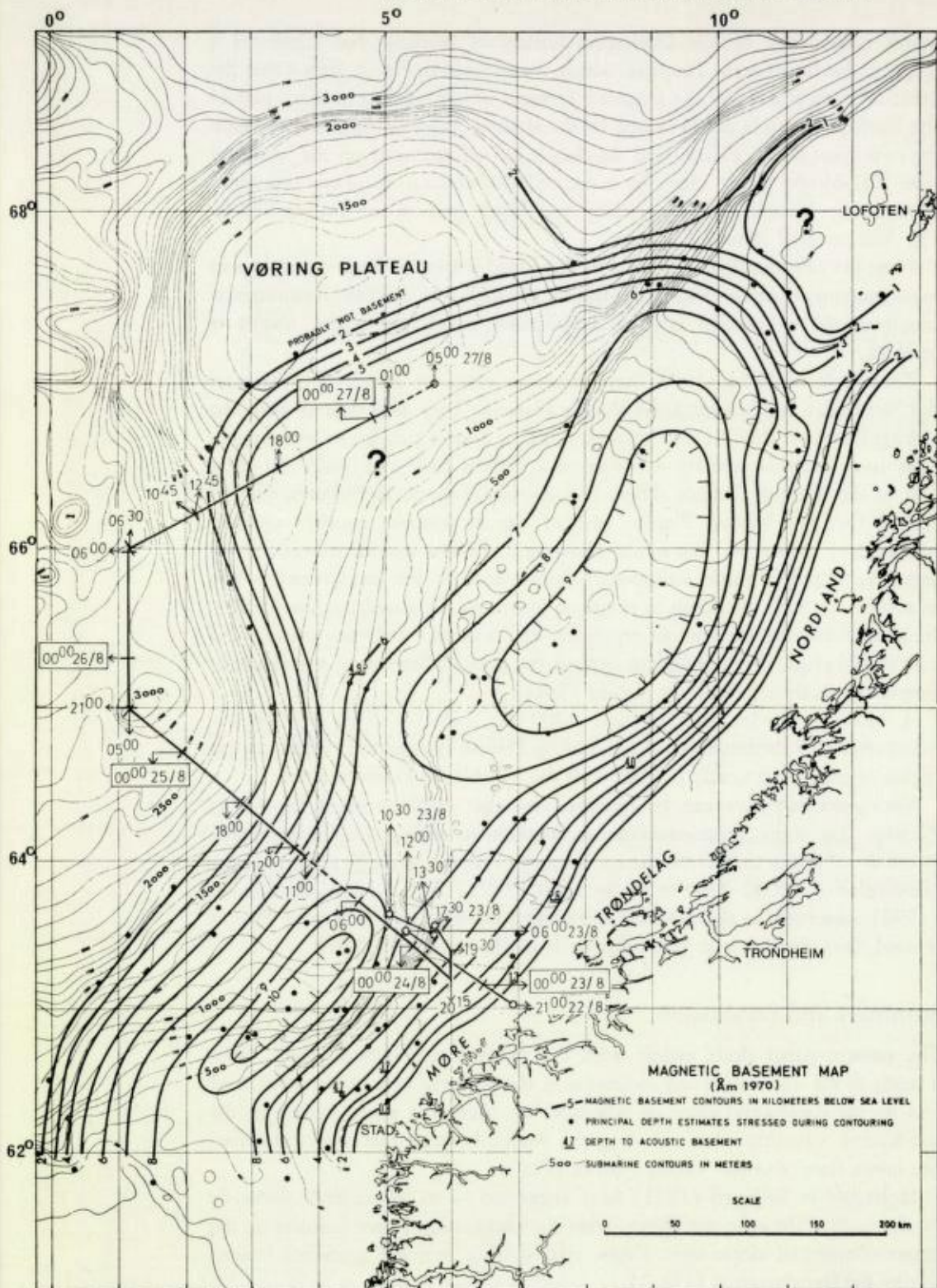
The sea-floor between the continental rise and the Vøring Plateau along our investigated profile is rather horizontal with a smooth bottom in the middle abyssal parts and a rougher bottom in the areas closer to the continental rise and the Vøring Plateau. Several reflecting horizons are observed beneath the ocean bottom.

Just at the foot of the Vøring Plateau a topographic feature has been observed, 200 m high and about 4 km 'broad' in the profile direction. The form of this feature cannot of course be determined on the basis of one traverse line. This topographic feature occurs where the profile crosses the Jan Mayen Fracture Zone according to Talwani & Eldholm (1972).

The Vøring Plateau

In recent years this area has received much attention from a scientific point of view. Johnson et al. (1968) gave a short description of the area on the basis of continuous seismic profiling. Avery et al. (1968) presented an aeromagnetic map which included the Vøring Plateau. The map shows strong irregular and narrow anomalies on the outer part of the Plateau, while the inner part of the continental shelf between Trondheim and Lofoten shows a weak and featureless magnetic picture. Åm (1970), on the base of magnetic measure-

Fig. 5. Magnetic basement map of the Vøring Plateau and adjacent parts of the continental shelf after Åm (1970), with the locations of the continuous seismic profiles of the present study added.



ments carried out by the Geological Survey of Norway, has presented a magnetic basement map. The map, which is presented in Fig. 5, shows that the great difference between the magnetic features on the outer and inner part of the Vøring Plateau is partly caused by the shallow magnetic basement beneath the outer part of the Plateau and the deeply buried basement on the landward side. In addition there must be a marked difference in magnetic properties between the basement on the outer and inner part of the Vøring Plateau (K. Åm, personal communication).

Hinz (1972) found, on the basis of combined marine geological-geophysical investigations, that the Vøring Plateau is divided into a western continental fragment and an eastern Graben Zone under which the upper mantle is uplifted.

Talwani & Eldholm (1972) have made an extensive geophysical study of the Norwegian Sea including the Vøring Plateau. They also found that the Vøring Plateau is divided into a western and an eastern part by an escarpment. They have demonstrated the existence of a shallow basement under the outer part of the Vøring Plateau. Hinz (1972) and Talwani & Eldholm (1972) agreed that the Vøring Plateau east of the escarpment consists of thick sedimentary sequences. The model showing a shallow basement west of the escarpment and a thick sedimentary basin east of the escarpment, is also in accordance with the depth to magnetic basement calculated by Åm (1970). If, in addition, the escarpment represents the boundary between oceanic and continental crust, it is possible to explain the great difference in the magnetic properties observed within the Vøring Plateau.

A fault is clearly observed near 1300 hrs (26/8 - Fig. 4). This is interpreted as a continuation of the Vøring Plateau escarpment, which in this region seems to run nearly parallel with the Jan Mayen Fracture Zone.

Very good reflectors can be observed on the profile crossing the Vøring Plateau. The most prominent one is marked A on Fig. 4. The maximum two-way reflection time from the sea bottom to this reflector is 1.4 sec. If the same velocity (2000–2500 m/s) as Hinz (1972) and Talwani & Eldholm (1972) observed in the assumed Cenozoic sediments on the Vøring Plateau is used, then the depth to this reflector is of the order of 1.7 km.

Summary and conclusion

The present paper deals mainly with two somewhat different topics: first, a study of the unconsolidated sediments in the adjacent area to the shelf edge and on the continental slope of NW-Norway. Second, a study mainly of the sub-bottom structure observed along the profile crossing the continental rise, the ocean floor, and the Vøring Plateau (Fig. 1).

Holtedahl & Sellevoll (1971) have suggested — as mentioned previously on the basis of the echo-soundings — that the undulating surface features on the upper continental slope were ridges, representing terminal moraines formed during the last glaciation (Fig. 3).

Another possibility is that these undulations on Fig. 3 represent megaripples (sandwaves) produced by strong bottom currents sweeping over or across the shelf slope. An important consideration in this proposed explanation is the composition and the nature of the sediments which constitute these features. If, as Holtedahl (1955) suggested, (and personal communication) they are heterogenous glacial deposits, then the action of traction-currents would presumably not produce sandwaves of the type documented from the shallow continental sea and continental margin. This explanation is consequently not very likely.

The continuous seismic sections now available from the shelf edge region and the upper continental slope (Fig. 2) indicate that oversedimentation of the shelf edge results at some stage in the instability of the superficial deposits which slump downslope along a curvilinear shear plane. The downslope movement of this unconsolidated material constantly modifies the form of the shelf edge by erosion of the more consolidated pre-Quaternary deposits, as indicated by the present form of the continental edge and upper slope (Fig. 2). Succeeding slump masses will pile up on preceding slides, whose form will become modified by the later ones, as shown by the diminution in amplitude with depth of these 'ridges' (see Fig. 3).

The investigation of the structure beneath the continental rise, the abyssal plain and the Vøring Plateau is rather limited, but several interesting features show up along the profile-line in Fig. 1.

The northward continuation of the Faroe-Shetland Escarpment is observed in the neighbourhood of 1600 hrs (24/8), but the exact position is difficult to point out. The magnetic feature is changing from a smooth increasing anomaly on the land side of the escarpment to an 'oscillating' magnetic anomaly on the sea side. According to our interpretation the magnetic high represents the crystalline basement on the west side of the escarpment (Fig. 4). Our evidence for such an interpretation is not very strong, but both the magnetic, seismic as well as the topographic features, contribute to such an interpretation. It is also in agreement with the observation of Talwani & Eldholm (1972).

Beneath the abyssal plain we have observed reflections from a depth corresponding to 1.5 sec two-way reflection time. According to the interpretation this corresponds to the crystalline basement. Assuming a velocity of 2000 m/s gives this a thickness of the total sedimentary sequences of 1500 m in this region 0500 (25/8 - Fig. 4). Some strong 'oscillating' magnetic anomalies are observed between 2300 hrs (24/8) and approximately 0600 hrs (26/8 - Fig. 4) indicating magnetic properties which are characteristic of an oceanic crust.

Clearly recognizable sedimentary sequences are observed on the continuous seismic sections in the Vøring Plateau area. A very good reflector (A in Fig. 4) with a maximum depth of approximately 1.7 km beneath the sea bottom, is assumed to represent the Cenozoic basement. The very distinct escarpment observed on the south-western side of the Vøring Plateau is

assumed to represent the continuation of the escarpment previously observed on the western part of the Vøring Plateau (Talwani & Eldholm, 1972).

The magnetic pattern is changing strongly from high amplitude anomalies which are associated with the sea floor spreading across the abyssal plain to smaller and less distinct anomalies on the Vøring Plateau.

The strong negative magnetic anomaly at 0200 hrs (28/8 – Fig. 4) is very peculiar. It may be due to diurnal variation, but since the rest of the magnetic anomalies are in good agreement with the maps of Avery et al. (1968), which also show similar anomalies on the Vøring Plateau, it is most likely a real anomaly. If the negative anomaly is real, it could be due to a shallow body with an essentially reversed magnetization, probably volcanic material in the sediments (K. Åm, personal communication).

Acknowledgements. – The author would like to thank Mr. K. Åm for his helpful comments and suggestions concerning the magnetic measurements which are presented in the paper, and he is also very much indebted to Professor Hans Holtedahl for his comments and great interest in the project. The study is supported by an N.A.V.F. grant through the Norwegian Geotraverse Project, which is gratefully acknowledged.

REFERENCES

- Åm, K. 1970: Aeromagnetic investigation on the Continental Shelf of Norway, Stad-Lofoten (62°–69°). *Norges geol. Unders.* 266, 49–61.
- Avery, O. E., Burton, G. D. & Heirtzler, J. R. 1968: An aeromagnetic survey of the Norwegian Sea. *J. Geophys. Res.* 73, 4583–4600.
- Hinz, K. 1972: Der Krustenaufbau des Norwegischen Kontinentalrandes (Vøring Plateau) und der Norwegischen Tiefsee zwischen 66° und 68°N nach seismischen Untersuchungen. *'Meteor' Forsch. – Ergebnisse No. 10*, 1–16.
- Holtedahl, H. 1955: On the Norwegian Continental Terrace, primarily outside More-Romsdal: Its geomorphology and sediments. *Årbok 1955, Mat.naturv. rekke nr. 14*, University of Bergen.
- Holtedahl, H. & Sellevoll, M. A. 1971: Geology of the Continental Margin of the eastern Norwegian Sea and the Skagerrak. *Institute of Geological Sciences, Report No. 70/14*, 33–52.
- Johnson, G. L., Ballard, J. A. & Watson, J. A. 1968: Seismic studies of the Norwegian Continental Margin. *Norsk Polarinstitutt, Årbok 1966*, 112–119.
- Talwani, M. & Eldholm, O. 1972: Continental margin off Norway: a geophysical study. *Geol. Soc. Am. Bull.* 83, 3575–3606.

Thermal Conductivities of Some Ores and Rocks in Norway

ØRNULF LOGN & EINAR EVENSEN

Logn, Ø. & Evensen, E. 1973: Thermal conductivities of some ores and rocks in Norway. *Norges geol. Unders.* 300, 11–19.

Thermal conductivities of 61 diamond core samples are given. Most of the samples are from the Joma pyrite deposit and its neighbouring rocks. The measurements from Joma show that there is a very high conductivity in compact pyrite ore, a considerably low conductivity in impregnated ore, a high conductivity in sphaleritic pyrite ore and a low conductivity in the surrounding greenstones and phyllites. Samples from other locations show that quartz and graphitic schists have intermediate conductivities and that magnetite has a relatively low conductivity. The conductivities of all measured specimens fall between 3 and 60 millical/cm.sec. °C.

Comparison of thermal and electrical conductivities reveals the following interesting features: compact pyrite ore, which is usually difficult to separate electrically from impregnated ore and graphitic rocks, has a thermal conductivity distinct from that of the impregnated ore and graphite-bearing rocks. Quartz, which has a poor electrical conductivity, has a relatively high thermal conductivity as compared with that of the ordinary rocks. These features may have direct applications in prospecting for compact ore deposits.

Ø. Logn & E. Evensen, *Norges geologiske undersøkelse, Box 3006, N-7001 Trondheim, Norway*

Introduction

The thermal conductivity measurements described here were undertaken to establish the thermal conductivities of ore types and country rocks in the Joma pyrite ore field to aid in the interpretation of a series of temperature gradient measurements carried out in diamond drill holes through this ore body to evaluate the possibility of using thermal methods in geophysical exploration of pyrite ores of the compact type (Logn, in preparation). Most of the thermal conductivities given in this paper are from specimens from Joma. A few conductivities from other localities in Norway are provided for comparison.

The Joma deposit is one of the largest pyrite deposits in Norway. It is situated at 65°N near the Swedish border (Fig. 1). The history and geology of the deposit are described briefly in a paper on self-potential measurements of this ore body (Logn & Bølviken, in preparation). The ore body is a broadly tabular mass which has been folded into an open synform. The greatest ore intersections are found along the axis (NE/SW) of this fold structure. The ore consists chiefly of compact pyrite with varying amounts of chalcopyrite, pyrrhotite and sphalerite. Galena occurs as a minor mineral. Greenstones occur both above and below the ore body. A phyllitic unit is situated in the footwall.

The greenstone is slightly calcareous with an average of about 2.5% Ca. In the hanging wall greenstone a horizon of mainly pyrrhotite disseminations occurs over a distance of about 50–100 m from the ore body. The phyllite

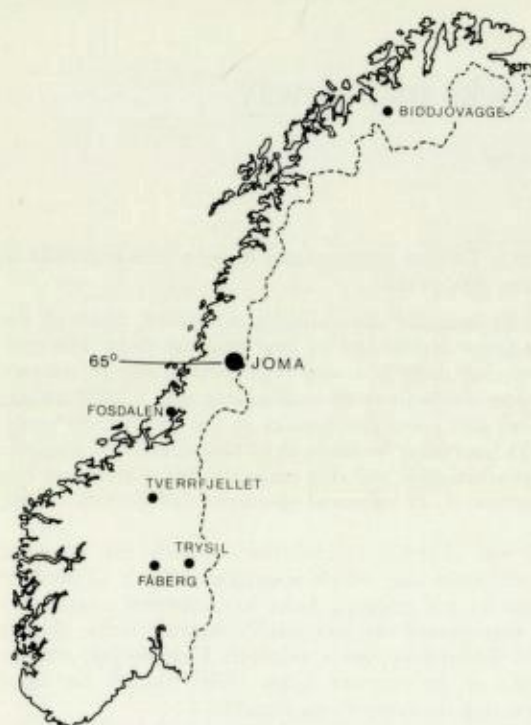


Fig. 1. Location of sample localities.

formation contains a number of graphitic zones which are good electrical conductors and cause strong electro-magnetic and geo-electric anomalies.

Thermal conductivity measurements have also been carried out on compact magnetite ore from the Fosdalen deposit situated at Trondheimsfjord to the south-west of the Joma pyrite deposit (Fig. 1). The ore contains about 45% Fe as magnetite with disseminated pyrites, and traces of chalcopyrite. The country rocks are greenstones and quartz keratophyres. The geology of the mine has been described earlier (Carstens 1955, Logn 1964).

One specimen of a quartz vein from the Tverrfjellet pyrite mine at Dovre, two specimens of sparagmite from Fåberg, one limestone from Trysil (Fig. 1) and three specimens of graphitic schists from Biddjovagge in Northern Norway comprise a supplementary collection on which thermal conductivity measurements were carried out. The complete specimen collection comprises 61 cores.

Methods of measurement

The thermal conductivities were measured by a divided bar method similar to that proposed by Birch (1950). The apparatus is shown in Fig. 2. The specimen, a circular diamond core 32 mm in diameter, was cut by diamond sawing to a disc of about the same thickness with flat parallel faces. The core (A, Fig. 2) is inserted between copper discs 8 mm thick. In the other side of this unit is placed the prototype, to which the specimen can be compared, capped at its outer face by another copper disc. The prototype has the same diameter

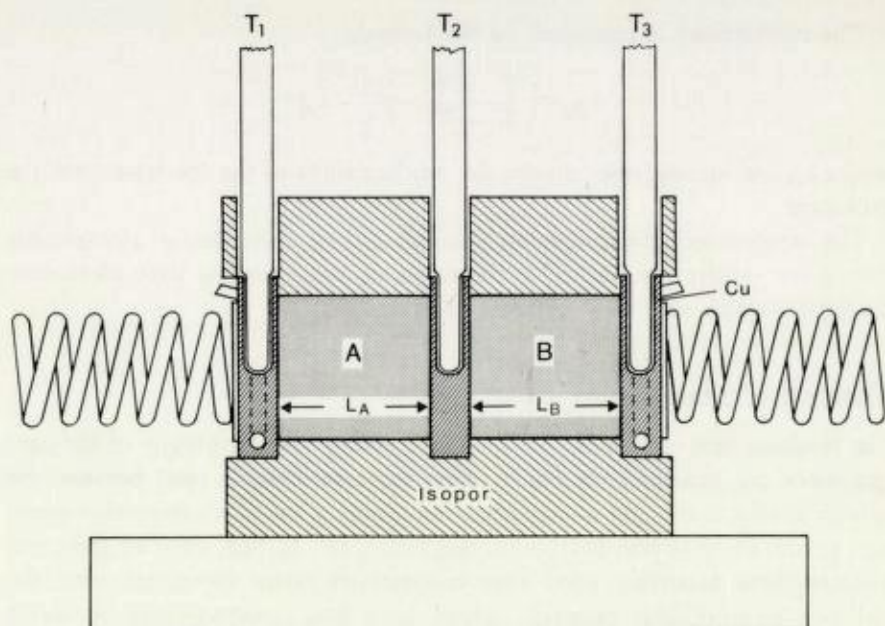


Fig. 2. Diagram of the apparatus used for measuring relative thermal conductivity.

and approximately the same thickness as the specimen. The end faces were covered by a thin film of SiC fine-fraction polish mixed with water in order to reduce the contact resistivity. This 'stack' is assembled in a unit pressed together by springs acting in the direction of the axis of the cylinders. The heating of one end face is supplied by warm water circulating in channels in one of the outer copper discs. A circulation of cold water is provided for the lower temperature side of the systems. The temperature of the water is adjusted so that the warm side of the unit is constantly about 12°C above room temperature and the cold side about 12°C below. The basic assumption in the use of this method is that all heat movement is parallel to the axis of the system. Non-axial heat flow can never be reduced to zero, but can be kept to a minimum by using insulating materials around the unit. For this purpose the unit was shielded by a cap of the 'isopor' insulating material. Three thermometers, scaled in tenths of degrees Celsius and fitting closely in wells drilled in the copper discs, are used to measure the temperature differences across the two poor conductors, i.e. the prototype and the specimen.

Two separate measurements were carried out on each sample by interchanging the specimen and prototype in the 'stack'. The results given in the following section are based on averages of these measurements.

The prototypes used in the measurements were kindly loaned to the authors by Dr. S. Werner, director of the Geophysical Department of the Swedish Geological Survey. The absolute conductivities on these prototypes were:

- 1) Vismuth: $20.12 - 0.02 \cdot t^{\circ}$ millical/cm · sec · $^{\circ}\text{C}$
 - 2) Invar: $22.8 + 0.065 \cdot t^{\circ}$ millical/cm · sec · $^{\circ}\text{C}$
- t° = room temperature (20°C).

The conductivity is computed by the formula:

$$\lambda_A = \frac{T_2 - T_3}{T_1 - T_2} \cdot \frac{L_A}{L_B} \cdot \lambda_B$$

where λ_A and λ_B are, respectively, the conductivities of the specimen and the prototype.

The conductivity measurements carried out by this sample arrangement have given satisfactory results, as the repeated measurements have given conductivities which vary only within narrow limits.

Thermal conductivities

The resulting heat conductivities vs. corresponding specific gravity of the core specimens are presented in Fig. 3. This representation is used because the specific gravity is thought to give some indication of the heavy mineral content, e.g., pyrite, chalcopyrite, pyrrhotite, magnetite, etc. In fact, most of these ore minerals have relatively good heat conductivity when compared with the ordinary rock-building minerals, which have heat conductivities of about 6–9 millical/cm · sec · °C (Herrin & Clark 1956; Puranen 1968). Impregnations of good-conducting ore minerals in rock-building mineral matrices are well expressed by the specific gravity of the specimen as there is a good correlation between the specific gravity and the heat conductivity of the rocks with impregnated ore minerals.

The specimens are separated into 10 groups (Fig. 3):

A. Rocks:

- 1) Graphitic schist (Gra, Fig. 3). 3 specimens from Biddjovagge. Average heat conductivity is 17 millical/cm · sec · °C. Average specific gravity is 2.55 g/cm³.
- 2) Quartz (Q, Fig. 3). 3 specimens, 1 from Tverrfjellet and 2 from Joma. Average heat conductivity is 15.7 millical/cm · sec · °C. Average specific gravity is 2.58 g/cm³.
- 3) Phyllite (Ph, Fig. 3). 12 specimens from Joma. Some of the specimens are graphitic. Average heat conductivity is 6.9 millical/cm · sec · °C. Average specific gravity is 2.74 g/cm³.
- 4) Greenstone (Gr, Fig. 3). 11 specimens from Joma. The greenstone has on average about 2.5%Ca. Average heat conductivity is 7.86 millical/cm · sec · °C. Average specific gravity is 2.87 g/cm³. Some of the heavier specimens are weakly impregnated with pyrite or pyrrhotite.
- 5) Miscellaneous. 3 specimens are not grouped. A dark Cambrian schist from Trysil (Cam, Fig. 3) has a heat conductivity 3.0 millical/cm · sec · °C and a specific gravity of 2.72 g/cm³. This specimen contains minor calcite. The other two specimens (Spa, Fig. 3) are dark-coloured sparagmites from Fåberg, which have heat conductivities of 4.8 and 9.4 millical/cm · sec · °C and specific gravities 2.73 and 2.67 g/cm³. The specimen with the heat conductivity of 9.4 millical/cm · sec · °C contains traces of graphite.

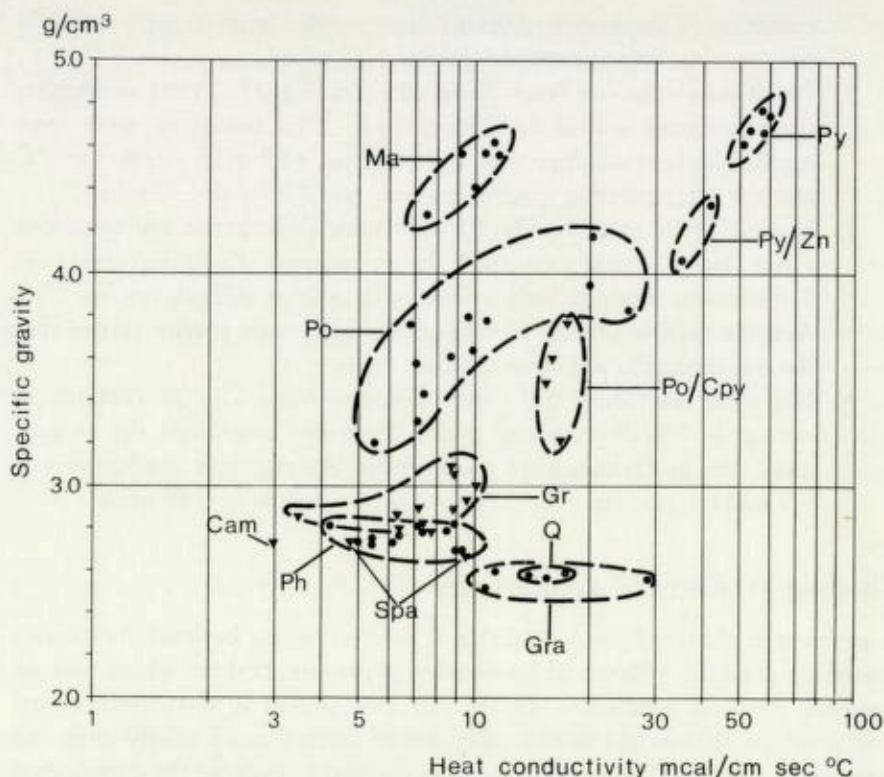


Fig. 3. Heat conductivity vs. specific gravity.

- Py = Massive pyrite ore from Joma deposit.
 Py/Zn = Sphalerite-pyrite from Joma.
 Po/Cpy = Chalcopyrite-pyrrhotite impregnations from Joma.
 Po = Pyrrhotitic impregnations in greenstone from Joma.
 Ma = Massive magnetite from Fosdalen deposit.
 Gra = Graphitic schist from Biddjovagge deposit.
 Gr = Greenstone from Joma.
 Ph = Phyllite from Joma.
 Q = Massive quartz from Joma and Tverrfjellet deposits.
 Spa = Sparagmite from Fäberg.
 Cam = Cambrian black schist from Trysil.

B. Ores and disseminated ores:

- 1) Impregnated pyrrhotite greenstones from Joma (Po, Fig. 3). The impregnations occur chiefly along schistosity bands or in irregular networks, which is probably the reason for the scattering of values obtained. The sample group comprises 12 specimens. Average heat conductivity is 11.6 millical/cm · sec · °C. Average specific gravity is 3.69 g/cm³. Some of the specimens with higher heat conductivity may contain traces of chalcopyrite or pyrite.
- 2) Impregnated pyrrhotite-chalcopyrite rocks from Joma (Po/Cpy, Fig. 3). The impregnations occur chiefly in bands or in networks. Ordinarily pyrrhotite is more abundant than chalcopyrite. The group

- comprises 4 specimens. Average heat conductivity is 16.6 millical/cm · sec · °C. Average specific gravity 3.67 g/cm³.
- 3) Pyrite-sphalerite ore from Joma (Py/Zn, Fig. 3). Pyrite constitutes the groundmass and is the main mineral. Two specimens were measured. The heat conductivities are 35.4 and 42.5 millical/cm · sec · °C and the corresponding specific gravities are 4.05 and 4.32 g/cm³.
 - 4) Massive pyrite ore (Py, Fig. 3) with some chalcopyrite and sphalerite (from Joma). Pyrite constitutes the groundmass. The group comprises 5 specimens. Average heat conductivity is 56.0 millical/cm · sec · °C. Average specific gravity is 4.68 g/cm³. The mean gravity shows that the ore specimens are quite compact types.
 - 5) Magnetite ore (Ma, Fig. 3) from Fosdalen Mine. The ore contains an average of 5% disseminated pyrite. Magnetite constitutes the groundmass. The group comprises 6 specimens. Average heat conductivity is 9.9 millical/cm · sec · °C. Average specific gravity is 4.50 g/cm³.

Thermal vs. electrical conductivity

A problem in electrical ore prospecting is to discriminate between indications caused by graphitic schists and by massive pyrite ore, both of which may be excellent electrical conductors. In the previous section it was demonstrated that graphitic schists had considerably lower thermal conductivity than the massive ore samples. The authors therefore decided to examine the correlations between thermal and electrical conductivity. Forty-six drill cores from the sample collection were selected for electrical conductivity measurements. The samples were placed under water pressure to fill dry open pores and were then measured by a four-point-method bridge arrangement. The resulting electrical conductivities vs. the thermal conductivities are presented in Fig. 4.

The most striking feature of the diagram is the great difference in thermal conductivity between two types which have strong electrical conductivity, namely, samples with pyrrhotite impregnations and samples of massive ore. In fact, the strongest electrical conductivities in the diagram are those of two cores with pyrrhotite banding almost parallel to the ore axis. These strong electrically conducting cores have thermal conductivities no higher than those of the ordinary greenstone or phyllite. Another interesting feature is the great difference between the heat conductivity of massive magnetite ore and that of massive pyrite ore, which is the reverse of the tendency shown by the electrical conductivities. The highest electrical conductivity in the magnetite ore is about the same as the lowest electrical conductivity in the pyrite ore.

The conductivity values in Table 1 are averages within the respective rectangles of Fig. 4.

The electrical conductivities of the pyrrhotite impregnations (Po, Fig. 4) vary between 0.36 and 52.4 mho/cm. The highest electrical conductivity is found in cores where the pyrrhotite bands pass more or less parallel to the core axis, and the lowest conductivity is found in those cores in which the banding is across the core axis.

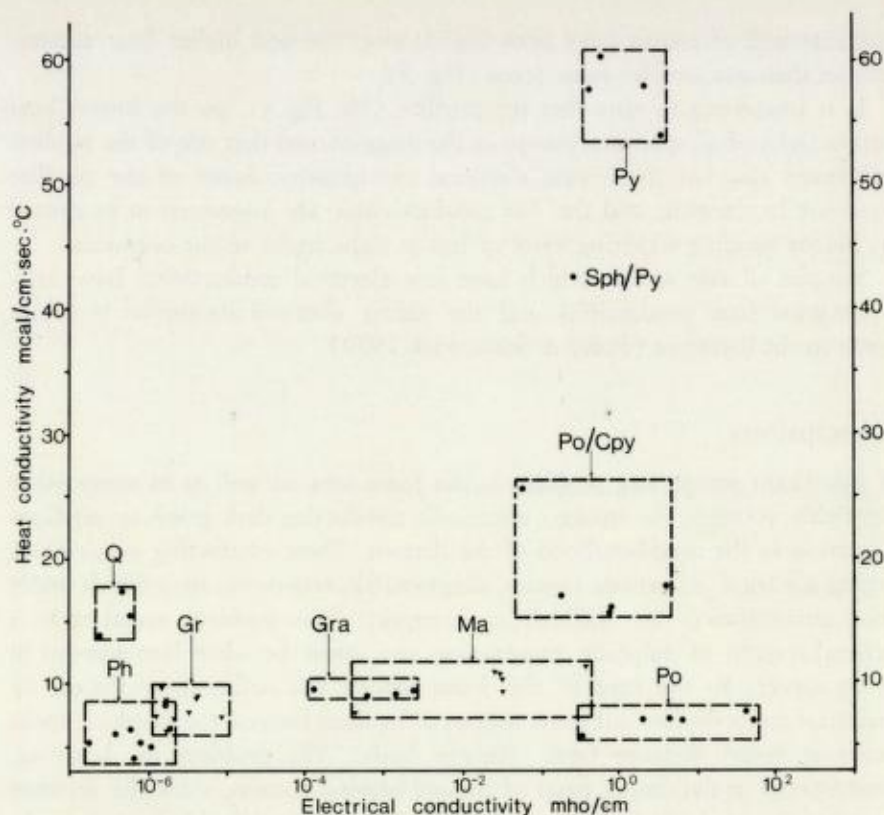


Fig. 4. Heat conductivity vs. electrical conductivity.
Symbols as in Fig. 3.

Table 1. Average thermal and electrical conductivities within the respective rectangles of Fig. 4

	Thermal (20°C)	Electrical
Massive pyrite ore	57.3 millical/cm · sec · °C	$1.70 \cdot 10^0$ mho/cm
Massive magnetite ore	9.9 » »	$8.50 \cdot 10^{-2}$ »
Chalcopyrite-pyrrhotite impregnations (banded)	18.5 » »	$1.20 \cdot 10^0$ »
Pyrrhotite impregnations (banded)	6.9 » »	$1.81 \cdot 10^1$ »
Graphitic phyllite	9.2 » »	$1.15 \cdot 10^{-3}$ »
Greenstone (calcitic)	8.0 » »	$3.01 \cdot 10^{-6}$ »
Phyllite	6.9 » »	$8.73 \cdot 10^{-7}$ »
Quartz (veins)	15.7 » »	$4.27 \cdot 10^{-7}$ »

Among the samples the highest thermal conductivity is found in the one chalcopyrite-pyrrhotite impregnations (Po/Cpy, Fig. 4), which contains some sphalerite, and this high value may be partly due to the high thermal conductivity of sphalerite.

The low electrical conductivity of the graphitic phyllite indicates that the graphite content in the samples is low. Graphite schists with higher graphite

contents will of course have both higher electrical and higher heat conductivities than our samples from Joma (Fig. 3).

It is interesting to note that the phyllite (Ph, Fig. 4) has the lowest heat conductivity of all specimen groups in the diagram, and that one of the phyllite specimens also has the lowest electrical conductivity. Some of the phyllite cores are biotite-rich, and the low conductivities are suggested to be caused by biotite banding occurring more or less at right angles to the core axis.

Samples of vein quartz which have low electrical conductivity, have relatively good heat conductivity and the values obtained are similar to values given in the literature (Poley & Steveninck 1970).

Conclusions

A significant prospecting problem in the Joma area, as well as in many other ore fields, concerns the strongly electrically conducting dark graphitic phyllites occurring in the neighbourhood of the deposit. These conducting zones cause strong electrical indications (turam, slingram, SP, resistivity, etc.) which under most circumstances are difficult to interpret. This problem seems to be a general feature of sulphide prospecting and must be taken into account in every survey. In the case of the Joma deposit the outlining of the ore by electrical methods does not cause serious difficulties because the graphitic rocks occur at some distance from the ore body. The problem is, however, encountered in the deeper parts of the ore-bearing horizon, since the distance between the ore body and the graphitic phyllites is considerably less at depth. The authors therefore believe that the registration of the heat flow through and around the ore body may possibly give valuable supplementary information about the ore extensions at deeper levels, which cannot be supplied by electrical methods. The heat conductivity contrast between ore and the surroundings is the basic physical parameter in this connection. The actual contrasts are apparent from Fig. 4. The compact pyrite ore has a thermal conductivity which is about 7 times stronger than that of the greenstone country-rock, and approximately 6 times stronger than that of the graphitic phyllites. Heat flow measurements thus appear to provide little possibility of discriminating between the graphitic phyllites and the greenstones. More strongly electrical-conducting graphitic schist from Biddjovagge has a slightly stronger thermal conductivity and its contrast with pyrite ore is from 1:5 to 1:3. These conductivities correspond with the data given by Halck (1958).

The thermal conductivity of magnetite ore from Fosdalen is of the same order of magnitude as the conductivity of most rocks, for instance the greenstones. Compact magnetite ore of the Fosdalen type is therefore not distinguishable by thermal methods. The conductivities are lower than the magnetite values given by Halck (1958). Our results, however, are similar to those of recent measurements carried out in Sweden (Malmquist & Werner, personal communication, 1973).

The relatively high thermal conductivity of sphalerite-rich pyrite ore suggested that sphalerite is also a fairly good heat conductor. Recent results from Sweden support this suggestion (Werner, personal communication, 1973). This conclusion is geophysically interesting, since sphalerite is a poor electrical conductor. The pyrrhotite impregnations have relatively low thermal conductivity, and most of the specimens show little contrast with results obtained from the surrounding greenstone. The higher conductivities of the impregnated pyrrhotite specimens can be attributed to the presence of chalcopyrite. Since the compact pyrite ore seems to be the only first class heat conductor in the Joma field, the possibilities of using thermal methods to outline the extension of this ore body seem promising.

Acknowledgements. – We thank Per Eidsvig for measuring the electrical conductivities and Aslak Kvalheim for critical reading of the manuscript.

REFERENCES

- Birch, F. 1950: Flow of heat in the front Range, Colorado. *Geol. soc. Am. Bull.* 61, 567–630.
- Carstens, H. 1955: Jernmalmen i det vestlige Trondheimsfelt og forholdet til kisforekomstene. *Norsk geol. Tidsskr.* 35, 211–220.
- Herrin, E. & Clark, S. P., Jr. 1956: Heat flow in West Texas and eastern New Mexico. *Geophysics* 21, 1087–1099.
- Logn, Ø. 1964: Exploration for deep magnetite ore. *Geoexploration* 2, 74–106.
- Logn, Ø. (in preparation): Geothermal anomalies on the Joma pyrite ore deposit, Norway.
- Poley, J. P. & Steveninck, J. v. 1970: Geothermal prospecting – delineation of shallow salt domes and surface faults by temperature measurements at a depth of approximately 2 metres. *Geophys. Prospecting* 18, 666–700.
- Puranen, M., Järvinäki, P., Hämäläinen, K. & Lehtinen, S. 1968: Terrestrial heat flow in Finland. *Geoexploration* 6, 151–162.

Distribution of Some Trace Elements in Different Beneficiation Fractions from the Bleikvassli Pyritic Lead-zinc Ore Body, Nordland

ANANDA DEB MUKHERJEE, RANENDRA N. SEN & EILIV STEINNES

Mukherjee, A. D., Sen, R. & Steinnes, E. 1973: Distribution of some trace elements in different beneficiation fractions from the Bleikvassli pyritic lead-zinc ore body, Nordland. *Norges geol. Unders.* 300, 21–25.

The distribution of some minor and trace elements at different stages of sulphide ore beneficiation in the Bleikvassli ore-dressing plant, has been studied using neutron activation analysis. Silver, gold, antimony and selenium are found to be concentrated along with lead. Cobalt is found in the pyrite concentrate. Arsenic is concentrated mainly with pyrite, but a minor fraction is also carried together with lead. Scandium and thorium are shown to be associated with the gangue minerals. Chromium present in the crude ore appears to have been removed to a great extent before the first flotation step.

A. D. Mukherjee, *Geological Institute, University of Oslo, Blindern, Oslo 3, Norway**

R. Sen, *Bleikvassli Gruber, N-8647 Bleikvassli, Norway***

E. Steinnes, *Institutt for Atomenergi, Isotope Laboratories, Kjeller, Norway*

Introduction

The palaeozoic stratabound pyritic lead-zinc ore body at Bleikvassli, Northern Norway (lat. 65° 50'N) has been classified mineralogically by Vokes (1963) as belonging to the fourth class of Caledonian massive sulphide ores (Carstens 1935). This ore consists of two main types (Vokes, *op. cit.*) a pyrite type comprising pyrite, sphalerite, galena, pyrrhotite, chalcopyrite, and a pyrrhotite-rich type comprising pyrrhotite, sphalerite, galena, chalcopyrite, and minor or no pyrite.

An ore-dressing plant situated close to the Bleikvassli mine is used for flotation of the lead and zinc sulphides and pyrite. After crushing and grinding, the usual procedure for selective flotation, involving three steps, is followed. Lead is concentrated in the first step, zinc in the second, and finally pyrite is separated. Copper is mainly separated along with lead, the concentration being 3–4% in the Pb concentrate. Some zinc is also separated in the first flotation step, amounting to 6–8% Zn in the Pb fraction.

The distribution of minor and trace elements between the different fractions resulting from this ore-beneficiation process has not been extensively studied so far. The present work was therefore undertaken in order to extend knowledge on this point, by means of instrumental neutron activation analysis.

* Present address: Department of Geology, Jadavpur University, Calcutta 32, India

** Present address: Department of Geology, Presidency College, Calcutta 12, India

Experimental

Samples for the present investigation were collected from the plant in a continuous series during five days. They are (a) crude ore, (b) concentrates of lead, zinc, and pyrite, (c) tailings of lead, zinc, and pyrite.

The samples were analysed for their content of Ag, As, Au, Co, Cr, Ir, Sb, Sc, Se, and Th, using neutron activation analysis according to a procedure described in detail elsewhere (Steinnes & Mukherjee 1973). Fractions of about 100 mg and appropriate standards of each element were irradiated for 20 hours in the JEEP II reactor (Kjeller, Norway) at a thermal neutron flux of $1.5 \cdot 10^{13}$ neutrons $\text{cm}^{-2}\text{sec}^{-1}$. After fixed intervals the samples were subjected to γ -spectrometry with a Ge(Li) solid-state detector system. Measurements for arsenic (^{76}As), antimony (^{122}Sb), and gold (^{198}Au) were performed after 6 days, while chromium (^{51}Cr), cobalt (^{60}Co), iridium (^{192}Ir), scandium (^{46}Sc), selenium (^{75}Se), silver (^{110}Ag), and thorium (^{233}Pa) were determined about 20 days after the irradiation.

Results and discussion

The results of this work are given in Table 1. Except for Ir, the content of which appeared to be too low for study by the purely instrumental technique employed, specific distribution trends have been observed for all elements investigated. In the following, the results obtained for each element are briefly discussed.

Ag

Silver is shown to be concentrated extensively in the lead concentrate, the average enrichment factor being 16.3 ± 3.7 as compared to the crude ore, which is similar to the corresponding factor for Pb (17.5 ± 1.0) calculated from data on the same fractions available from Bleikvassli Gruber. This can be explained by the well-known fact that silver is readily camouflaged in galena. The contribution of free silver minerals, however, cannot be excluded.

Au

Although the results clearly reflect the fact that the fractions taken for analysis were not sufficiently homogeneous with respect to gold, it seems clear that this element is also concentrated in the Pb fraction. In a similar study concerning the distribution of Ag, Au, and Hg in concentrates from various Norwegian ores, Rehman et al. (in press) found the highest concentrations of Au in the Cu concentrates, and indicated a possible substitution of gold in copper sulphide minerals. In the Bleikvassli plant, where copper is concentrated along with lead in the flotation process, gold is therefore likely to be found mainly in the lead concentrate.

Co

Cobalt is enriched in the pyrite concentrate, as could be expected from the similar ionic radii of Co^{2+} and Fe^{2+} (0.82 Å vs. 0.83 Å). Only a very minor fraction of cobalt appears to be associated with the gangue minerals.

As

Arsenic is found mainly in the pyrite concentrate, where its concentration is about four times that of the crude ore. A certain amount, of the same order as in the crude ore, is also found in the Pb concentrate. Vokes (1963) in his mineralogical study of the Bleikvassli ore, found that arsenopyrite (FeAsS) occurs sparsely and sporadically in the pyrite type of the ore, and in the sections where it is more abundant, the mineral often appears crystallized together with pyrite in composite grains or crystals. Furthermore, he observed a rather widespread occurrence of fahlerts ($\text{Cu}_3(\text{As,Sb})\text{S}_4$) in the ore, intimately associated with the galena. The distribution pattern observed in the present work is consistent with these observations.

Sb

Antimony shows a strong concentration in the Pb fraction, in accordance with the fact that this element is a common constituent of many hydrothermal galena deposits (Goldschmidt 1954), replacing either S or Pb. Possible Sb occurring in fahlerts would also tend to be concentrated with lead. The minerals gudmundite (FeSbS), boulangerite ($\text{Pb}_5\text{Sb}_4\text{S}_{11}$), and bournonite (CuPbSbS_3) have also been identified in the Bleikvassli ore (Vokes 1963), but these minerals appear to be less abundant than fahlerts. The observed concentration factor for Sb from the crude ore to the lead concentrate (11.6 ± 1.2) is somewhat lower than the corresponding value for Pb.

Se

Selenium, which is present in a concentration of about 10 ppm in the crude ore, also shows a very distinct enrichment in the lead concentrate (average concentration factor 15.7 ± 2.8 , in agreement with the Pb value within the observed standard deviations). This fact may be explained by a substitution of Se for S in galena or chalcopyrite. It could also in part be associated with the presence of Se in one or more trace minerals, possibly together with silver, which is known to have a pronounced affinity towards selenium. Such minerals, however, have not been observed so far in the Bleikvassli ore.

Ir

The iridium content of the present samples is so low (< 0.05 ppm) that no discussion seems to be appropriate at this point.

Sc, Tb

The strongly lithophile character of these elements suggests their association with the gangue minerals, an assumption which is supported by the occurrence

of these elements in the pyrite tailings while their abundance in the metal concentrates is very low.

Cr

This element exhibits a somewhat peculiar behaviour. While apparently present in the crude ore at a concentration level of about 150 ppm, it has not been observed in any of the fractions studied. It might have been present in part in the Zn or Pb concentrates, where analytical interference did not permit its determination at levels below 100 ppm. Some fractions were therefore re-analysed for Cr using a radiochemical variant of neutron activation analysis. In this case, the irradiated samples were decomposed with $\text{Na}_2\text{O}_2/\text{NaOH}$ in the presence of 10 mg inactive chromium carrier, and the insoluble hydroxides occurring upon leaching the melt with water were removed. By this means, most of the analytically interfering radionuclides were eliminated. The results thus obtained are given in the extreme right hand column of Table 1. The occurrence of Cr in the crude ore samples is confirmed, while the content in the Zn and Pb concentrates appears to be very low. Consequently the major part of chromium seems to be removed before the first flotation step. This seems difficult to explain, unless the Cr observed in the crude ore samples is present in an easily soluble mineral, or simply due to contamination from the equipment used during crushing and grinding of the ore. As neither of these possibilities seems very likely, the virtual disappearance of Cr during the processes involved still remains unsolved.

Acknowledgements. - The authors are grateful to Professor J. A. W. Bugge, Institutt for Geologi, Universitetet i Oslo, and Professor F. M. Vokes, Institutt for Geologi, Universitetet i Trondheim, Norges Tekniske Hogskole, for valuable discussions. Thanks are due to Fangel & Co. A/S for permission to publish the results.

REFERENCES

- Carstens, C. W. 1935: Zur Genese der Kiesvorkommen des Trondhjemgebietes. *K. norske Vitensk. Selsk. Skr.* 11, 40 pp.
- Fazal-Ur-Rehman, Brunfelt, A. O. & Finstad, K. G., (in press): Gold, silver and mercury in materials from Norwegian sulphide mines. *Norges geol. Unders.*
- Goldschmidt, V. M. 1954: *Geochemistry*. Clarendon Press, Oxford. 477 pp.
- Steinnes, E. & Mukherjee, A. D. 1973: Instrumental neutron activation analysis of a sulphide ore and some ore beneficiation products. *J. Radioanal. Chem.* 14, 129-138.
- Vokes, F. M. 1963: Geological studies on the Caledonian pyritic zinc-lead orebody at Bleikvassli, Nordland, Norway. *Norges geol. Unders.* 222, 126 pp.

Table 1. Results for some trace elements in samples collected from the mineral dressing plant at Bleikvassli.
All values are given in ppm

Date (1970)	Fraction	Co	Ag	Au	As	Sb	Se	Ir	Cr	Sc	Th	Cr*
2.11	Crude ore (CO)	39	46	<0.04	157	73	14	<0.05	154	1.8	21	159
"	Zn concentrate (ZnC)	6.5	51	0.29	9.3	35	43	<0.3	<100	-	<5	2.9
"	Zn tailings (ZnT)	47	<5	0.01	200	23	<5	<0.05	21	2.5	22	
"	Pb concentrate (PbC)	13.8	690	3.0	150	950	190	<0.3	<100	-	5.0	<10
"	Pb tailings (PbT)	44	12	0.03	188	23	7.0	<0.05	14	2.3	22	
"	Pyrite concentrate (PyC)	146	4.8	<0.04	640	32	<5	"	18	<0.5	6.3	
"	Pyrite tailings (PyT)	2.5	<5	<0.01	13	14.6	<5	"	10	2.4	29	
3.11	CO	43	44	0.23	194	80	14	<0.05	143	2.0	21	151
"	ZnC	<5	<50	0.08	3.8	28	<40	<0.3	<100	-	<5	3.7
"	ZnT	49	<5	0.07	174	25	<5	<0.05	13	2.2	22	
"	PbC	5.6	840	0.78	116	890	200	<0.3	<100	-	<5	<10
"	PbT	45	12	0.19	171	27	13	<0.05	18	2.3	20	
"	PyC	167	8.5	0.04	620	26	2.9	"	14	<0.3	5.5	
"	PyT	5.5	<5	0.01	22	17.6	<5	"	13	3.1	27	
4.11	CO	31	68	0.17	117	93	11	<0.05	162	2.6	23	172
"	ZnC	4.6	51	0.03	17	29	<40	<0.3	<100	-	<5	1.6
"	ZnT	41	<5	<0.02	144	17.7	<5	<0.05	15	2.9	35	
"	PbC	16.5	760	0.71	128	960	167	<0.3	<100	-	5.3	<10
"	PbT	36	8.1	0.02	142	23	5.5	<0.05	13	3.7	27	
"	PyC	140	<5	0.05	550	35	<5	"	24	<0.4	6.4	
"	PyT	1.1	<5	<0.01	8.3	19.1	<5	"	<10	4.1	28	
5.11	CO	35	39	0.05	138	80	8.8	<0.05	132	3.0	28	
"	ZnC	4.7	<50	0.02	13	22	<40	<0.3	<100	-	<5	
"	ZnT	41	<5	<0.02	178	18.0	<5	<0.05	14	3.4	25	
"	PbC	<5	770	16.8	148	970	173	<0.3	<100	-	4.5	
"	PbT	34	<5	0.04	153	15.9	<5	<0.05	12	3.1	26	
"	PyC	109	5.1	0.04	510	30	<5	"	21	<0.4	4.7	
"	PyT	0.9	<5	<0.02	5.8	7.6	<5	"	7.1	4.5	29	
6.11	ZnC	5.7	55	<0.02	12	57	<40	<0.3	<100	-	<5	
"	ZnT	46	5.3	<0.02	157	20	<5	<0.05	18	2.8	24	
"	PbC	<5	1250	1.3	179	1640	220	<0.3	<100	-	<5	
"	PbT	38	15	0.12	152	33	4.2	<0.05	10	2.9	26	
"	PyC	139	<5	0.09	520	42	<5	"	14	0.2	4.6	
"	PyT	2.7	<5	0.02	9.1	12.1	<5	"	7.9	4.1	30	

* Values obtained using radiochemical separation of ^{51}Cr .

Change in Chemical Composition of Rock Samples during Preparation for Analysis

PER REIDAR GRAFF

Graff, P. R. 1973: Change in chemical composition of rock samples during preparation for analysis. *Norges geol. Unders.* 300, 27-31.

It has been shown that up to 3% of the volume of rock samples may escape as dust during their preparation (crushing and grinding) for chemical analysis. The mineral and chemical composition of the escaping rock dust may frequently differ from that of the main sample, as demonstrated by analytical examples. The effect of such selective separation can, in most cases, be regarded as negligible, though in some instances it may be of considerable importance in an evaluation and classification of the sample.

Per Reidar Graff, Norges geologiske undersøkelse, P.O.Box 3006, N-7001 Trondheim, Norway

Introduction

The preparation of rock samples for chemical analysis is a very important process. This first stage as a rule includes the crushing, splitting, grinding, mixing and, if necessary, the drying of the sample (Kolthoff & Sandell 1964). The equipment generally used is a jaw crusher, a splitter and an agate mortar or mill with agate inset. Jaw crushers are widely employed in laboratories to reduce the large fragments of silicates to pea size or smaller. This step always leads to the formation of rock dust, some of which escapes from the main sample. The amount of rock dust formed depends on several factors, the most important apparently being the brittleness, the fissility and the hardness of the mineral (Taggart 1950). Jaw crushers are frequently equipped with a suction device to eliminate the dust nuisance. Clearly, the greater the efficiency of the suction, the larger will be the amount of the rock dust removed. In the present study, the amount of rock dust escaping during the preparation of samples was estimated to be about 3 per cent. A comparison of the chemical composition of the main sample and that of the derived dust is therefore of interest.

In the present investigation dust and main samples of rock types with lithologies varying in chemical composition from acid to ultrabasic were analysed by normal wet chemical methods. In addition, X-ray diffractometer determinations were carried out on the same samples to establish the distribution of minerals in the main powder and in the corresponding dust fraction.

Crushing and pulverizing. Analytical methods

In the present investigation a jaw crusher from Morgaardshamar Mek. Verksted AB. has been used. The jaw crusher was connected to a cyclon with a hose, and a special filter (100 mesh) for collecting the rock dust was placed

inside the hose. The desired reduction of the fragments was achieved by narrowing the gap between the two metal plates of the jaw crusher. Each sample was treated twice in the crusher, first with a wide gap and secondly with a narrow gap. After this step, the sample consists of rock fragments ranging in size from about one mm to the finest rock dust. The main samples are then repeatedly halved until the weight of the powder is about 30 g. This is then treated in a mill with agate inset for about 1½ minutes, after which all the fragments are smaller than 100 mesh. The pulverized rock sample is then transferred to a sample box.

The technique employed in the determination of the major components is based partly on gravimetric, spectrophotometric and flamephotometric methods. The determination of silica, alumina, calcium, magnesium and total iron has been carried out after the conventional classical method. The determination of titanium, manganese, sodium, potassium and ferrous iron has been based on a method described by Langmyhr & Graff (1965). For the determination of water the method of Penfield was employed, while the carbon dioxide determinations were carried out by the direct method described by Kolthoff & Sandell (1959). Further, the determination of principal minerals both in the main sample and in the dust fraction was made by X-ray diffractometry (Table 1).

Results

As can be seen from Table 1, there is some change in the proportion of the main minerals in the two fractions. According to E. Evensen (personal communication 1972), these changes can be quite large for some trace elements. In specimens I–V the minerals somewhat concentrated in the rock dust are those of microcline, mica, chlorite and calcite, as well as rutile and sphene. The last two minerals are accessories and are omitted from Table 1. Acid plagioclase is found to be relatively concentrated in the main fraction, while quartz is either weakly concentrated in the main sample or shows an equal distribution. Equal distributions seem to be the rule for the minerals pyroxene and epidote.

As a consequence of these changes in the mineral concentrations, some differences will also occur in the chemical compositions of the two fractions. Table 2 shows the average chemical compositions of 38 rock samples and the average differences in the corresponding dust fractions. The mineral composition of the rock samples is shown in Table 1, columns I–V. Possible accessory minerals have not been considered in this example.

The differences between the chemical composition of the main fraction and that of the dust fraction can be completely explained by the change in mineral content in these two fractions, with the exception of the higher content of divalent iron in the rock dust. This iron increase would probably be partly due to contamination from the crusher. Minute fragments (< 150 mesh) of iron would tend to tear from the jaws and mix with the rock dust.

Table 1. Comparison of mineral contents in the main samples and the corresponding dust fractions

Sample number	I	II	III	IV	V	VI	VII	VIII
Acid plagioclase	D	D	D	D	D	D		
Microcline	I			I		I		
Quartz	E	D	E	D				
Mica	I	I		I	I			I
Pyroxene				E				
Hornblende			I		D			
Epidote	E	E	E					
Chlorite		I	I		I			E
Dolomite								D
Magnesite								D
Calcite	I	I						
Serpentine							I	
Talc								I
Olivine							D	

D Mineral proportion decreased in the rock dust relative to that in the main fraction.

I Mineral proportion increased in the rock dust relative to that in the main fraction.

E Equal distribution of the minerals in the two fractions.

Table 2. The average of chemical analyses for 38 rock samples and the oxide variations in the corresponding dust fraction in absolute per cent

Average composition of 38 rock samples	Average deviation in the corresponding dust fraction
SiO ₂	69.00 — 2.70
TiO ₂	0.448 + 0.063
Al ₂ O ₃	12.07 + 0.71
Fe ₂ O ₃ (tot)	4.12 + 0.83
FeO	2.62 + 0.65
MnO	0.08 + 0.02
MgO	3.40 + 0.20
CaO	1.81 + 0.22
Na ₂ O	3.51 — 0.21
K ₂ O	2.72 + 0.15
H ₂ O ⁻	0.31 + 0.10
H ₂ O ⁺	1.08 + 0.41
CO ₂	0.29 + 0.12
P ₂ O ₅	0.058 + 0.020

The mineral combination shown in Table 1, column VI, is representative of feldspar. The average of the chemical composition of the main fraction of 10 feldspar samples and the differences in the corresponding dust fraction are presented in Table 3.

The results (Table 3) show smaller variations between the dust fraction and the main sample, but the tendencies are the same as those noted in Table 2.

Table 1, column VII, represents serpentine rocks. The results show a relative increase of serpentine concentration and a decrease of the olivine concentration in the rock dust. In Table 4 the average chemical composition of the main fraction of 6 serpentine rocks is presented together with the average deviation in the corresponding dust fraction.

Table 3. Average of 10 analyses of feldspar and the variation in the corresponding dust fraction in absolute per cent

Average of 10 feldspar samples		Average of the deviation in the corresponding dust fraction
SiO ₂	64.34	- 0.40
Al ₂ O ₃	20.08	+ 0.24
Fe ₂ O ₃ (tot)	0.07	+ 0.08
MgO	0.13	+ 0.01
CaO	0.46	+ 0.15
Na ₂ O	4.35	- 0.01
K ₂ O	9.91	+ 0.05
CO ₂	0.14	+ 0.01

Table 4. Average chemical composition of serpentine rocks and the differences in oxide contents in the corresponding dust fraction (absolute per cent)

Average of 6 serpentine rocks		Average of the deviation in the corresponding dust fraction
SiO ₂	37.14	- 0.43
Fe ₂ O ₃ (tot)	8.55	- 0.83
FeO	5.06	- 0.28
MnO	0.09	+ 0.04
MgO	44.10	+ 0.24
H ₂ O ⁻	0.01	+ 0.09
H ₂ O ⁺	6.68	+ 1.22

Table 5. Average chemical composition of 6 steatite samples and the deviation in corresponding dust fraction (absolute per cent)

Average of 6 steatite samples		Average of the deviation in the corresponding dust fraction
SiO ₂	36.33	+ 3.30
TiO ₂	0.38	- 0.07
Al ₂ O ₃	6.42	- 1.27
Fe ₂ O ₃ (tot)	9.71	- 0.38
FeO	7.63	- 0.04
MnO	0.15	+ 0.02
MgO	28.60	+ 0.56
CaO	3.07	- 0.62
Na ₂ O	0.04	- 0.04
K ₂ O	0.60	- 0.07
H ₂ O ⁻	0.12	+ 0.09
H ₂ O ⁺	6.33	+ 0.65
CO ₂	9.33	- 2.19
P ₂ O ₅	0.04	+ 0.01

As a consequence of the mineral separation, the oxide percentages presented in Table 4 show considerable deviations for iron and chemically bound water.

Some experiments were also carried out on rock samples containing the mineral combination shown in Table 1, column VIII, and the results of these analyses, showing the average of 6 rock samples (Steatite), are presented in Table 5.

From Table 1, column VIII, it can be seen that talc and mica are enriched in the dust fraction and that dolomite and magnesite are less dust-forming in this particular mineral assemblage. These differences are sufficient to explain the deviation in the chemical composition as shown in Table 5. In this case there is no contamination of iron in the dust fraction since we are dealing with a soft rock type.

Conclusions

It can be concluded from the present investigation that a certain measure of separation of minerals from rock samples occurs during the crushing process. Because the content and combination of minerals vary so much from sample to sample, it does not, however, appear feasible to advance any theory as to how much this separation will influence the ultimate analytical result. In most cases the oxide variations can be regarded as negligible, but in some instances these would have a bearing on the evaluation of the sample. The deviation and variation trends reported here should therefore be borne in mind when considering the results of chemical analyses, particularly those judged to be critical for interpretation or classification purposes.

Acknowledgements. - The author wishes to thank his co-workers for technical assistance, and Dr. D. Roberts for kindly correcting the English manuscript.

REFERENCES

- Kolthoff, I.M. & Sandell, E. B. 1959: *Textbook of Quantitative Analysis*. Third edition, 700 pp. Macmillan Co., New York.
- Langmyhr, F. J. & Graff, P. R. 1965: A contribution to the analytical chemistry of silicate rocks: a scheme of analysis for eleven main constituents based on decomposition by hydrofluoric acid. *Norges geol. Unders.* 230, 128 pp.
- Taggart, A. F. 1950: *Handbook of Mineral Dressing*. 1845 pp. John Wiley & Sons Inc., New York.

Age Determinations from the Iveland-Evje Area, Aust-Agder

SVEND PEDERSEN

Pedersen, S. 1973: Age determinations from the Iveland-Evje area, Aust-Agder. *Norges geol. Unders.* 300, 33-39.

A Rb/Sr isochron age determination on intrusive granite and monzonite from the Iveland-Evje area gave an age of 1038 ± 43 m.y. Biotite from the granite dated by the K/Ar method gave an age of 845 ± 60 m.y. These values are very similar to other age determinations on intrusive rocks from Southern Norway.

The initial $\text{Sr}^{87}/\text{Sr}^{86}$ ratio of the granite and monzonite is very low: 0.7048 ± 0.0003 .

The rocks must be genetically related to the Iveland-Evje pegmatites, which are among the latest intrusions within the Sveconorwegian igneous period.

S. Pedersen, *Institute of General Geology, Østervoldsgade 5, DK-1350 Copenhagen K, Denmark*

Introduction

The paper describes some new age determinations from the Iveland-Evje area in Southern Norway. These were carried out on intrusive rocks, granite and monzonite, which had not previously been described. The method used was the Rb/Sr whole rock isochron method. One age, however, was obtained on biotite from granite by the K/Ar method.

The author mapped part of the Iveland-Evje amphibolite during the summers 1967 and 1968, with a final short stay in 1970; during the first field season the author was a member of the team working on the 'Telemark Project'. This mapping, being more detailed than that carried out by Barth (1947), revealed the granitic and monzonitic rocks.

Prior to the present study, all the age determinations from the Iveland-Evje area had been made on pegmatite minerals (Herr & Mertz 1958; Herr et al. 1958; Polkanov & Gerling in Neumann 1960; Kulp & Neumann 1961; Obrochev & Gerling in Broch 1964, and Herr & Wölfle 1967). Ages and methods are shown in Table 1.

Both Neumann and Broch remark that there is doubt about the significance of some of these ages. For instance, regarding the Re/Os determinations, the results suggest that the half-life of Re should be increased by about 20%. The Russian K/Ar determinations are 4 to 5% too high, because Russian geochronologists prefer the value $5.5 \times 10^{-11} \text{yr}^{-1}$ for the decay constant λ_e , whereas the value $5.85 \times 10^{-11} \text{yr}^{-1}$ is normally used in other laboratories. From these early age determinations Neumann (1960) concluded that the pegmatites were emplaced 900-1000 m.y. ago.

Table 1. Previous age determinations from the Iveland-Evje area

Ref.	Method	Mineral	Age m.y.	Revised age m.y.	Locality
1.	RaD/Pb	Gadolinite	755		Frikstad
2.	Re/Os	Gadolinite	838		Frikstad
2.	Pb ²⁰⁷ /Pb ²⁰⁶	Gadolinite	820		Frikstad
2.	RaD/Pb	Blomstrandine	884		Kåbuland
2.	Pb ²⁰⁷ /Pb ²⁰⁶	Blomstrandine	920		Kåbuland
2.	Re/Os	Molybdenite	882		Tveit
2.	Re/Os	Molybdenite	962		Tuftan
3.	K/Ar	Biotite	880	835	Håverstad
4.	K/Ar	Muscovite	860		Iveland
5.	K/Ar	Biotite	1650	1582	Eptevann
5.	K/Ar	Biotite	1750	1679	Eptevann
6.	Re/Os	Molybdenite	1120		Tuftan
6.	?	Uraninite	1040		Tuftan

References:

- Herr et al. (1958).
- Herr & Mertz (1958).
- Gerling & Polkanov in Neumann (1960).
- Kulp & Neumann (1961).
- Obruchev & Gerling in Broch (1964).
- Herr & Wölflé (1967).

Outline of the geology in the northern part of the Iveland-Evje area

The Iveland-Evje area is famous for its nickel mineralisation (Vogt 1893, 1923; Bjørlykke 1947) and the many pegmatites carrying rare minerals (for general descriptions see Barth 1928, 1931, 1947; Andersen 1926, 1931; Bjørlykke 1934, 1937).

The nickel mineralisation and the pegmatites appear in an amphibolitic body described by Barth (1947) as the Iveland-Evje amphibolite. This body is 35 km in a north-south direction and its maximum width is 15 km.

Recent investigations by the present author (not yet published) have shown that, at least in the northern part, the Iveland-Evje amphibolite is made up of several bodies. One of these bodies, situated NE of Evje, is called here the Høvringsvatn Complex. It has a rather complicated structure; amphibolite is not the only rock type, contrary to what was previously thought. The complex consists of an older basic intrusion representing part of the Iveland-Evje amphibolite and a younger intermediate to acid intrusion of granite and monzonite. Some monzonitic rocks seem to be developed as thin cone sheets cutting amphibolite, granite, monzonite and the surrounding gneisses. Granite pegmatites and some aplites end this igneous activity.

It has to be emphasised here that the relations are very complicated, especially those between the granite and the cone sheets, as the granite has often been reactivated in connection with the intrusion of the sheets.

The Rb/Sr whole rock isochron age determinations described in the following were carried out on rocks from the Høvringsvatn Complex: granite

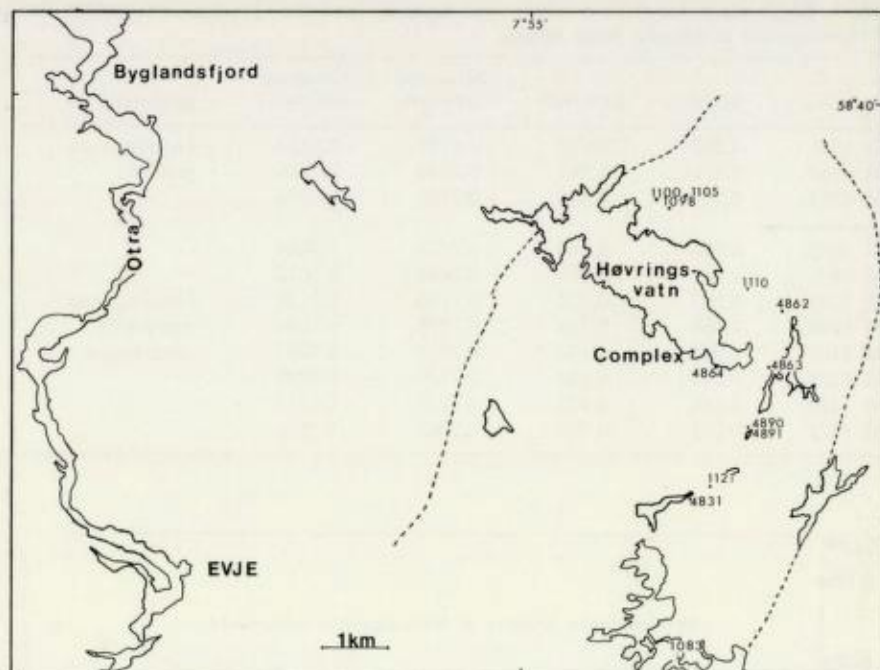


Fig. 1. Map of sample location.

(called Høvringsvatn granite), and monzonitic cone sheets (called Høvringsvatn monzonite). One K/Ar determination was carried out on biotite from the Høvringsvatn granite. The location of samples dated is shown in Fig. 1.

The Høvringsvatn granite is a medium- to coarse-grained rock, which is dominated by red, mainly euhedral potassium feldspar, and is characterised by a very homogeneous look and uniform grain size throughout the entire area.

Høvringsvatn monzonite embraces several structural types, all grey rocks carrying blue-green hornblende and green biotite as dark minerals and with a characteristic, marked content of abundant accessory sphene and apatite.

A thorough description of the rocks is planned in a later publication.

Rb/Sr age determinations and isotope analyses

Determination of Rb/Sr ratios: For the measurements of the ratio between Rb and Sr a Philips X-ray fluorescence apparatus with a W-tube (20 mA, 10 kV), an LiF 200 analysing crystal and a fine collimator were used. The peaks and background have been counted for 40 seconds.

The measurements were corrected for counter dead time, background curvature and peak interferences. These corrections have been described by Pankhurst (1968). All determinations were made in duplicate. The experimental error is in the range of 2% (1 σ level).

Table 2. Rb/Sr analytical data of whole rock samples from the Høvringsvatn granite and the Høvringsvatn monzonite (cone sheets)

Sample No.	Rb/Sr	Rb ⁸⁷ /Sr ⁸⁶	Measured Sr ⁸⁷ /Sr ⁸⁶	Corrected Sr ⁸⁷ /Sr ⁸⁶	Rock type
MM 4831	0.302	0.874	0.7195	0.7183	Høvringsvatn granite
MM 4862	0.426	1.233	0.7230	0.7218	
MM 4864	0.119	0.345	0.7106	0.7094	
MM 4890	0.050	0.144	0.7076	0.7064	Høvringsvatn monzonite cone sheets
MM 4891	0.061	0.175	0.7084	0.7072	
MM 1083	0.207	0.602	0.7140	0.7128	
MM 1098	0.086	0.248	0.7098	0.7086	
MM 1100	0.066	0.190	0.7079	0.7067	
MM 1105	0.112	0.324	0.7109	0.7097	
MM 1110	0.146	0.425	0.7129	0.7117	
MM 1121	0.072	0.207	0.7088	0.7076	

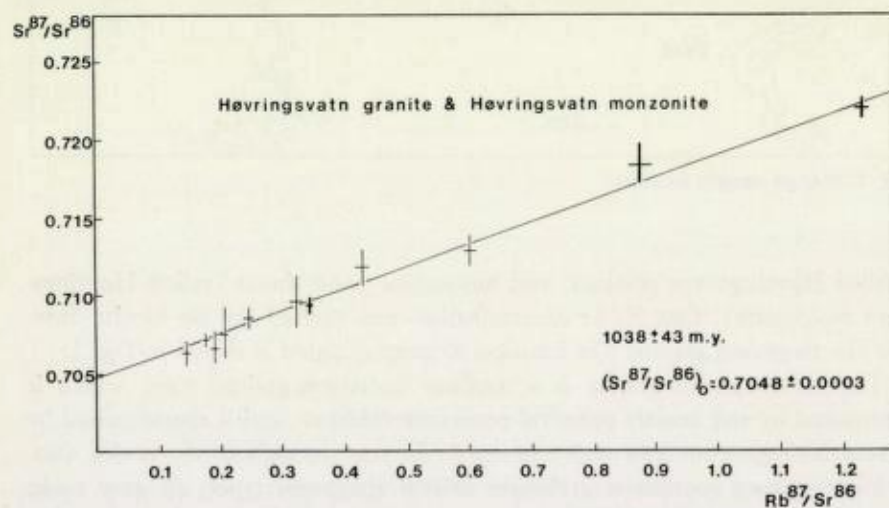


Fig. 2. Isochron plot for Høvringsvatn granite (heavy crosses) and Høvringsvatn monzonite cone sheets (light crosses).

Measurements of Sr isotope ratios: The chemical analyses were carried out at the dating laboratory of the Petrological Institute, University of Copenhagen, whereas the mass spectrometric investigations were undertaken on the Atlas CH-4 mass spectrometer at the Institute of Theoretical Meteorology, University of Copenhagen. A Faraday collector was attached to the mass spectrometer.

The Sr^{87}/Sr^{86} ratio obtained on the Eimer and Amend $SrCO_3$ standard (lot 492327) was 0.7092 ± 0.0004 ; all measured ratios were normalised to Sr^{86}/Sr^{88} values of 0.1194. The average obtained here is scarcely $2^0/00$ higher than the normally accepted value of 0.7080, and for this reason just under $2^0/00$ was subtracted from all the measured Sr^{87}/Sr^{86} ratios.

The experimental error varies between $0.5^0/00$ and $2.5^0/00$ (1σ level).

Table 3. K/Ar analytical data of biotite from the Høvringsvatn granite

Sample No.	% K ₂ O	Ar ⁴⁰ _R /K ⁴⁰	Age in m.y.
MM 4864 (Biotite)	9.4 ± 0.3	0.0627	845 ± 60

Results: All the values obtained (see Table 2) are plotted in the diagram Fig. 2. It is remarkable that these values, which represent both granite and monzonite, plot on a single isochron, giving an age of 1038 ± 43 m.y. with an initial Sr⁸⁷/Sr⁸⁶ ratio of 0.7048 ± 0.0003 . The decay constant used is $\lambda = 1.39 \times 10^{-11} \text{yr}^{-1}$ (Aldrich et al. 1956).

This isochron needs an explanation, as it contrasts with the field relations. In the field the monzonitic cone sheets are clearly seen to cut the granite; in places, however, the granite has been reactivated in connection with the monzonite intrusion. It may be either that the monzonite and granite are penecontemporaneous and have a common initial ratio, or that the granite is older, but was reworked at the time of monzonite intrusion with the result that a resetting of the isotopic systems took place.

K/Ar determinations

K determinations: These were made on a Perkin Elmer 303 atomic absorption spectrometer. The samples were decomposed with the aid of hydrofluoric acid following a method described by Langmyhr & Paus (1968). The details of this method as used in the laboratory in Copenhagen have been described by Larsen (1971).

Ar determinations: The amount of radiogenic Ar was determined by isotope dilution on an AEI MS 10 mass spectrometer. A full description of this method has been given by Larsen & Møller (1968) and by Larsen (1971).

Results: The K/Ar determination was carried out on biotite from the Høvringsvatn granite. It gave an age of 845 ± 60 m.y. The results are shown in Table 3.

Concluding remarks

The Rb/Sr dating shows that intrusion of monzonite (and perhaps granite) took place about 1038 m.y. ago in the Iveland-Evje area.

There is a remarkable consistency between this age and the ages of the youngest intrusive, basic rocks of the Bamble area (1040 m.y., O'Nions et al. 1969) and the mangerites and farsundites of the Rogaland area (967 m.y. and 993 m.y. old respectively, according to Pasteels et al. 1970).

The earlier age determinations on pegmatite minerals showed that the pegmatites of the Iveland-Evje area are 900–1000 m.y. old (Neumann 1960) and consequently they must belong to the same intrusive period as the granite and

monzonite. This period corresponds with the Sveconorwegian igneous period of Welin (1966).

The K/Ar age of 845 m.y. is in accordance with some of the earlier K/Ar determinations on pegmatite micas. Polkanov & Gerling (in Neumann 1960) obtained an age of 835 m.y. on biotite (converted age, see Table 1). Kulp & Neumann (1961) obtained 860 m.y. on muscovite from a pegmatite. On the other hand the results of Obruchev & Gerling (in Broch 1964), who obtained figures of 1582 m.y. and 1679 m.y. (converted ages, see Table 1), are not in agreement with these ages.

It is remarkable that K/Ar ages on biotite from the neighbouring Bamble area are higher than the result obtained here, i.e. about 970 m.y. (O'Nions et al. 1969).

Acknowledgements. - I wish to thank Professor A. Berthelsen, Dr. J. A. Dons and Professor H. Neumann for their help during the mapping and geological interpretation. I am also very much indebted to O. Larsen and J. Møller for help and criticism in connection with the experimental work. T. C. R. Pulvertaft kindly corrected the English.

REFERENCES

- Aldrich, L. T., Wetherill, G. W., Tilton, G. R. & Davis, G. L. 1956: Half life of ^{87}Rb . *Phys. Rev.* 103, 1045-1047.
- Andersen, O. 1926: Feldspat I. *Norges geol. Unders.* 128a.
- Andersen, O. 1931: Feldspat II. *Norges geol. Unders.* 128b.
- Barth, T. F. W. 1928: Zur Genesis der Pegmatite im Urgebirge. *N. Jahrb. f. Min. etc.*, B. Bd. 58, Abt. A., 385-432.
- Barth, T. F. W. 1931: Feldspat III. *Norges geol. Unders.* 128b.
- Barth, T. F. W. 1947: The nickeliferous Iveland-Evje amphibolite and its relation. *Norges geol. Unders.* 168a.
- Bjørlykke, H. 1934: The mineral paragenesis of the granite pegmatites of Iveland, Setesdal, Southern Norway. *Norsk geol. Tidsskr.* 14, 211-309.
- Bjørlykke, H. 1937: The granite pegmatites of Southern Norway. *J. Min. Soc. Am.* 22, No. 4, 241-255.
- Bjørlykke, H. 1947: Flåt Nickel Mine. *Norges geol. Unders.* 168b.
- Broch, O. A. 1964: Age determination of Norwegian minerals up to March, 1964. *Norges geol. Unders.* 228, 84-112.
- Herr, W. & Mertz, E. 1958: Zur Bestimmung der Halbwertszeit des Re^{187} . *Z. Naturf.* 13a, 231-233.
- Herr, W., Mertz, E., Eberhardt, P. & Signer, P. 1958: Zur Bestimmung der β -Halbwertszeit des Lu^{176} durch Nachweis von radiogenem Hf^{176} . *Z. Naturf.* 13a, 268-273.
- Herr, W. & Wölflé, R. 1967: Development and recent applications of the Re/Os method. *Radioactive Dating and Methods of Low-level Counting*, 499-508. International Atomic Agency, Vienna 1967.
- Kulp, J. L. & Neumann, H. 1961: Some potassium-argon ages on rocks from the Norwegian basement. *Am. N.Y. Acad. Sci.* 91, 469-475.
- Langmyhr, F. J. & Paus, P. E. 1968: The analysis of inorganic siliceous materials by atomic absorption spectrophotometry and the hydrofluoric acid decomposition technique. Part 1: The analysis of silicate rocks. *Analytica chim. Acta* 43, 397-408.
- Larsen, O. 1971: K/Ar age determinations from the Precambrian of Denmark. *Danmarks geol. Unders.* 11, række nr. 97.
- Larsen, O. & Møller, J. 1968: Radiometrisk datering af geologisk materiale efter kalium-argon metoden. *Fysisk Tidsskrift* 66. årgang nr. 1, 1-18.
- Neumann, H. 1960: Apparent ages of Norwegian minerals and rocks. *Norsk geol. Tidsskr.* 40, 173-191.

- O'Nions, R. K., Morton, R. D. & Baadsgaard, H. 1969: Potassium-argon ages from the Bamble section of the Fennoscandian Shield in South Norway. *Norsk geol. Tidsskr.* 49, 2, 171-190.
- Pankhurst, R. J. 1968: Strontium isotope and geochronological studies of the basic igneous province of NE Scotland. Unpublished Ph. D. thesis.
- Pasteels, P., Michot, J. & Lavreau, J. 1970: Le complexe éruptive du Rogaland Méridional (Norvège). Signification pétrogénétique de la Farsundite et de la mangerite quartzitique des unités orientales; arguments géochronologiques et isotopiques. *Annales de la Société Géologique de Belgique, Tome 93*, 453-476.
- Vogt, J. H. L. 1893: Bildung von Erzlagerstätten durch Differentiationsprozesse in basischen Eruptivmagmata. *Z. Prakt. Geol.*, 4-11, 125-143 and 257-269.
- Vogt, J. H. L. 1923: Nickel in igneous rocks. *Econ. Geol.* 18, 4, 307-353.
- Welin, E. 1966: The absolute time scale and the classification of Precambrian rocks in Sweden. *Geol. Fören. Stockholm Förh.* 88, 29-33.

Petrochemistry and Origin of the Raudhamaren Ultramafites, Jotunheimen

S. R. N. MURTHY

Murthy, S. R. N. 1973: Petrochemistry and origin of the Raudhamaren ultramafites, Jotunheimen. *Norges geol. Unders.* 300, 41–52.

The ultramafites show gradual petrochemical variation and Mg/Fe ratios indicative of crystallisation differentiation from the stratiform type mafic magma series. The country rocks with which they are in primary association, however, have a calc-alkaline trend of evolution, more indicative of affiliation with the alpine type. The ultramafites are essentially spinel peridotites thought to have formed in a dry environment by diapiric upwelling during the basaltic (gabbroic) evolution of the Upper Mantle.

S. R. N. Murthy, *Mineralogisk-Geologisk Museum, Sarsgt. 1, Oslo 5, Norway*
Present address: *Geological Survey of India, Manoranjan, Hyderabad-1, A.P., India*

Introduction

Ultramafites are rather special rocks because of their extreme femic mineralogy and restricted distribution. Since they are possibly the closest representatives of the Upper Mantle they serve as 'Petrological Windows' to the internal Earth. The traditional classification of ultramafites into alpine and stratiform types has genetic implications in undoubted geological environment, but the catazonal and mesozonal ultramafites cannot be simply attributed to any one of these types.

The ultramafites of Jotunheimen are examples of this, and earlier work by Münster (1884), Rekstad (1904, 1905), Bjørlykke (1905), Goldschmidt (1916), Carstens (1918), Dietrichson (1955, 1958), and Battey (1960, 1965) revealed interesting aspects of these rocks. Carstens (1918) demonstrated that lenses of peridotite occur by the hundreds, possibly by the thousands in the igneous rocks of Jotunheimen, that they are usually surrounded by pyroxenite, and they display gradational contacts towards gabbroic country rocks. Dietrichson (1955, 1958) suggested stratiform magmatic origin for the igneous rocks of Jotunheimen, while Battey (1960) first proposed an intrusive alpine origin for the ultramafites and later (1965) accepted a stratiform origin. This paper is devoted to a study of a single large body, the Raudhamaren ultramafite, and some smaller bodies adjacent to it.

The area in which the ultramafic bodies have been examined is bounded by N latitudes $61^{\circ}24'$ and $61^{\circ}40'$ and E longitudes $8^{\circ}44'$ and $9^{\circ}00'$ on the E30A Sjødalen and E30V Gjende quadrangular topographic maps (Fig. 1). The rocks which belong to the Upper Jotun Nappe, which extends NE-SW for nearly 150 km with a width of about 50 km, are now considered as Precambrian crystallines emplaced during the Caledonian orogeny (Heier et al. 1972).

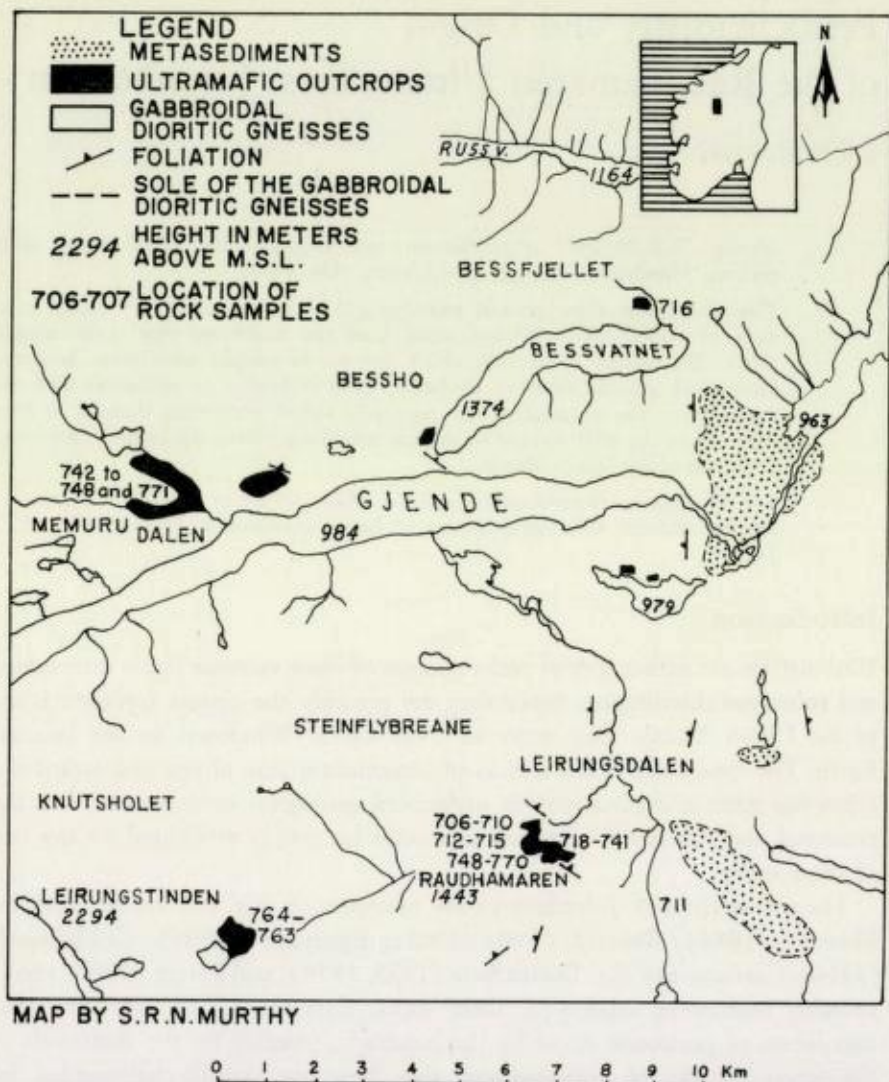


Fig. 1. Geological setting of the ultramafic rocks with location of rock samples.

The lithological units and rock types of the examined area are given below:

Age	Rocks
Precambrian igneous rocks of the Caledonian nappes.	Pegmatites and epidote veins; anorthosites, amphibolites and ultramafic rocks; gabbroidal dioritic gneiss, amphibole gabbro gneiss and amphibole biotite gneiss.
Late Precambrian-lower Palaeozoic metasediments.	Thrust Quartz and feldspar veins, phyllites, mica schists, chlorite schists, amphibole schists and amphibole-biotite gneisses.

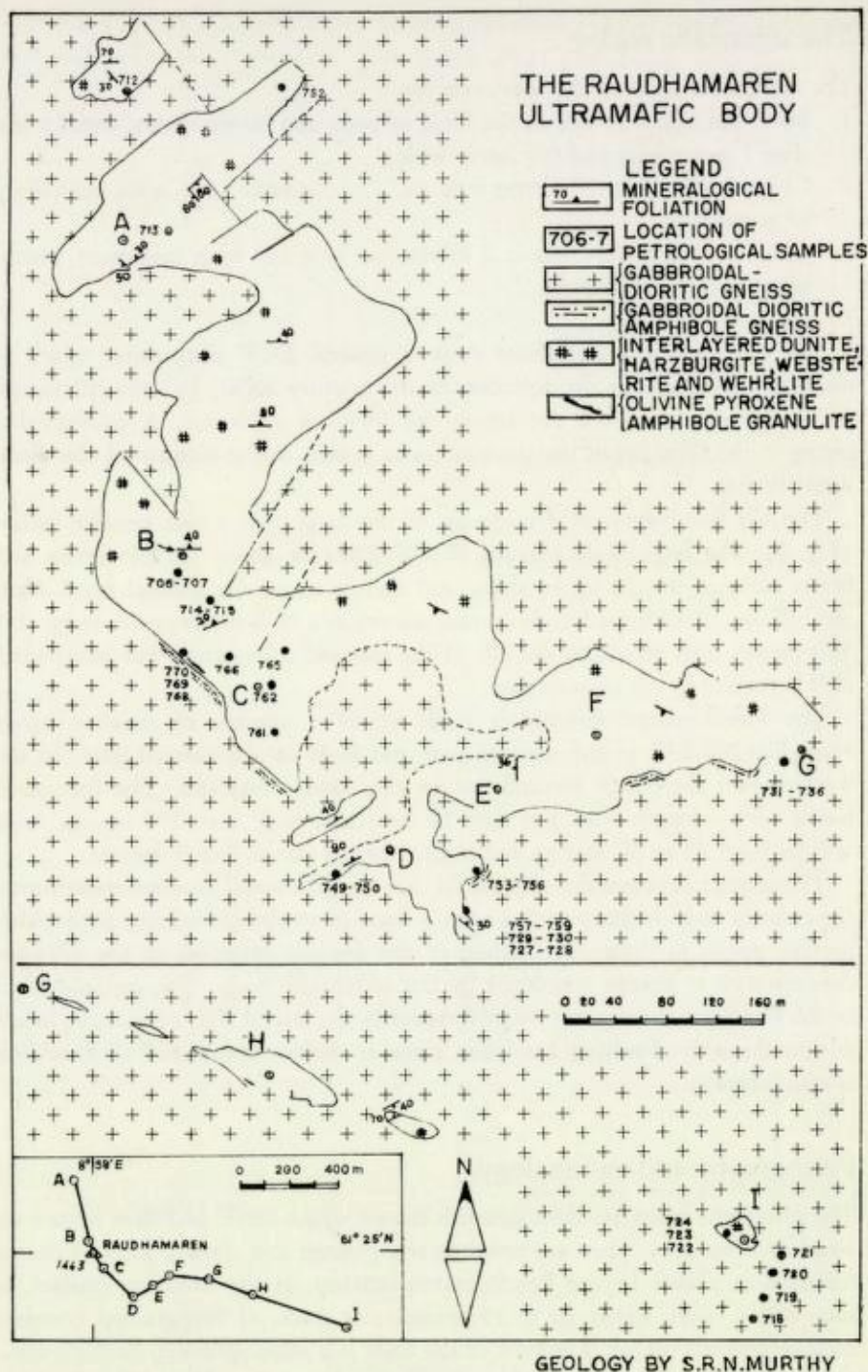


Fig. 2. The ultramafic bodies at Raudhamaren. Upper and lower part of the map are to be joined orthogonally at points G.

The ultramafic rocks

The ultramafic rocks in the area occur as;

1. Small individual bodies in the form of pods and minor lenses, usually less than 1 metre long and 0.5 metre wide;
2. Larger bodies, 5 to 10 metres long and 1 to 3 metres wide, with a tendency to group; and
3. Large lensoid bodies, nearly 2 kilometres long and with maximum widths of more than 500 metres.

The outcrops of ultramafites show a general E-W disposition which is usually at an angle to the foliation of the country rocks, but the ultramafic rocks themselves do not cut across the foliation anywhere. A conformable swing in the foliation of the country rocks is seen in the vicinity of the ultramafic bodies.

The hill Raudhamaren is made up of one large and a few smaller bodies (Fig. 2). The large body extends WNW-ESE for about 1.5 kilometres and forms elevated terrain up to about 500 metres above the general level. Near the hill top, it outcrops for about 600 metres in a N-S direction. A steep cliff 300 metres high occurs to the NE of the top and a less steep but continuous cliff is present in the eastern part.

The Raudhamaren outcrop is made up of a number of massive bands extending NE-SW in the western part and E-W in the eastern part. In the western part the bands succeed one another northwestwards. The individual bands vary in length from less than 10 metres to more than 500 metres, with widths from 20 to 30 metres and thicknesses of about 2 to 3 metres.

The contact between the ultramafite and the gabbroidal gneisses constituting the country rocks is sharp with a narrow band of amphibole-bearing gabbroidal-dioritic gneiss in between. Folding of the gneissic foliation in the adjacent country rock is always simulated by the ultramafic body. The apparent fold in the Raudhamaren outcrop largely expresses the lateral shift of massive bands within the body. Faulting has taken place at various places and slickensiding is also common.

Petrography and mineralogy

The ultramafic rocks are dark greenish brown where fresh, and dark brown on weathered surfaces. They are rather coarse-grained and show a kind of coarse foliation in places. In the Raudhamaren outcrop, at the southern contact, is seen a thin band, about 10 to 15 centimetres thick, of fine-grained compact rock of greenish colour. The bulk of the body is a coarse-grained, dark greenish peridotite with interbanded dark brownish dunite in places. The body is transected by dunite veins, with coarse metamorphic foliation, which may be mistaken for igneous layering.

Table 1. Modal composition (vol%) of ultramafites from Raudhamaren

Minerals	Ol	Opx	Cpx	Amph & Bi	Sp & Ore	nd	Carb	Nomenclature
Sample No.								
758	96				1	2	1	Dunite
731	52	15	29	1	1		2	Websterite
733	62	11	26		1			Wehrlite
735	85	10	5					Ol. Harzburgite
736	58	16	25		1			Websterite
737	83	10	1		4		2	Ol. Harzburgite
739	40	9	47		4			Wehrlite
761	50	19	16		3	11	1	Websterite
762	34	22	36		3	5		Websterite
764	40	17	39		4			Wehrlite

The rock samples are registered at the Mineralogisk-Geologisk Museum, Oslo.

Olivine, clinopyroxene, orthopyroxene and green spinel make up the peridotite varieties while the compact greenish rock at the southern contact contains much amphibole, chlorite and some carbonate. Modal composition of ten samples demonstrates that the Raudhamaren body contains dunite, olivine harzburgite, websterite and wehrlite (Table 1). (Classified according to a scheme adopted from Malakhov 1964.) The peridotitic varieties are difficult to recognise by visual examination alone, but the dunite veins and the compact greenish rock at the base of the outcrop can be distinguished by their habit and compactness respectively.

Olivine ($Fe_{80}-Fe_{92}$) is the main constituent of the peridotites and its composition was determined by microprobe to be Fe_{80} in three samples (Table 2). The grains are euhedral to subhedral, varying from 1 to 4 mm but commonly 1 to 2 mm wide with pale yellow serpentine filling cracks at places. Simple twinning and a characteristic ribbon banding formed by minute inclusions of green spinel and opaque ores can sometimes be seen. Olivines enclosed in tabular grains of pyroxene show effects of resorption and colour zoning. Extremely fractured olivine grains make up the veined dunite, and show preferred orientation by which the coarse foliation of this rock is defined.

Pyroxenes, similar in grain size to the olivines, show well developed (100) and (010) cleavages and distinct partings. Simple lamellar twinning, intergrowth between ortho and clino varieties are present. Olivine, green spinel, some wasps of amphibole and opaque ores are present as inclusions. Orthopyroxene occurs as a coloured variety with pleochroism: X = pink, Y = pale greenish brown and Z = pale green and En content around 70, and as a colourless variety with En about 88-92. Partial microprobe analyses of pyroxenes and their associated olivine are given in Table 2. An interesting point is that the clinopyroxenes are chemically zoned with decreasing alumina outwards.

The amphiboles, occurring as inclusions and forming the greenish compact rock, are secondary tremolite-actinolite varieties. Their formation from

Table 2. Chemical composition and structural formula of minerals from the Raudhamaren ultramafites

Sample No.	750			766			769								
	Cpx	Opx	Ol	Cpx	Opx	Ol	Cpx		Opx	Ol					
Minerals	(Col)			(Col)			core	mantle	rim	(Col)					
Oxides															
SiO ₂	55.5			53.4			50.4	50.2	51.3						
TiO ₂	0.1			0.1			0.1	0.1	0.1						
Al ₂ O ₃	2.9	3.2		3.2	2.9		3.4	2.4	2.0	3.2					
FeO (tot)	4.5	12.5	18.4	4.4	13.0	18.4	4.4	4.5	4.3	12.4	18.6				
MgO	16.1			16.2			16.4	16.7	16.5						
CaO	24.0			22.7			23.9	24.3	24.2						
Total	103.1			100.3			98.9	98.2	98.4						
Number of ions on the basis of 6 oxygens															
Si	1.963	} = 2.000		1.943	} = 2.000		1.881	} = 2.000		1.890	} = 1.997		1.921	} = 2.000	
Al	0.037			0.057			0.119			0.107			0.079		
Ti	0.003			0.003			0.003			0.003			0.003		
Al	0.084			0.080			0.031						0.009		
Fe	0.133	} = 1.979		0.143	} = 1.990		0.147	} = 2.248		0.142	} = 2.062		0.135	} = 2.039	
Mn															
Mg	0.849			0.879			0.912			0.937			0.921		
Ca	0.910			0.885			0.955			0.980			0.971		

Electron probe analyses by B. Griffin and I. Bryhni. Formula obtained on a computer programme.

pyroxene in the compact green rock suggests effects of local water pressure in an otherwise essentially dry environment.

Opaque ores, generally magnetite, and green spinel occur as accessories in these rocks.

The essential mineralogical assemblages are:

1. Olivine-orthopyroxene-spinel,
2. Olivine-orthopyroxene-clinopyroxene-spinel, and
3. Olivine-clinopyroxene-spinel.

Chemistry

Major and selected trace element analyses of 36 rock samples have been analysed out of which 30 are from the Raudhamaren outcrop. The samples from Raudhamaren are from four 'profiles', two in the eastern part, one from the central and one from the western part. Since the base of the nappe is to the SE of the area, it is contended that sampling from SE to NW along the western profile would show variation, if any, in a singular mass from bottom to top of some 150 m thickness, subject to lateral variation due to shifting of bands.

The chemical analyses were carried out by the writer at the Mineralogisk-Geologisk Museum using a Phillips X-ray fluorescence spectrograph. Sample

VARIATION OF OXIDES IN THE RAUDHAMAREN ULTRAMAFITES

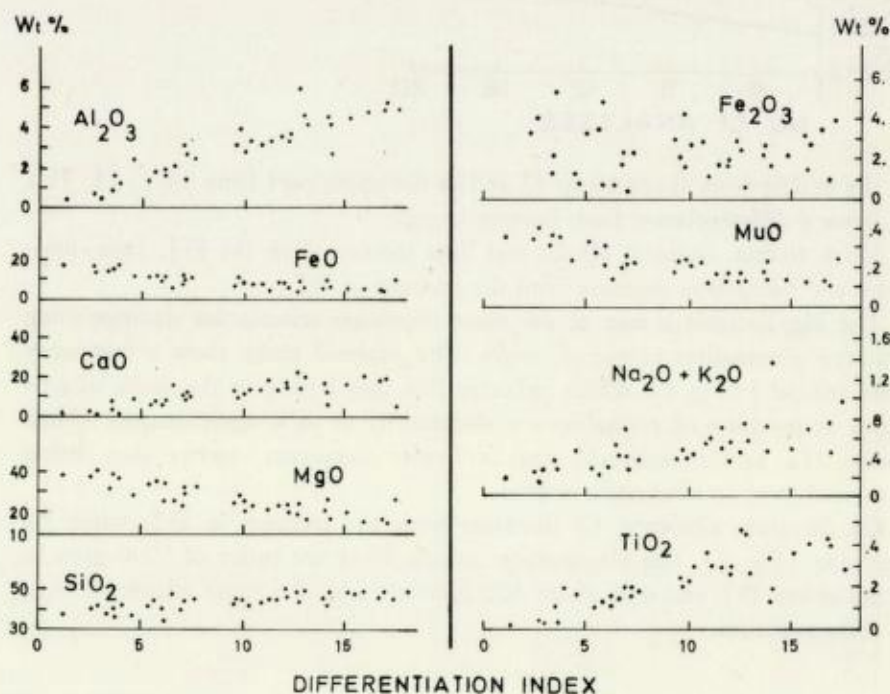


Fig. 3. Major oxides plotted against the differentiation index (D.I.).

pellets (pressed pellets and fused pellets) were prepared in duplicate. Fused pellets were prepared by fusing finely powdered, homogenised sample material with sodium tetraborate in 1:9 dilution. All the major elements (excepting Na₂O, K₂O and FeO) and the trace elements were determined utilising International Geochemical Rock Standards. Counting times were chosen to keep the relative standard deviation of the counting statistics well below 1%. FeO was determined by wet analyses. Na₂O and K₂O were determined by flame photometric techniques, using standard solutions.

The petrochemical variations within the analysed rock samples are illustrated in Fig. 3. The oxides are plotted against the total wt% of normative silic minerals quartz, orthoclase, albite, anorthite, leucite, nepheline, and kaliophilite, a parameter only slightly different from the differentiation index (D.I.) of Thornton & Tuttle (1960). The illustration demonstrates clearly that there is almost a gradual passage from the most silic to the most femic rock types. The differentiation trend in these rocks is almost linear and the D.I. varies from 3 to 18. The Raudhamaren outcrop shows an overall – although internally inconsistent – increase in the D.I. from southeast to northwest. In the lower southeast part the body shows D.I.s varying from 3 to 7.

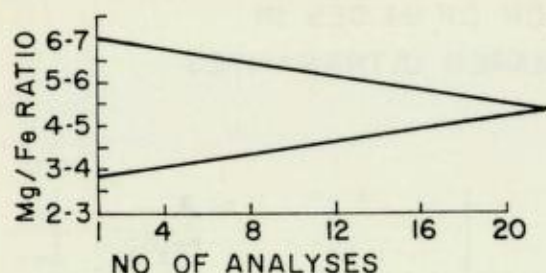


Fig. 4. Frequency of occurrence of Mg/Fe ratios (36 analyses).

in the middle from about 10 to 12 and in the upper part from 14 to 18. This suggests a differentiation from bottom to top.

Silica, titania, alumina, alkalis and lime increase with the D.I. Iron, magnesia and manganese decrease with the increase in D.I.

The Mg/Fe ratio is one of the most important criteria for distinguishing between ultramafites of varied origin. The analysed rocks show a frequency peak around 5 (Fig. 4), which indicates that they belong to the mafic magma series as products of crystallisation differentiation of a mafic magma (Hess 1938) like in the Bushveld and Stillwater complexes, rather than being produced from an ultramafic magma.

Of the trace elements, Cr increases with the increase in D.I. while Ni decreases (Fig. 5). The ultramafites contain Ni of the order of 1000 ppm in rocks of low D.I. and only about 300 ppm in rocks of a more advanced stage of differentiation.

Petrogenesis

Occurrence of the ultramafites in gabbroidal dioritic gneisses, massive banding and coarse foliation (pseudomagmatic), gradual petrochemical variation and almost a lack of serpentinisation as well as the frequency peak of Mg/Fe ratio around 5 are strong evidence suggesting a stratiform origin. Habit and distribution, apparent xenolithic relationship characteristic of 'root zone' ultramafites (Den Tex 1969) are equally strong items of evidence suggesting an alpine origin for these rocks. However, the analyses of known alpine type intrusives suggest a magnesian differentiation trend that crosses the A-F-M triangle nearer to the typical calc-alkaline trend than the Skaergaard trend (Thayer 1967). By this criteria the Jotunheimen ultramafites are certainly 'Alpine type' (Fig. 6). The variation diagram (Dietrichson 1958) shows that the alkali-lime index of the Upper Jotun Nappe rocks is around 57.

Carstens (1918) observed that;

1. Peridotite lenses are generally surrounded by pyroxenite which displays gradational contacts to gabbro and peridotites.
2. Sharp contacts between the lithological units are rare.
3. Transecting relations serve to define the intrusion sequence peridotite-pyroxenite-gabbroic and granitic rocks.

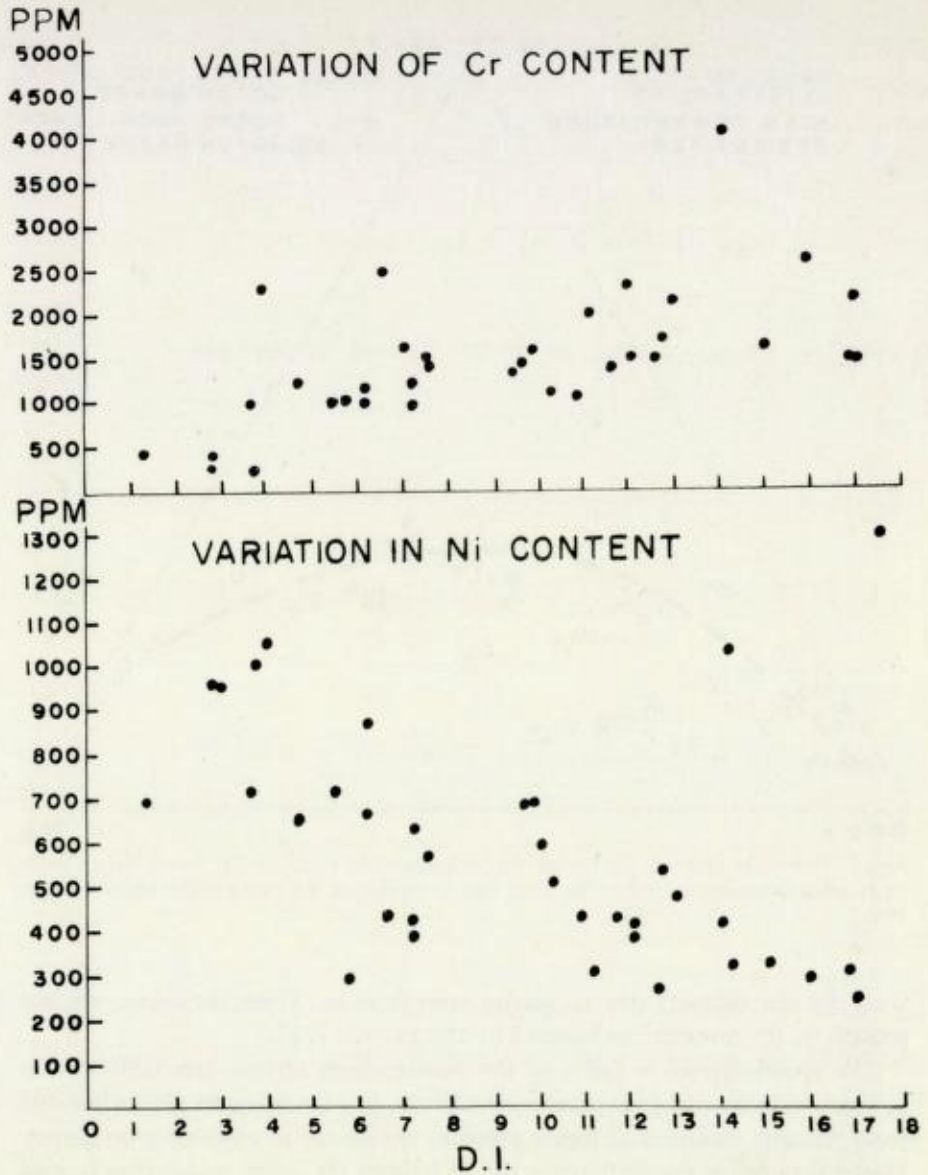


Fig. 5. Chromium and nickel contents plotted against the differentiation index (D.I.).

4. Lithological sequence could be explained in terms of in situ concentration of the first crystallised minerals from the parental magma.

The present study has not confirmed observations 1, 2 and 3, but the mineralogical paragenesis confirms the intrusion sequence given by Carstens. Absence of chilled contacts between the individual rock types does not support the intrusive sequence. The in situ concentration of the first crystallised minerals from the parental magma in the order mentioned by Carstens (1918) would produce reaction and cumulate textures and in large bodies also layering

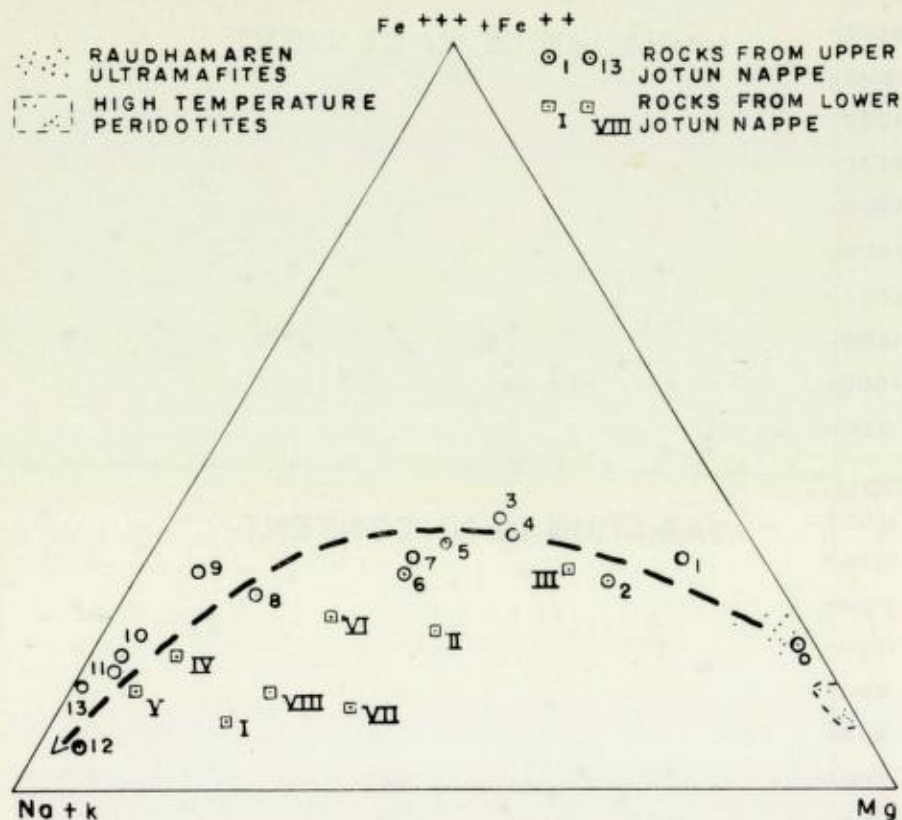


Fig. 6. Triangular diagram illustrating the differentiation trend of the Jotun Nappe rocks (data from Dietrichson 1958). The trend line is typical of the calc-alkaline series (Thayer 1967).

with distinct contacts due to gravity stratification. These, however, are not present in the ultramafites covered by the present study.

The spinel-lherzolite facies of the Jotunheimen ultramafites differs from Seiland subfacies of lower pressure conditions in containing no plagioclase and from Ariegite subfacies of higher pressure conditions in containing no garnet. Hence they define the restricted stability field of the spinel-peridotites formed under high temperature and moderately high pressure conditions (MacGregor 1967).

The origin of alpine ultramafite-gabbro association was explained by Thayer (1963) as due to gravity stratification of peridotite and gabbro in the upper mantle and their emplacement into shallower levels. Such a gravity-stratified intrusive hypothesis is difficult to reconcile with the origin and emplacement of the Jotunheimen ultramafites because undoubted gravity strata are not seen there. The Jotunheimen ultramafites rather occur as numerous xenoliths and podiform bodies of limited dimensions. Reaction and cumulate textures, cryptic layering, etc. characteristic of stratiform bodies are absent in this area.

High pressure ultramafic mineralogy has shown (Green & Ringwood 1967)

that plagioclase disappears between 13.5 and 15.7 kb pressure at 1200°C temperature, and that garnet will disappear from pyrolite composition at about 21 kb pressure around 1300°C temperature. In the light of these data the absence of plagioclase and garnet in the Jotunheimen ultramafites indicates load pressure between 13.5 and 21 kb at magmatic temperatures (1200° to 1300°C).

The origin of the calc-alkaline magma is uncertain (O'Hara 1968). Spinel peridotites have been correlated with the Upper Mantle composition (MacGregor 1967) and it is now believed that the low velocity zone of the Upper Mantle can cause basaltic magmatism by diapiric upwelling (Green 1970). Hence, the alpine peridotite-gabbro association appears to be due to the Upper Mantle evolution of basalts due to diapiric upwelling in orogenic zones and segregation of gabbro or basalt leaving residual peridotite. The anhydrous differentiation of ultramafites is complementary to the segregation of gabbro and basalt magma, the evolutionary trend of which possibly depends upon the level of partial fusion and the local composition of the mantle on fusion.

Acknowledgements. - I thank Professor K. S. Heier and all other members of Mineralogisk-Geologisk Museum, University of Oslo, for help and friendly guidance throughout the research. I. Bryhni and T. Torske assisted in abbreviating the original manuscript for publication.

I also thank the Norwegian Agency for International Development for awarding me a fellowship during 1970-1971 which made the research possible, and the Mineralogisk-Geologisk Museum for providing funds for field work.

REFERENCES

- Batthey, M. H. 1960: Observations on the peridotites and pyroxenites of the Jotunheimen complex in Norway. *XXI Int. Geol. Congr., part XIII*, 198-207.
- Batthey, M. H. 1965: Layered structures in rocks of Jotunheimen complex, Norway. *Min. Mag.* 34, 268, 35-51.
- Bjørlykke, K. O. 1905: Det centrale Norges fjeldbygning. *Norges geol. Unders.* 39, 595 pp.
- Carstens, C. W. 1918: Norske peridotiter II. *Norges geol. Unders.* 5, 43-73.
- Den Tex, E. 1969: Origin of ultramafic rocks, their tectonic setting and history. *Tectonophysics* 7, 457-488.
- Dietrichson, B. 1955: Spessartite and pseudotachylite on the thrusting zone of the upper Jotun eruptive nappe near Nautgardstind, East Jotunheimen. *Norges geol. Unders.* 191, 30-35.
- Dietrichson, B. 1958: Variation diagrams supporting the stratiform, magmatic origin of the Jotun eruptive nappes. *Norges geol. Unders.* 203, 5-34.
- Goldschmidt, V. M. 1916: Geologisch-petrographische Studien in Hochgebirge des südlichen Norwegens. IV. Übersicht der Eruptivgesteine im kaledonischen Gebirge zwischen Stavanger und Trondhjem. *Vitensk.selskapets Skrifter I. Matemat.-Naturv. Kl. Nr. 2*, 140 pp.
- Green, D. H. 1970: Peridotite-gabbro complexes as keys to petrology of mid-oceanic ridges: Discussion. *Geol. Soc. Am. Bull.* 81, 2161-2166.
- Green, D. H. & Ringwood, A. E. 1967: The stability of aluminous pyroxene peridotite and garnet peridotite and their relevance in upper mantle structure. *Earth Planet. Sci. Letters* 3, 151-160.
- Heier, K. S., Naterstad, J. & Bryhni, I. 1972: A Rb-Sr whole-rock isochron date from the Stavanger area, south Norway. *Norsk geol. Tidsskr.* 52, 377-383.

- Hess, H. H. 1938: A primary peridotite magma. *Am. Jour. Sci.* XXXV 209, 321-344.
- MacGregor, I. D. 1967: Mineralogy of modal mantle compositions. pp. 372-392 in Wyllie, P. J. (ed.) *Ultramafic and Related Rocks*. John Wiley & Sons, Inc., New York.
- Malakhov, I. A. 1964: Some problems in the nomenclature of Uralian ultrabasic rocks. *Int. Geol. Rev.* 6, 1413-1415.
- Münster, T. 1884: Dagbog fra reise i Jotunfjeldene juli 1882. *Nyt Mag. Naturvid.* 28, 194-214.
- O'Hara, M. J. 1968: The bearing of phase equilibria studies in synthetic and natural systems on the origin and evolution of basic and ultrabasic rocks. *Earth Sci. Rev.* 4, 69-133.
- Rekstad, J. 1904: Fra det nordøstlige af Jotunfjeldene. *Norges geol. Unders.* 37, No. 6, 24 pp.
- Rekstad, J. 1905: Fra indre Sogn. *Norges geol. Unders.* 43, No. 7, 53 pp.
- Thayer, T. P. 1963: The Cangon Mountain Complex, Oregon, and the alpine mafic magma stem. *U.S. Geol. Surv. Profess. Paper* 475C, C82-C85.
- Thayer, T. P. 1967: Chemical and structural relations of ultramafic and feldspathic rocks in alpine type intrusive complexes. pp. 227-238 in Wyllie, P. J. (ed.) *Ultramafic and Related Rocks*. John Wiley & Sons Inc., New York.
- Thornton, C. P. & Tuttle, O. F. 1960: Chemistry of igneous rocks. I. Differentiation Index. *Am. Jour. Sci.* 258, 664-684.

Permian Rocks and Faulting in Sandsv er at the Western Margin of the Oslo Region

ERIK ROHR-TORP

Rohr-Torp, E. 1973: Permian rocks and faulting in Sandsv er at the western margin of the Oslo region. *Norges geol. Unders.* 300, 53-71.

In the Sandsv er area, a Permian quartz conglomerate and great thicknesses of both the B₁-basalt and the rhomb porphyry RP₂ are found above the Ringerike sandstone and the underlying Cambro-Silurian sediments. The younger Permian supracrustal units are engulfed by larvikite and ekerite. The larvikite is intersected by aplite, a granitic rock possibly formed by assimilation of Ringerike sandstone by the larvikite magma.

The area is cut by a number of dip-slip faults, most of which are connected to the subsidence of the Oslo graben. The steep dip of the supracrustals towards the intrusives at the contact was caused by sinking of the supracrustals into the melt, while dip-slip faults parallel to the contact possibly were formed by a later pushing upwards of the half-consolidated magma.

E. Rohr-Torp, *Norges geologiske unders kelse, Oslo-kontoret, Eilert Sundtsgt. 32, Oslo 2, Norway*

Introduction

The area described is situated at the western margin of the Oslo region, just south of the town of Kongsberg, Southern Norway (Fig. 1). The north-western part of the area consists of Precambrian Telemark- and Kongsberg-Bamble rocks (not dealt with in this report). Permian intrusives (larvikite and ekerite) make up the southern and eastern parts of the area. A belt of Cambro-Silurian and Permian supracrustal rocks is preserved between the Precambrian gneisses and the Permian intrusives. The area is cut by a number of faults, ranging in age from Precambrian to late Permian.

As early as 1824, Naumann described a section through the Cambro-Silurian sediments southwards to the igneous rocks in the mountain Skrim. Dahll (1861), in a corresponding section, gives the sediments a synclinal structure between the Telemark rocks and the Permian intrusives.

In 1877 Corneliussen investigated the area dealt with in this text. A detailed map and description were published in 1880. The map clearly shows the geological main features. One marked fault is treated in detail.

Kjerulf (1879) gives two sections through the Cambro-Silurian sediments. Both seem to rest on observations made by Corneliussen. The geological quadrangle map Kongsberg was published in 1926 by Br gger & Schetelig. In spite of a more detailed stratigraphy within the Cambro-Silurian sediments, data concerning the area treated in this text seem to a large extent to rest on observations made by Corneliussen.

Strand's diary notes (1937) have been most useful during the present writer's fieldwork. St rmer (1953) describes the Middle Ordovician sediments

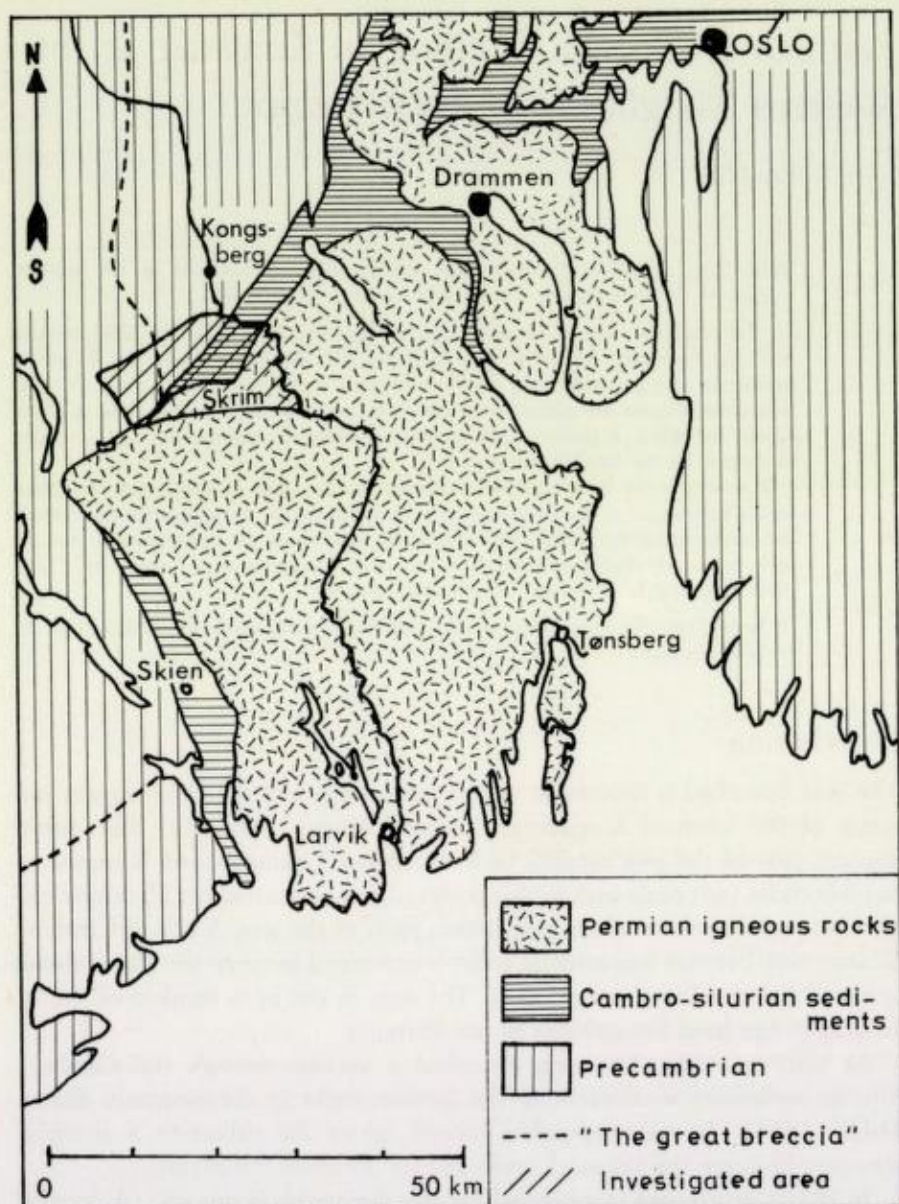


Fig. 1. The geographical and regional geological position of the investigated area.

from the Eiker-Sandsvær district. Heintz (1953) gives a detailed section from the Precambrian rocks in the north-west through the sediments to the larvikite in the mountain Evjuseterfjell. He has also made an unpublished excursion map of the area, which has been of great help to the present writer.

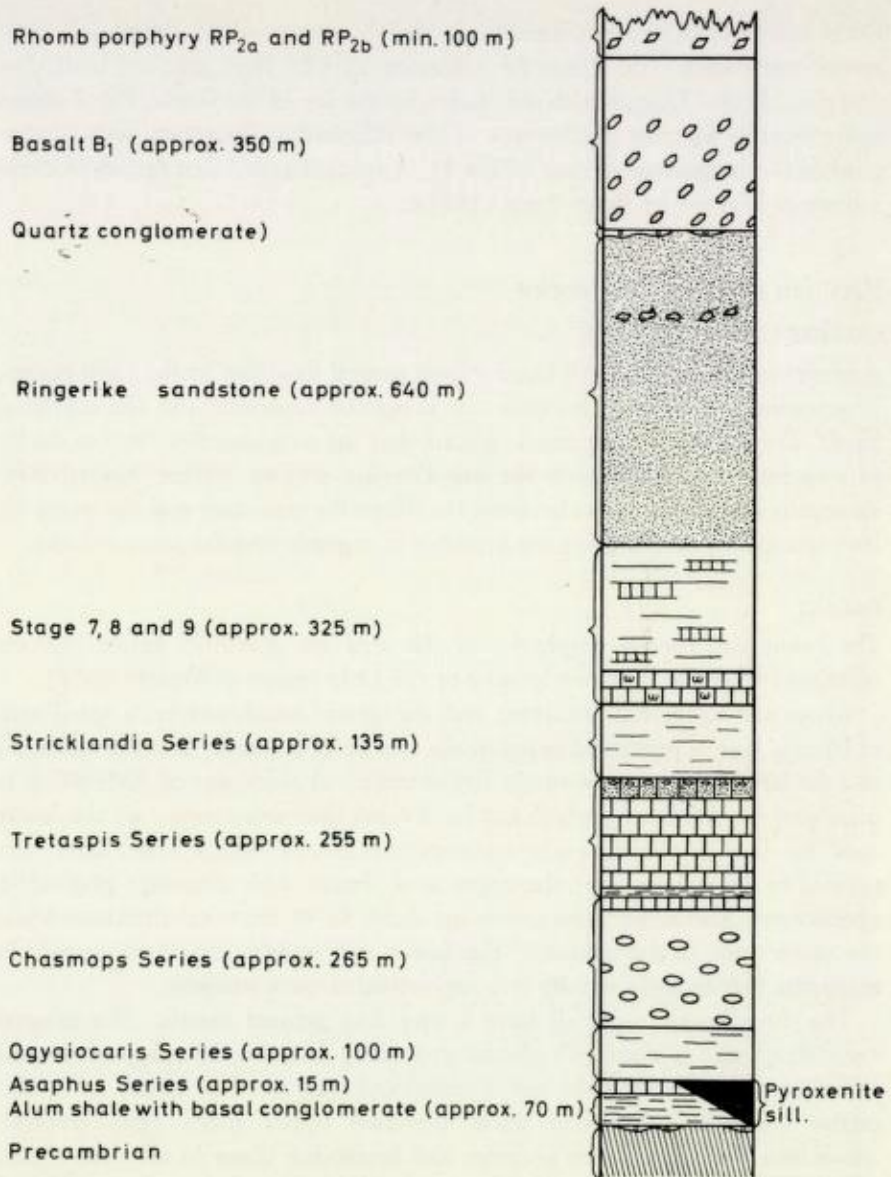


Fig. 2. The supracrustal rocks overlying the Precambrian in the investigated area.

Cambro-Silurian sedimentary rocks

The sediments of the described area rest with an angular unconformity upon the Precambrian gneisses. They have not been folded during the Caledonian orogeny. The dip is rather constant, $10-20^\circ$ towards the south-east (the same as the dip of the Precambrian peneplain). Only in the vicinity of the Permian intrusives does the dip rapidly increase towards the intrusions, as will be discussed later. Locally the Precambrian border is controlled by faults.

A basal conglomerate is overlain by Cambrian alum shales. The marine

Ordovician and Silurian sediments are mainly composed of alternating limestones and shales. The Ringerike sandstone of Old Red type, of Ludlovian and possibly also Downtonian age, makes up the top of the strata. Fig. 2 shows some features and the thicknesses of the different sedimentary units distinguished on the geological map (Plate I). A more detailed description of these sediments is given by Rohr-Torp (1971).

Permian supracrustal rocks

QUARTZ CONGLOMERATE

A quartz conglomerate, well known from several localities in the Oslo region, is occasionally developed between the Ringerike sandstone and the overlying basalt. The scattered occurrences indicate that the conglomerate (0–3 m thick) fills up small irregularities in the sub-Permian erosion surface. Several measurements along the contact between the Ringerike sandstone and the overlying lava (conglomerate) suggest the presence of a gentle angular unconformity.

BASALT

The basalt and rhomb porphyries of the area are described below and are correlated with the lava stratigraphy of the Oslo region (Oftedahl 1952).

Above the Ringerike sandstone and the quartz conglomerate, a small area of basaltic lava is preserved between the ekerite of the mountain Hovdebofjell and the larvikite of the mountain Evjuseterfjell. A thickness of 300–400 m is calculated for the basalt, which can be divided into three zones: a) the lower zone, basalt with abundant augite phenocrysts, b) the middle zone, more even grained to dense basalt, c) the upper zone, basalt with abundant plagioclase phenocrysts. The lower zone makes up about $\frac{2}{3}$ of the total thickness while the upper zone is the thinnest. The lower and middle zones are so rich in magnetite that in their vicinity it is impossible to use a compass.

The three basalt types all have a very fine grained matrix. The mineral associations are: titanomagnetite phenocrysts along with biotite, plagioclase, and titanomagnetite. Accessories are titanite and apatite. The lower zone also carries common hornblende while the two upper zones carry chlorite. Amygdules filled mainly by prehnite and heulandite occur in all three zones. The plagioclase phenocrysts of the upper zone have an An-content of 53 and are not markedly zoned. The minute plagioclase grains of the two lower zones have not been determined.

According to Oftedahl (1952) the B₁-basalt of the Vestfold area has the same subdivision into three zones as described above. In Vestfold, east of the described area, the maximum thickness of B₁ is 120–150 m, B₂ approx. 10 m, and B₃ approx. 40 m.

The three divisions of the present basalt, its great thickness and the fact that it is overlain by RP₂ show that it must represent the B₁-basalt, the lowermost lava formation of the Oslo area sequence.

The expected thickness of B₁ in the described area is a little more than 100 m

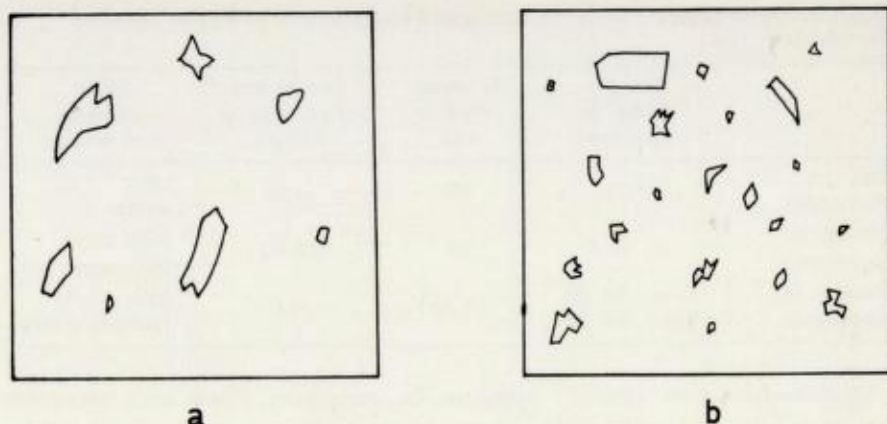


Fig. 3. a. Rhomb porphyry, lower part.
b. Rhomb porphyry, upper part. Natural size.

(Oftedahl 1952, p. 43). The calculated thickness of 300–400 m is not due to repetitions by faulting, and must be explained in another way. If the area described had represented a depression in the sub-Permian peneplain, one would have expected a greater thickness of Permian sediments below the lavas. The explanation must be that the area was situated in the vicinity of a volcanic vent (see p. 60).

RHOMB PORPHYRY

Above the basalt a small area of rhomb porphyry is preserved, dipping steeply towards the south-east. The thickness of the rhomb porphyry is at least 100 m. It can be divided into two zones (Fig. 3), both with fine-grained grey matrix. The lower zone carries a few small and a few medium grained pink plagioclase phenocrysts, making up approximately 10% of the rock volume. The upper zone carries more phenocrysts. They are nearly always small, often forming 'star-shaped' twins. The phenocrysts, which make up 10–20% of the rock volume, are pink or greyish white.

The phenocrysts of the lower zone are less than 1 cm across, usually rhomb-shaped and heavily altered. They are often broken apart and almost completely recrystallized into smaller plagioclase grains (An-30–31, low temperature), lath shaped along (010). The original plagioclase is not determinable. The matrix is composed of perthite, often mesoperthite, biotite, common hornblende, chlorite, apatite, titanite, white mica, and opacite. Grain size, 0.1–0.2 mm.

The upper zone often has a glomeroporphyritic texture. The phenocrysts are approx. 1.5 mm in size, often zoned (core: An-30, rim: An-25, high temperature). The matrix feldspar is not determinable. The other minerals are the same as for the lower zone, with a grain size of less than 0.1 mm.

Aggregates composed of biotite and hornblende with small amounts of apatite and opacite, which frequently occur in both zones, may represent either

Table 1. Rhomb porphyry from the investigated area compared to RP₂ as described by Oftedahl (1946)

	Comp. of plag. in phenocrysts	% pheno-crysts in rock	Size in mm of groundmass feldspar	Other minerals than feldspar
RP ₂ (Oftedahl)	An 20	10	0.02	chlo. quartz
Present RP lower part	An 30.5	10	0.1-0.2	chlo. amph. bio.opaque min.
Present RP upper part	Core: An 30 Rim: An 25	10-20	0.1	chlo. amph. bio.opaque min.

pseudomorphs after primary pyroxene or amygdules filled with secondary minerals, altered by the later contact metamorphism towards the larvikite. A complete lack of crystal outlines favours the latter hypothesis.

Mesoscopically the bottom of the present rhomb porphyry has the greatest resemblance to RP_{2a} and the top to RP_{2b} as compared to the different rhomb porphyries of the Oslo region.

Table 1 shows some features of the present rhomb porphyry compared to dates on RP₂ given by Oftedahl (1946).

Only RP₁-RP₃ and RP₉ have plagioclase phenocrysts in the range An 20-An 35, and except for RP₂ they all look quite different from the present rhomb porphyry (op. cit.).

Oftedahl (1946, Table 9) has not distinguished between RP_{2a} and RP_{2b}. The average of the phenocryst content from top and bottom of the present rhomb porphyry is close to 10%. Only RP₂, RP₁₀ and RP₁₂ have such a small amount of phenocrysts, whereas the others have 20% or more. RP₁₀ looks quite different from RP₂, and RP₁₂ has phenocrysts of An 45 composition.

The grain size of the matrix feldspar is quite different from the value given by Oftedahl, but as this value depends on local temperature conditions during the crystallisation process, it seems to be of little diagnostic value.

The differences between the other matrix minerals must be expected because of the later contact metamorphism of the present rhomb porphyry.

Except for RP_{17v}, which is quite different from the present rhomb porphyry, only RP₂ has a thickness greater than 100 m in Vestfold, east of the described area (Oftedahl 1952). Since the thickness of the present rhomb porphyry is at least 100 m, this argument also indicates that it represents RP₂.

In parts of Vestfold RP₁ is missing (Oftedahl 1952), giving the same picture as in the described area, where RP₂ lies directly above B₁.

Permian intrusive rocks

Larvikite and ekerite occupy the south-eastern and eastern part of the mapped area. As my investigations of these rocks brought little new, they are not treated in this text. Brøgger & Schetelig (1926) have mapped kjelsåsité east of the lake Ravalsjøen (G-13). In my cand. real. thesis I have shown that the

Table 2. Modal analyses of aplite

	8-19-A	11-A-2	11-A-3	11-A-13	J-27-2	J-27-3
Alkali feldspar	54.2	47.2	52.4	49.4	58.2	43.0
Quartz	25.6	28.1	18.2	31.4	18.8	24.4
Plagioclase	16.2	22.1	20.3	16.2	12.4	24.4
Biotite	x	2.4	3.5	2.2	2.4	3.2
Amphibole			4.4		2.4	0.2
Pyroxene	2.2					
Muscovite	x	x	x	x	0.2	0.4
Titanite	1.6	x	0.6	x	1.4	0.8
Zircon		x	x	x	0.2	0.2
Apatite		x			0.4	0.2
Allanite	x	x	x		x	x
Opaque minerals	0.2	0.2	0.6	0.8	3.6	3.2
Limonite				x		
Total	100.0	100.0	100.0	100.0	100.0	100.0
An cont. of plg.	30.0	28.0	28.5	29.0	30.0	28.0

area is composed of larvikite which is often hybrid in composition because of heavy assimilation of basalt.

APLITE

The larvikite massif is cut by a number of aplite dikes, the width of which varies from 1 to more than 100 m. The dikes always show sharp borders against the larvikite; they are cut by the younger ekerite. Chilled margins never occur, indicating that the larvikite was hot during intrusion of the aplite. Aplite is not separated from larvikite in Plate I.

The aplite is greyish- to brownish red, with a fine grained saccharoidal texture; 1-2 cm rhomb-shaped plagioclase phenocrysts, identical to the plagioclase of the larvikite, may occur.

Modal analyses of the aplite are given in Table 2. The composition is granitic (Streckeisen 1965). The An-content of the 'matrix plagioclase' is given at the bottom of the Table.

The alkali feldspar is an irregular patchy perthite, often 30 Ab, 70 Or, but variable within a single thin section. The amphibole is common hornblende and the pyroxene, which is often zoned, has core and rim composed of titanite. The opaque mineral is titanomagnetite while the titanite is often keilhauite (yttrotitanite).

The intimate connection in space and time and the occurrence of the same characteristic plagioclase phenocrysts in larvikite and aplite, make it unlikely that the aplite evolved from a magma independent of the larvikite magma. Three theories for the formation of the aplite are possible:

1. Anatexis of consolidated larvikite gave a granitic neosome. A squeezing upwards of the neosome gave rise to the aplite dikes, while the paleosome was left in the deeper regions of the larvikite intrusion.

2. The aplite magma was formed by a special differentiation of the larvikite magma. Primarily the differentiation is characterized by an increase in silica. Thus the aplite has nearly the same amount of quartz as has the ekerite of the described area (ca. 25%). Also, the alkali content of the magma is slightly increased by the differentiation. This is seen by a higher alkali feldspar/plagioclase ratio in the aplite than in the larvikite. In the described area this ratio is 2.6 for the aplite and 0.6 for the larvikite. The increase of alkalis is much less than in ekerite, where alkali pyroxene and alkali amphiboles occur.
3. The alteration of larvikite magma to aplite magma may be explained by assimilation of quartz-rich country rocks (Ringerike sandstone). This last theory is favoured by the author.

The described area is not unique in having the larvikite cut by a number of aplite dikes. The same feature is mentioned by Sæther (1962) from Nordmarka, north of Oslo.

DIKE ROCKS

The Cambro-Silurian as well as the Precambrian rocks are cut by a number of different dike rocks. They have not been more closely examined, except for one approx. 50 m thick metapyroxenite sill between D-13 and I-7.

Mesoscopically the dike rock is identical to the bottom of the B₁-basalt. It is so rich in titanomagnetite that it makes the use of a compass difficult. The titanomagite phenocrysts are nearly completely altered to a bluish green common hornblende containing rutile inclusions. The matrix is composed of calcite, titanite, titanomagnetite and apatite. Plagioclase is absent.

In mineral composition the sill corresponds to the pyroxenite from the central parts of the Vestby volcanic neck (Ramberg 1970).

A volcanic neck composed of Oslo essexite (Brøgger 1933) is situated at the lake Eiangsvann approx. 1 km south-west of the south-western corner of Plate I (A-14). The pyroxenite sill is possibly related to this neck.

The fact that the B₁-basalt is situated only some 15 km from a volcanic neck seems to be the explanation of the great thickness of this basalt in the described area.

Discussion of the increasing dip of the supracrustals towards the intrusive contacts

An increasing dip of the supracrustal rocks towards the intrusive contacts is well known from several localities in the Oslo region. A list of references is given by Oftedahl (1960).

In the Sandsvær area, the dip of the supracrustals is constant (10–20° south-east) from the Precambrian border and south-eastwards until approximately 1 km away from the intrusive contacts. Further on towards the contacts, the dip increases rapidly to 70–100° SE at the contact. The dip *does not* increase when crossing faults striking more or less parallel to the strike of the supracrustals

Table 3. Density of natural glasses compared to density of contact metamorphosed supracrustal rocks from the investigated area

Rock/glass	Density (g/cm ³)
Tretaspis Shale	2.79
Tretaspis Limestone	2.87
Calcareous sandstone	2.78
Stricklandia Shale	2.84
Pentamerus Limestone	2.77
Downtonian Sandstone	2.65
Augite porphyry (B ₁)	3.21
Rhomb porphyry (RP _{2b})	2.72
Rhyolite obsidian	2.37
Trachyte obsidian	2.45

(faults of group 3, see later), as described from the Skien-Langesund area (Brøgger 1883).

To maintain a constant thickness of the different supracrustal units towards the intrusives, where the dip is so rapidly increasing, the supracrustals have to be folded down towards the contacts by a flexure around axes approximately parallel to the contacts. The simplest explanation of such a flexure is a gravity sinking of the supracrustals into the melt.

In Table 3, the densities of contact metamorphosed supracrustals from the investigated area are compared to the densities of natural rock glasses. Rhyolite obsidian corresponds approximately to an ekeritic melt, trachyte obsidian to a lavikitic melt. (Values for the rock glasses are given by Daly 1966.)

The densities given in Table 3 are determined at room temperature, but as rocks and their glasses all have a coefficient of linear thermal expansion very close to 10^{-5} centigrade⁻¹ (Skinner 1966), the differences in density are also real at the actual intrusion temperature.

If the supracrustals are considered to have represented a comparatively thin cover above an overhead stoping intrusion, the differences in density between the rocks and the glasses are sufficient to allow a sinking of the supracrustals into the melts.

The increasing south-easterly dip of the supracrustals towards the intrusions can thus in a simple way be explained by the differences in density between the supracrustals and the melts. More complicated theories therefore seem unnecessary.

Faults

The area described is cut by a number of faults. They can be divided into three groups:

1. Those with fault planes striking close to north.
2. Those with fault planes striking north-east (or south-east), where the north-western (north-eastern) side is relatively lifted.
3. Those with fault planes striking north-east, where the south-eastern side is relatively lifted.

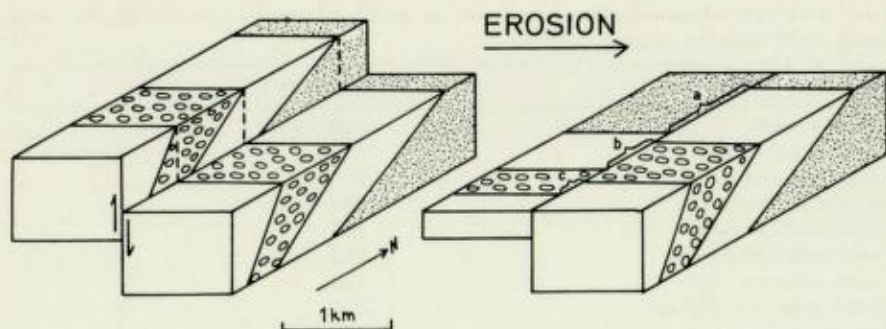


Fig. 4. Dip-slip fault crossing layered rocks with increasing dip towards the south. After erosion, note $a > b > c$.

FAULTS OF GROUP 1

The 'great breccia' in the Precambrian is described by Bugge (1928, 1936, 1937). It enters the described area from the north, south of the lake Kolsjø (E-5) and splits into several branches towards the south. Along two branches the Cambro-Silurian is disrupted.

Along the hill Kisgruveåsen (I-2) another breccia is described in the Precambrian by Bugge (1936). Later movements along this breccia have disrupted the Cambro-Silurian sediments to the south.

Less than 1 km east of the hill Kisgruveåsen is another, less prominent fault belonging to group 1.

These faults all form marked breccia zones in the Precambrian, while the younger sediments are sharply cut without brecciation.

Inside the Cambro-Silurian area the faults of group 1 are linear, independent of the topography, showing that they must have nearly vertical fault planes. The linear trace also shows that the faults must be younger than the down-bending of the sediments towards the intrusions (p. 61). If the age relation were the opposite, the steeply dipping north striking fault planes would have curved traces on the map after having been bent along with the sediments around north-easterly directed fold axes.

The picture along the faults of group 1 may have been formed in two ways or a combination of both: 1. The western side is horizontally dislocated towards the south relative to the eastern side. 2. The western side is vertically lifted relative to the eastern side. Constant dip when crossing a fault shows that no rotation has taken place. From the map it is seen that the dislocation of rock-borders along the faults decreases towards the south. This decreasing dislocation as the dip increases towards the intrusions, indicates that the western block is vertically lifted relative to the eastern block. If the movement along one fault had been horizontal and constant, the dislocation of rock borders along this fault should also have been constant.

Fig. 4 shows to the left a block where the western part is vertically lifted. By erosion of the two sides down to the same level (right hand side of the

Table 4. Calculated dip-slip by the faults of group 1

Dislocated border	W. branch of 'great breccia'	E. branch of 'great breccia'	Fault S. of Kis- gruveåsen	Fault W. of Mugge- rud
Precambrian - alum shale			105 m	40 m
Top of alum shale	75 m	160 m	95 "	30 "
Top of Ogygiocaris Series	75 "	165 "	100 "	
Top of Chasmops Series	70 "	175 "	100 "	
Top of Tretaspis Series			105 "	
Average dip-slip (approx.)	75 m	165 m	100 m	

Figure), the same picture will arise as is shown on the geological map along faults of group 1. Note: $a > b > c$.

In Table 4. is shown the dip-slip calculated at different rock borders dislocated by faults of group 1. Except for the eastern fault which 'dies' towards the south, the figures are quite constant along each individual fault. This also indicates that the group 1 faults are formed by a vertical relative dislocation of the western block.

One can see from Plate I (I-6, J-6) that a certain horizontal drag has taken place along the fault by the hill Kisgruveåsen. However, the constant dip-slip along this fault shows that any horizontal displacement must have been negligible. The drag may have been caused by horizontal forces acting along the old breccia zone at an early stage, giving a plastic deformation without disrapture of the overlying sediments.

The limestone enclosed in the larvikite (G-10) appears to have been dislocated by the western branch of the 'great breccia'. In that case, the dislocation of the limestone is the opposite of the dislocation of the sediments further towards the north (see Plate I). As a constant dip on either side of the fault shows that no rotation has taken place, the two limestone bands rather seem to represent two stratigraphically different limestones. This is supported by the fact that the limestone east of the fault has twice the thickness of the limestone west of the fault.

Faults of group 1 may also have been active at an early stage. A lifting above sea level of the western side of the 'great breccia' (same relative displacement as the later described movements), before or contemporaneously with the deposition of the alum shales, can explain the stratigraphic wedging out of the alum shales west of this fault.

Corresponding movements along the fault south of the hill Kisgruveåsen before or contemporaneously with the deposition of the Orthoceras Limestone (also here the same relative displacement as the later observed movements) can explain the stratigraphic wedging out of the Orthoceras Limestone west of this fault. If the theory is valid, the Orthoceras Limestone has to be a shallow water deposit as the vertical displacement which gave dry land in the west has to be small. If the displacement had not been small, it would have manifested itself in Table 4, by somewhat higher values for the dip-slips below the

Orthoceras Limestone than for the higher units which were not yet deposited at the time of this movement.

The conclusion is that within the Cambro-Silurian area the faults of group 1 are dip-slip faults on which the western side is relatively lifted. The latest movements are younger than the downfolding of the sediments towards the intrusions (see p. 61). The group 1 faults are mainly reactivated Precambrian fault zones.

FAULTS OF GROUP 2

Only two faults belong to this group. One is seen in Plate I between (M-2) and (L-3). The area has a thick drift cover so that the downfaulted south-eastern side is exposed only in the river Dalselv, which runs in a 30-40 m deep canyon composed of alum shales down to the bottom. Little is known about this fault. It is younger than the heavily tectonized alum shales. A determination of the relative vertical displacement is impossible as the alum shales are eroded away on the up-faulted side, but it must be more than approx. 40 m. From the topography the strike of the fault plane is calculated to approx. N-50°, and the dip is unknown.

The other fault belonging to group 2 is seen in the river Dalselv (K-4) where the fault plane makes a sharp bend of almost 100°. South-westwards and south-eastwards from this bend there is no continuation into the alum shales of the fault. The alum shales are markedly dragfolded, showing that the fault is younger than the deposition of the alum shale. Because of the sharp bend, this fault must be a dip-slip fault. In the river Dalselv the fault plane is seen to dip almost vertically. For the same reason as for the other fault of this group, only a minimum value of 25-30 m is calculated for the dip-slip.

FAULTS OF GROUP 3

One fault belonging to this group has been traced from Sørby (O-2) to Trengen (M-5). South-west of Trengen it continues as a joint-zone with no dislocation. The fault possibly splits into two branches south-west of Dalen (M-4) and one branch follows a marked depression between Dalen and Skumtjern (L-5).

Another fault of group 3 is traced from Lintveit (P-3) along Rosstjerdalen to Store Lauvarvann (M-6), where it splits into three branches as seen between the two lakes (L-7). A more detailed map of this area is shown in Fig. 5. South-westwards from Lille Lauvarvann (K-8) only the two south-eastern faults can be traced. The north-western one continues as a joint-zone with no perceptible dislocation.

A generalized map along faults of group 3 is shown in Fig. 6. At a glimpse the relative movements seem to be horizontal with the south-eastern side dislocated towards the south-west. It is, however, shown by slickensides that vertical movements also have taken place. Actually there are more arguments against the faults of group 3 being strike-slip faults:

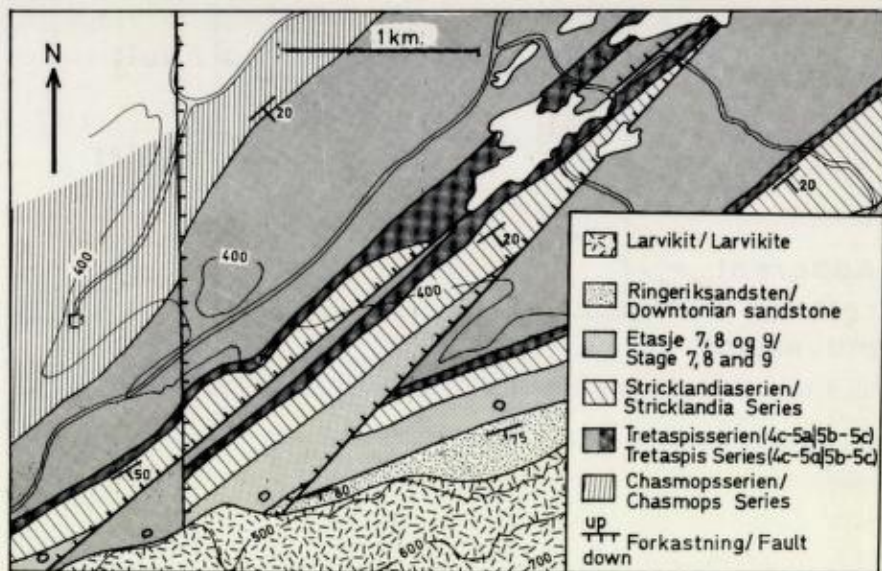


Fig. 5. Detailed map of the area south-west of the lake Store Lauvarvann.

1. Between P-3 and M-6, the strike of the fault plane makes a bend of some 10° (not clearly seen from the map). By horizontal movements, the rocks along the fault in this area should have been brecciated, not undeformed as they are.
2. The bedding dip changes from the usual $10-20^{\circ}$ SE to almost horizontal near the faults of group 3. This effect on the bedding must have been caused by vertical drag along the fault planes by a relative lifting of the south-eastern side.

If the bedding, as in the described area, is dipping south-east, the dislocations shown on the generalized map (Fig. 6), will also develop if the south-eastern side of the fault is relatively lifted vertically. This is illustrated in Fig. 7.

By accepting the group 3 faults to be dip-slip faults, the above described dislocations of the borders near the intrusive contact, show that these faults are younger than the flexure towards the intrusions, which gave the supracrustals their increasing south-easterly dip.

This age relation can also be shown in another way. The fault north-east of Store Lauvarvann in the area O-3, as seen from aerial photographs, passes linearly through a canyon and a marked ridge. The terrain is here elevated some 50 m per 200 m. In this area, outside the flexure towards the contacts, the fault plane thus must be quite steep. (A dip of 70° would give a deflection of some 6° .)

If the faults of group 3 had been older than the downbending of the supracrustals towards the contacts, the fault planes near the intrusions would have been folded along with the supracrustals. The result would have been that for the last kilometre towards the contact, where the dip of the bedding changes

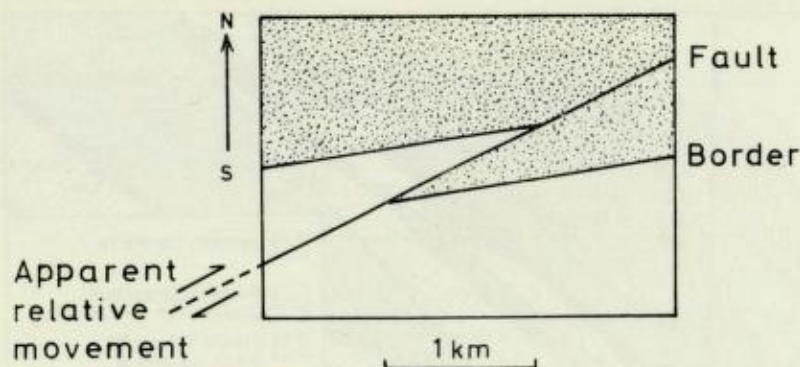


Fig. 6. Generalized map along faults of group 3.

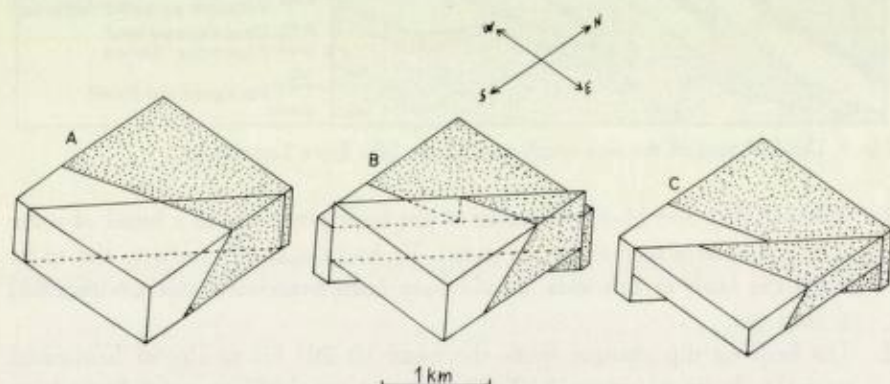


Fig. 7. Disrupture of a border by a vertical dip-slip fault.

- A. Before faulting, the fault plane and a border are seen.
- B. The south-eastern block is lifted relatively.
- C. After erosion. The map is similar to that in Fig. 6.

from approximately 15° SE to 80° SE, the dip of the fault planes would have changed from nearly vertical (as by O-3) to some 35° NW at the contact.

South-westwards from the lakes Store- and Lille Lauvarvann, however, the two faults of this group continue linearly to the contact, although the terrain is elevated some 100 m per kilometre along the faults. This shows that the faults must be *younger* than the downbending of the supracrustals, as the fault planes are nearly vertical all the way to the contact.

The conclusion is that the faults of group 3 are almost vertical dip-slip faults on which the south-eastern side is relatively lifted. The faults are younger than the downbending of the supracrustals towards the intrusive contacts. The total displacement along the subparallel group 3 faults is estimated to some 400 m throughout the faulted area.

AGE RELATIONS BETWEEN FAULTS OF GROUPS 1 AND 3

The formation of group 3 faults and the latest movements along group 1 faults took place after the downbending of the supracrustals towards the intrusives.

The age relations between the two groups of faults are difficult to solve, since both groups, inside the Cambro-Silurian area, are dip-slip faults with almost vertical dipping fault planes.

However, marked valleys along swarms of aplite dykes continue southwards into the larvikite along the extension of faults of group 1. This indicates that the latest movements took place after the larvikite was to a large extent consolidated. The somewhat younger aplite (see p. 59), found its way along the weak zones represented by the faults in the larvikite. Accordingly the aplite is not brecciated or mylonitized along the fault lines.

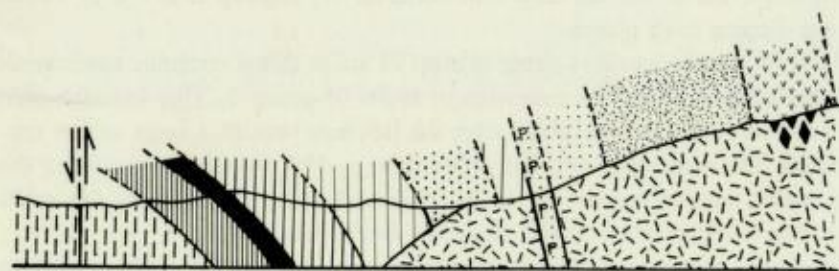
The faults of group 3 cannot be traced into the larvikite. This could be explained by the larvikite at this stage still being a melt. However, the faults are younger than the downfolding of the supracrustals, which most probably took place after the intrusion of larvikite, while it was still a melt (see below). My opinion is that the faults of group 3 were formed after the larvikite was partly consolidated, so that the supracrustals were no longer sinking into it. At this stage the core of the intrusion was still a melt, able to merge along weak zones in the outer shell, thus 'healing' the faults and blotting out the traces of them. If this is the case, the faults of group 3 must be somewhat older than the latest movement along faults of group 1.

TECTONIC HISTORY

1. Precambrian: Large movements along the 'great breccia' (E-5) and the breccia along the hill Kisgruveåsen (J-2); possible movements also along the fault by Heistadmoen (M-2).
2. Before or contemporaneously with deposition of the alum shales: possible minor relative lifting of the western block along the 'great breccia'.
3. Before or contemporaneously with deposition of the Orthoceras Limestone: possible minor relative lifting of the western block along the fault by the hill Kisgruveåsen.
4. After deposition of the alum shales: formation of the fault in the river Dalselv (K-4) by a relative sinking of the south-eastern block. Movements also along the fault by Heistadmoen (M-2). Both faults belong to group 2.
5. After deposition of the Asaphus Series: formation of the fault (group 1) west of Muggerud (J-5), probably by a relative lifting of the western block.
6. Contemporaneously with the intrusion of larvikite: downfolding of the supracrustals into the melt.
7. After intrusion of the larvikite, before complete consolidation: formation of faults of group 3 by a relative lifting of the south-eastern blocks.
8. Larvikite just consolidated, before or contemporaneously with intrusion of aplite: new relative lifting of the western blocks along the 'great breccia' and the fault by the hill Kisgruveåsen. The less prominent group 1 fault west of Muggerud was possibly formed at this stage.

(G-9)

(H-11)



◆◆ Basalt-xenolither
(Basalt-xenolithes)

⦿⦿ Pentameruskalk
(Pentamerus Limestone)

1 km

Fig. 8. Section from the Precambrian rocks in the north-west (G-9) to the mountain Skrimtoppen (H-11). Legend is given on the geological map (Plate I).

ORIGIN OF THE FAULTS, DISCUSSION OF THE BORDER RELATIONS TOWARDS THE INTRUSIONS

All the faults described, except those of group 3, have in post-Cambrian time caused a relative sinking of the land mass east and south-east of the faults. Together they may represent a system of faults, activated at different times, connected to the downfaulting of the Oslo Graben. If the latest movements along the 'great breccia' and the fault along the hill Kisgruveåsen are parts of the Oslo region subsidence, this subsidence must have lasted until after the intrusion of larvikite.

The faults of group 3, which have caused a relative lifting of the south-eastern land mass, must be explained in another way. In the area described these faults are considered younger than the downfolding of the supracrustals towards the intrusions.

The same general picture is seen at different places in the Oslo region near the big intrusions; only the age relations between downfolding and upfaulting towards the intrusions are not yet straightened out.

Some mechanisms which might have given these border relations are discussed below.

- 1) In the area described the downfolding of the supracrustals may have been connected to the intrusion of larvikite, while the upfaulting towards the intrusions could have been a result of the later intrusion of more viscous ekerite (see Plate I). This theory, however, does not seem valid, as elsewhere in the Oslo region similar border relations exist towards only one intrusive body.
- 2) The intrusive contact may represent an old fault zone, along which the south-eastern land mass has sunk, either as part of the Oslo region

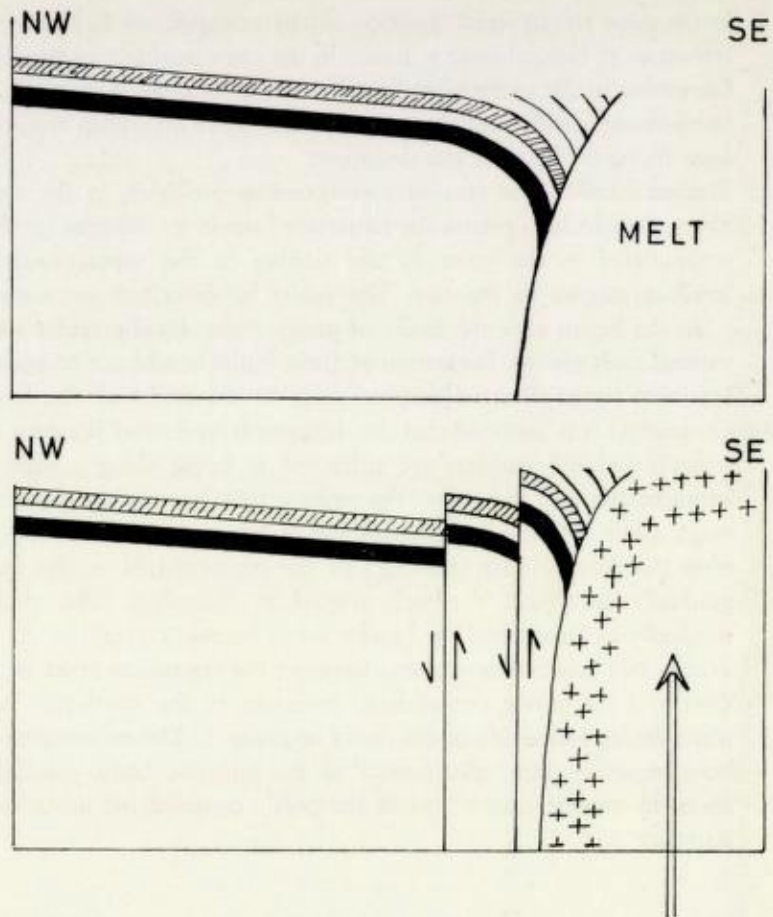


Fig. 9. Top: The supracrustals are sinking into the hot magma because of their higher density.

Bottom: A late upward movement of the partly crystallized magma leads to formation of the faults of group 3.

subsidence, or as a cauldron subsidence. The steep dip of the supracrustals towards the contact is caused by a drag along the old fault plane. Later the intrusives have forced their way up to their present position during formation of the group 3 faults.

A couple of hundred metres north-west of the mountain Skrimtoppen (H-11), huge xenoliths of augite porphyry are found within the larvikite. At the summer farm Grønnliseter (H-10) a limestone bed, approx. 50 m thick, is enclosed in the larvikite. In Fig. 8 is shown a section from the Precambrian border (G-9), through the limestone at Grønnliseter and further towards the south-east through the basalt xenoliths to the mountain Skrimtoppen. The bedded sequence is extrapolated south-eastwards from the contact. The different sedimentary units are drawn with correct thicknesses and the same steep dip as measured by the contact.

As seen from the section, the augite porphyry-xenoliths are found exactly

in the same stratigraphic position as the extrapolated B₁-basalt, while the limestone at Grønnliseter is found in the same position as the Pentamerus Limestone in the extrapolated section. With an older down-faulting of the south-eastern land mass along the contact, these inclusions would not have been found in the positions described.

- 3) Brøgger (1883) has treated corresponding problems in the Langesund-Skien area. In his opinion the faults are formed to compensate the tension accumulated in the crust by the sinking of the supracrustals into the larvikite magma in the east. The faults he described are normal faults.

In the Skrim area the faults of group 3 are dip-slip faults with almost vertical fault planes. Formation of these faults would not compensate such tensional forces directed perpendicular to the strike of the fault planes.

- 4) On page 61 it is assumed that the differences in density between the supracrustals and the magmas are sufficient to bring along a sinking of the supracrustals into the melts. The sinking must have taken place at an early stage, while the melt was still hot and of low viscosity (Fig. 9, top). Later, after the downfolding (sinking) of the supracrustals, as the temperature gradually decreased, the melt started to crystallize. The viscosity was markedly increased and the border zones became crystalline. At this stage (see p. 67) relative movements between the crystalline crust in the north-west and the partly consolidated intrusion in the south-east have taken place during formation of the faults of group 3. The movements may have been caused by late 'adjustments' of the intrusive body, possibly brought about by vapour activity inside the partly consolidated intrusion (Fig. 9, bottom).

Acknowledgements. - This paper is a revised part of the thesis submitted for my cand.real. examination in 1969, University of Oslo. The work was completed under the supervision of Professor T. Strand and Førstekonservator J. A. Dons, to whom I am indebted. I also wish to thank Amanuensis J. Naterstad, Professor I. Th. Rosenqvist and Professor A. Heinz for valuable discussions and advice; and Dr. W. L. Griffin for critically reading the manuscript and correcting the English.

REFERENCES

- Brøgger, W. C. 1883: Spaltenverwerfungen in der Gegend Langesund-Skien. *Nyt Mag. f. Naturv.* 28, 253-419.
- Brøgger, W. C. 1933: Essexitrekkens erupsjoner. Den eldste vulkanske virksomhet i Oslo feltet. *Norges geol. Unders.* 138, 103 pp.
- Brøgger, W. C. & Schetelig, J. 1926: Geologisk kart Kongsberg, 1:100 000. *Norges geol. Unders.*
- Bugge, A. 1928: En forkastning i det syd-norske grunnfjell. *Norges geol. Unders.* 130, 124 pp.
- Bugge, A. 1936: Kongsberg-Bambleformasjonen. *Norges geol. Unders.* 146, 117 pp.
- Bugge, A. 1937: Flesberg og Eiker, beskrivelse til de geologiske karter F. 35 Ø og F. 35 V. *Norges geol. Unders.* 143, 118 pp.
- Corneliussen, O. A. 1880: Dislokationslinjen ved Skrim i Hedenstad annex. *Nyt Mag. f. Naturv.* 25, 1-11.
- Dahll, T. 1861: Om Tellemarkens Geologi. *Nyt Mag. f. Naturv.* 11, 137-172.

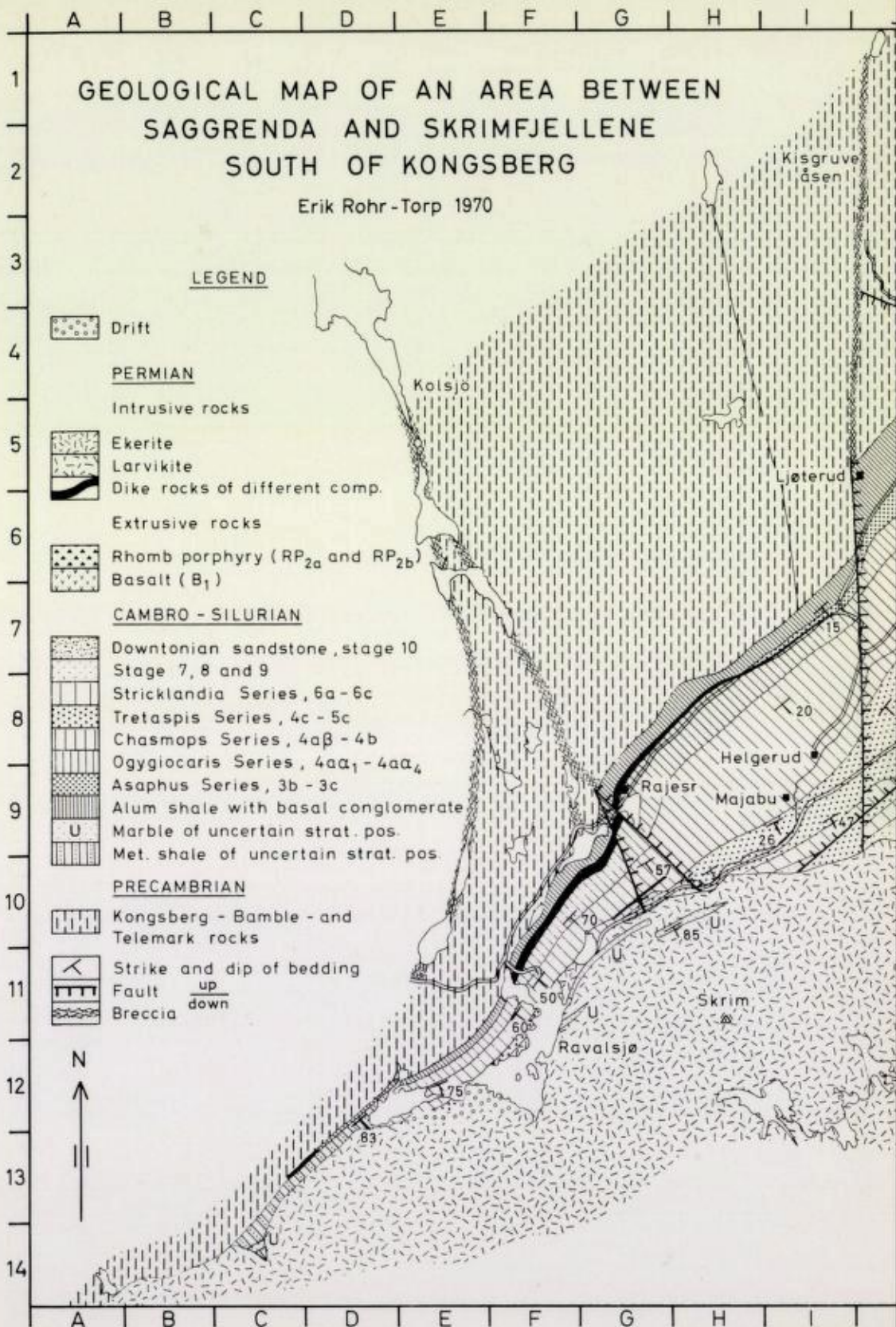
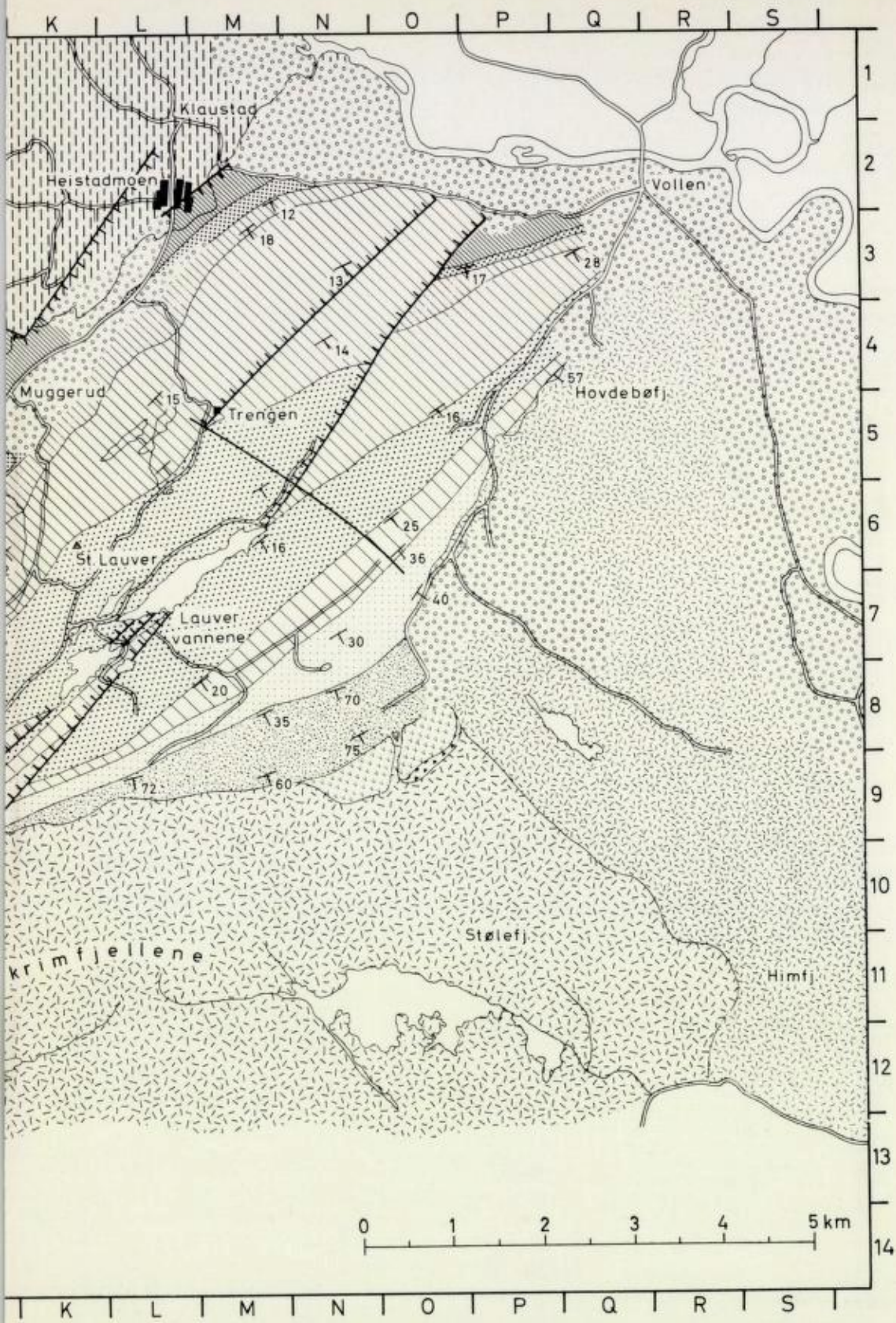


Plate I. Geological map of an area b



en Sagrenda and Skrimfjellene.

- Daly, R. A. 1966: Average densities of natural glasses, Table 4-2, p. 20 in Clark, S. P. (ed.) *Handbook of Physical Constants. Rev. Ed., Geol. Soc. America Mem. 97*, 587 pp.
- Heintz, A. 1953: Fig. 233, p. 526 in Høltedahl, O. (ed.) *Norges Geologi. Bd. 1. Norges geol. Unders. 164*, 583 pp.
- Heintz, A.: *Geologisk kart over øvre Sandsvær*. Unpubl. excursion map. Univ. of Oslo.
- Kjerulf, T. 1879: *Udsikt over det sydlige Norges geologi*. Fabritius, Christiania (Oslo), 262 pp.
- Naumann, C. F. 1824: *Beyträge zur Kenntnis Norwegen's. Erster Teil*. Leipzig. 263 pp.
- Oftedahl, C. 1946: Studies on the Igneous Rock Complex of the Oslo Region. VI. On akerites, felsites and rhomb porphyries. *Skr. Norske Vidensk.-Akad. i Oslo. Mat.-Naturv. Kl. 1946, No. 1*, 51 pp.
- Oftedahl, C. 1952: Studies on the Igneous Rock Complex of the Oslo Region. XII. The lavas. *Skr. Norske Vidensk.-Akad. i Oslo, Mat.-naturv. Kl. 1952, No. 3*, 108 pp.
- Oftedahl, C. 1960: Permian rocks and structures of the Oslo region, in Høltedahl, O. (ed.) *Geology of Norway. Norges geol. Unders. 208*, 298-343.
- Ramberg, I. B. 1970: Vulkanpluggene ved Vestby. *Nytt fra Oslofeltgruppen*, 1970, No. 1, 26-40.
- Rohr-Torp, E. 1971: Oversikt over den kambro-siluriske lagrekke nord for Skrim i Sandsvær. *Nytt fra Oslofeltgruppen*, 1971, No. 1, 14-25.
- Sæther, E. 1962: Studies on the Igneous Rock Complex of the Oslo Region. XVIII. General investigation of the igneous rocks in the area north of Oslo. *Skr. Norske Vidensk.-Akad. i Oslo. Mat.-naturv. Kl. Ny ser., No. 1*, 184 pp.
- Skinner, B. J. 1966: Thermal expansion of rocks, Tables 6-10, and thermal expansions of a few commercial glasses, Tables 6-11, pp. 94-95 in Clark, S. P. (ed.) *Handbook of Physical Constants. Rev. Ed., Geol. Soc. America Mem. 97*, 587 pp.
- Stormer, L. 1953: The middle Ordovician of the Oslo Region, Norway. I. Introduction to stratigraphy. *Norsk geol. Tidsskr. 31*, 37-141.
- Strand, T. 1937: Reiser på gradteigsbladet E 31 aust Slidre og på rektangelbladet 14 A Kongsberg (kambro-silur). Unpubl. diary notes.
- Streckeisen, A. 1965: Die Klassifikation der Eruptivgesteine. *Geol. R.schau 55*, 478-491.

Structural Interpretation of a Double-folded Gneiss-amphibolite Sequence, Bunnefjorden, Akershus

OLE GRAVERSEN

Graversen, O. 1973: Structural interpretation of a double-folded gneiss-amphibolite sequence, Bunnefjorden, Akershus. *Norges geol. Unders.* 300, 73-82.

Garnet amphibolite bands folded together with gneiss lamellae in tight to isoclinal folds are described. A structural analysis shows that the folds were formed during two separate deformation episodes. This conclusion has in particular a bearing on the problem of distinguishing between primary intrusive structures and simple and multiple fold-structures.

O. Graversen, *Institut for almen Geologi, Københavns Universitet, Østervoldgade 5-7, DK-1350 København K, Danmark*

Introduction

The structures under consideration occur in an area within the Precambrian basement of south-eastern Norway situated around the southern part of Bunnefjorden, 25 km south of Oslo (Fig. 1). Amphibolite facies paragneisses underlie most of the area; the dominant rock type is a rather heterogeneous granitic augen-gneiss. The megascopic structure is outlined by 100-200 m thick horizons of fine-grained two-mica gneisses (Fig. 1).

The bedrock of the area is often hidden by Quaternary deposits and only very seldom are there continuous exposures. It has therefore been of the utmost importance to the study of the mesoscopic structures, which are usually outlined by the numerous amphibolite horizons in the gneisses, that continuous exposures have been created during the enlargement of highway E 6, which crosses the area.

When amphibolite bands of intrusive origin are used in structural interpretation, one must distinguish between structures of primary origin and structures which have been generated during a later deformation. Further complications arise if the gneisses have been through several episodes of deformation, or if several generations of intrusive basic rocks occur. These problems will be treated in the following detailed analysis of a gneiss-amphibolite sequence exposed in a road-section along E 6. Some of the problems have already been briefly discussed by Graversen & Hageskov (1971).

Description of the road-section

Along the eastern side of E 6 several hundred metres of road-sections have been surveyed at the scale 1:100. The section which has turned out to be the most valuable is shown in Plate 1, and the location is given on the map in

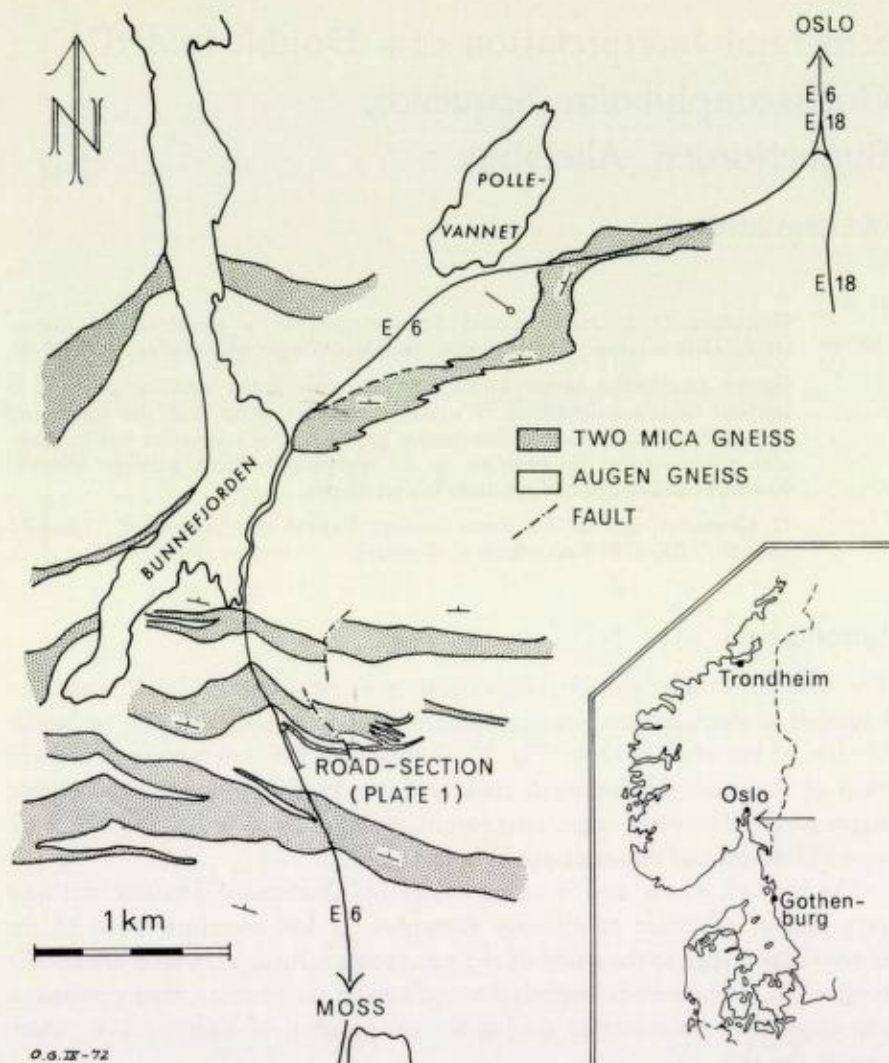


Fig. 1. Geological map (with inset location map) showing the position of the road-section shown in Plate 1. Compiled from field maps by O. Graversen, J. Thygesen and C. Zetterstrom.

Fig. 1. The section surface is nearly vertical over long distances and the height varies from 10 m to about 25 m. The dominant rock type is the augen gneiss; in places it shows migmatitic veins, but in other areas the veins have been broken apart and augen are formed. The augen may have ellipsoidal form and a linear orientation, but it has not yet proved possible to carry out a meaningful strain analysis on the gneiss. However, the gneiss gives the impression of having undergone a very strong compression (Fig. 2). The general structure is indicated by concordant garnet amphibolite sheets of intrusive origin whose thickness varies from about 10 cm to 1 m. (The intrusive origin of the amphibolite has been demonstrated in gneisses from other parts of the area

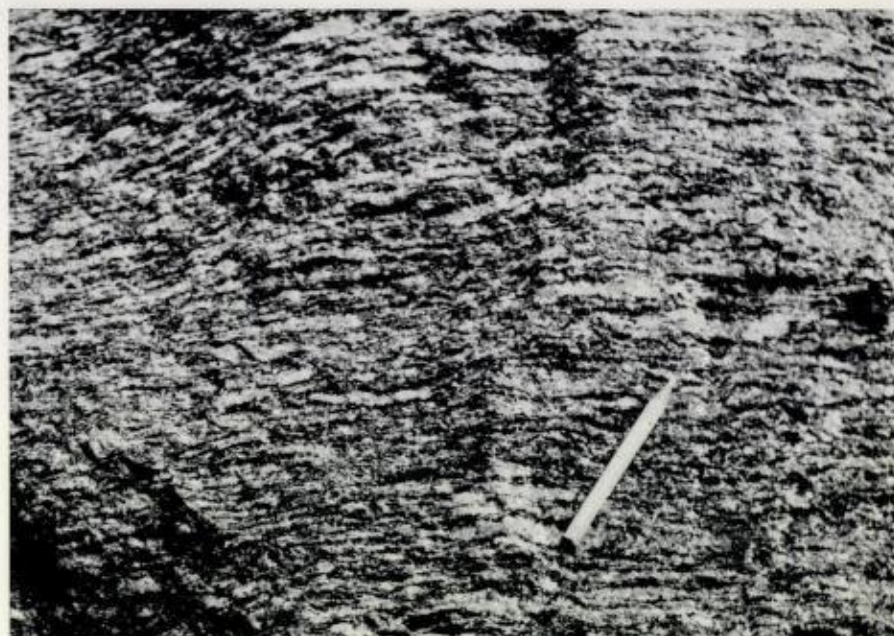


Fig. 2. Augen gneiss from the central part of the road-section shown in Plate 1.

which can be correlated with the rock sequence described in this paper.) This sequence is cut by discordant pegmatites deriving from the Bohuslän-Iddefjord granite, and by Permian dolerites. As can be seen from the section in Plate 1, the folded structure has not been disturbed by the cross-cutting dykes.

The garnet amphibolite sheets are folded in tight to isoclinal folds. At two places, central gneiss lamellae can be seen in amphibolite; both the amphibolite and the gneiss lamellae have been folded around a NW-plunging axis. One example of this is seen at the northernmost end of the section shown in Plate 1 and in Fig. 6, and the other is shown in the photo Fig. 3a, which was taken 110 m SSE of the section shown in Plate 1. One of the problems that will be treated in the analysis is whether these gneiss lamellae are remnants of screens in intrusive amphibolites, or whether they represent the cores of folds belonging to a fold episode older than the NW folding.

Much of the steep section is only accessible with difficulty, and it is not always possible to carry out accurate measurements. Where it has been possible to measure the fold axes, they always plunge to the NW, a direction that is also known from the regional mapping. Where observed, the NW axes always make a distinct angle with the section surface, because of the orientation of the road-section ($N 20^{\circ} W$). On the flanks of the NW folds, the foliation is deformed around fold axes that trend almost parallel to the section surface – so, obviously, two axial directions are present.

Between the isoclinally folded amphibolites there occur amphibolite sheets which do not show a folded structure in the exposed part of the section, but nevertheless show concordant contacts against the gneiss (see for example

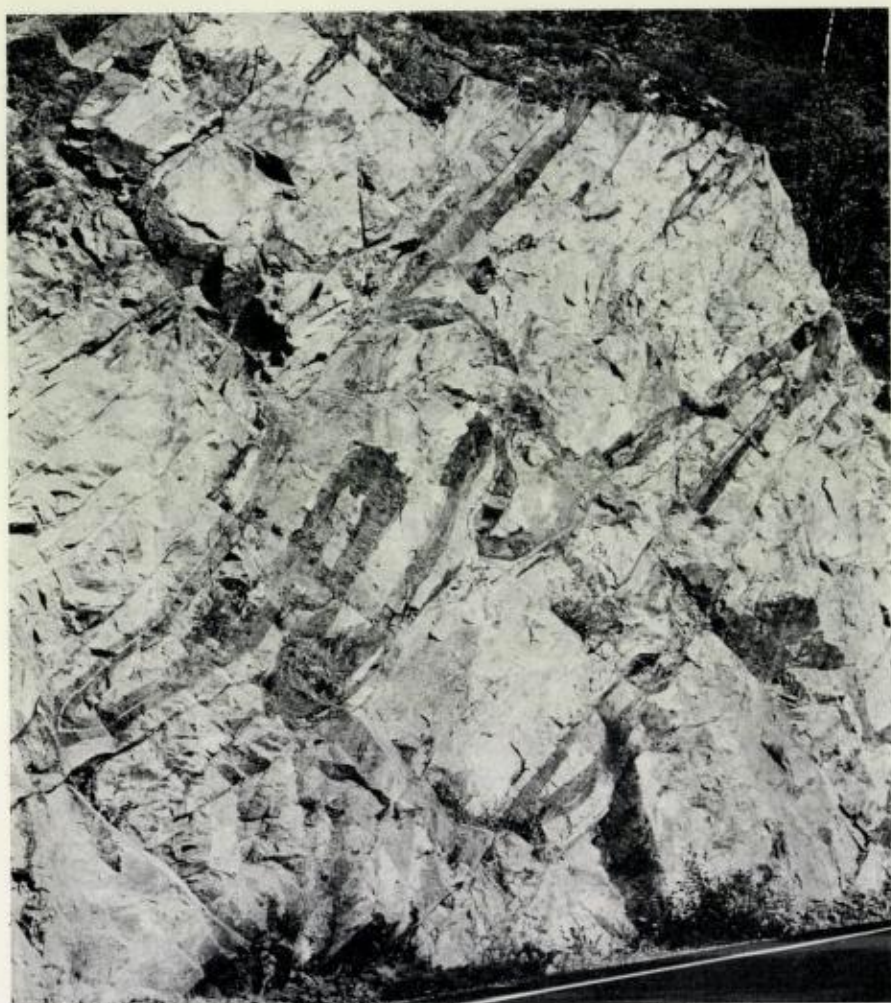


Fig. 3 a and b. Garnet amphibolite with central gneiss lamellae folded in tight to isoclinal NW plunging folds. (Photo along east side of E 6, 110 m SSE of the section in Plate 1).

Plate 1, 40–50 m, and in the southern part of the section). The question arises whether these seemingly unfolded amphibolites belong to the same generation as the remainder of the amphibolites, or whether they are sills belonging to an intrusive phase later than the NW folding. In order to clarify these and the questions mentioned above a more detailed structural analysis will now be given.

Structural analysis

During the analysis of the main structure the author used the 'paper and scissors method', which involves reproducing the structure in a model in which sheets of paper represent the marker layers, trimming these with scissors

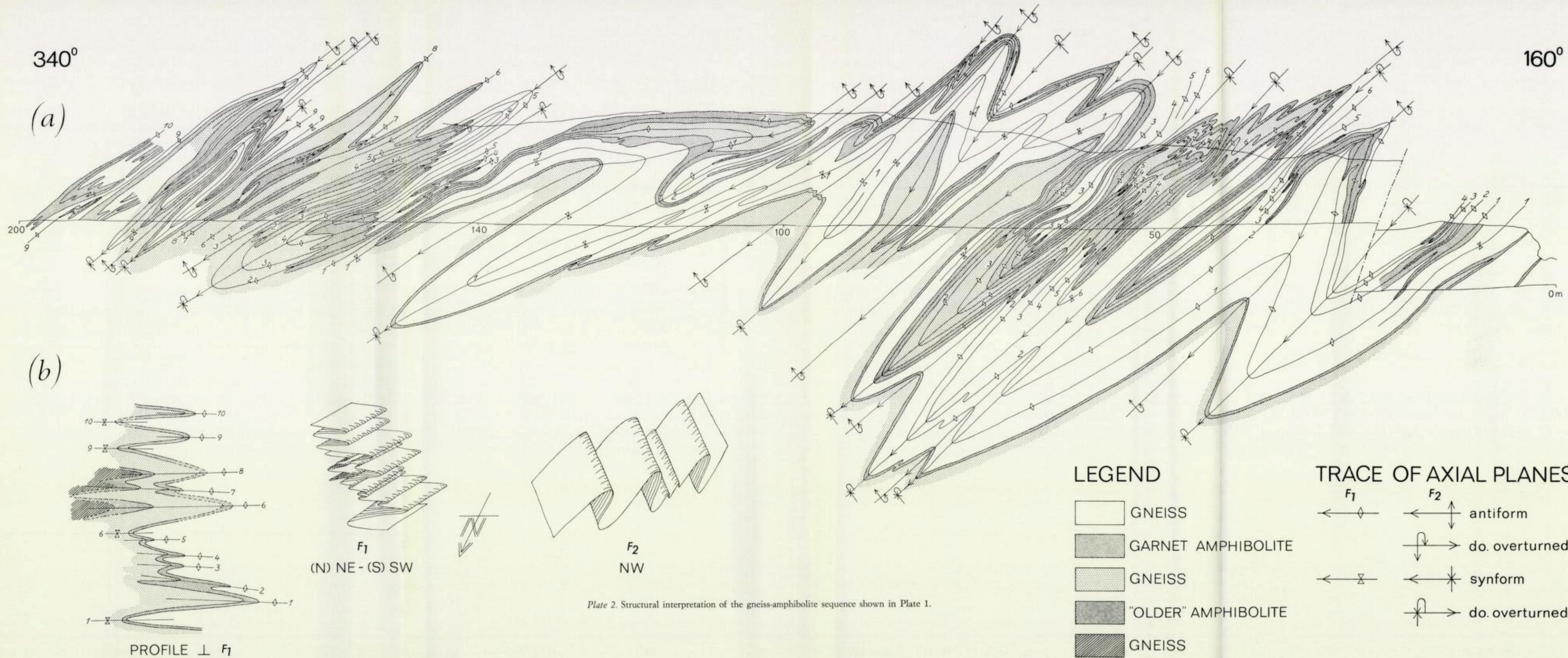
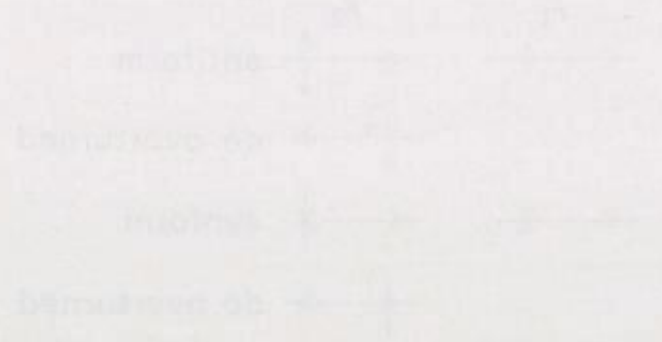


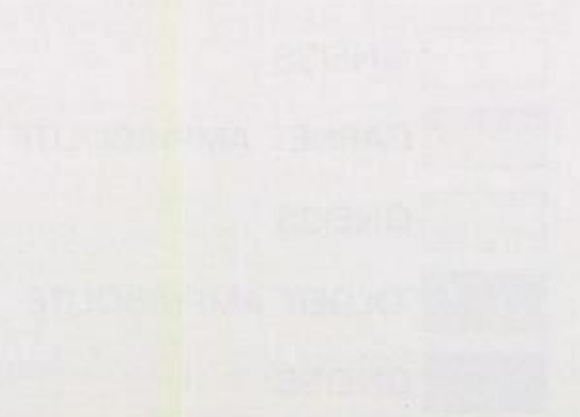
Plate 2. Structural interpretation of the gneiss-amphibolite sequence shown in Plate 1.

100

TRACE OF AXIAL PLANES



LEGEND



100

(10)

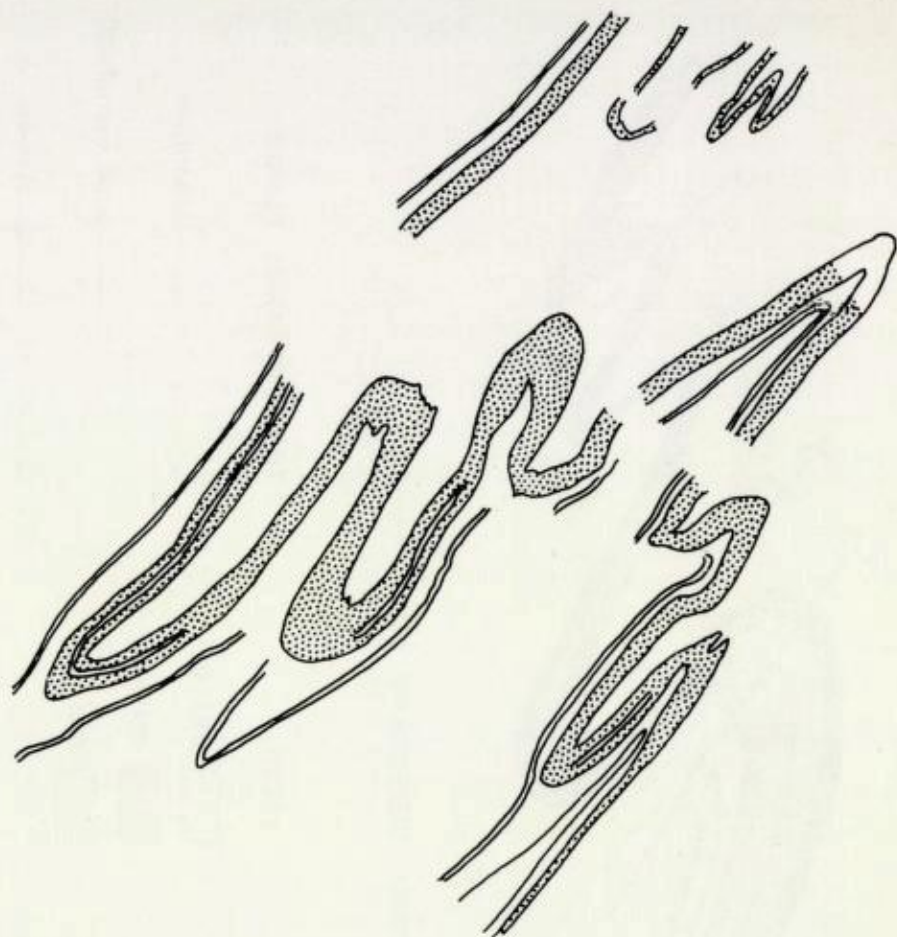


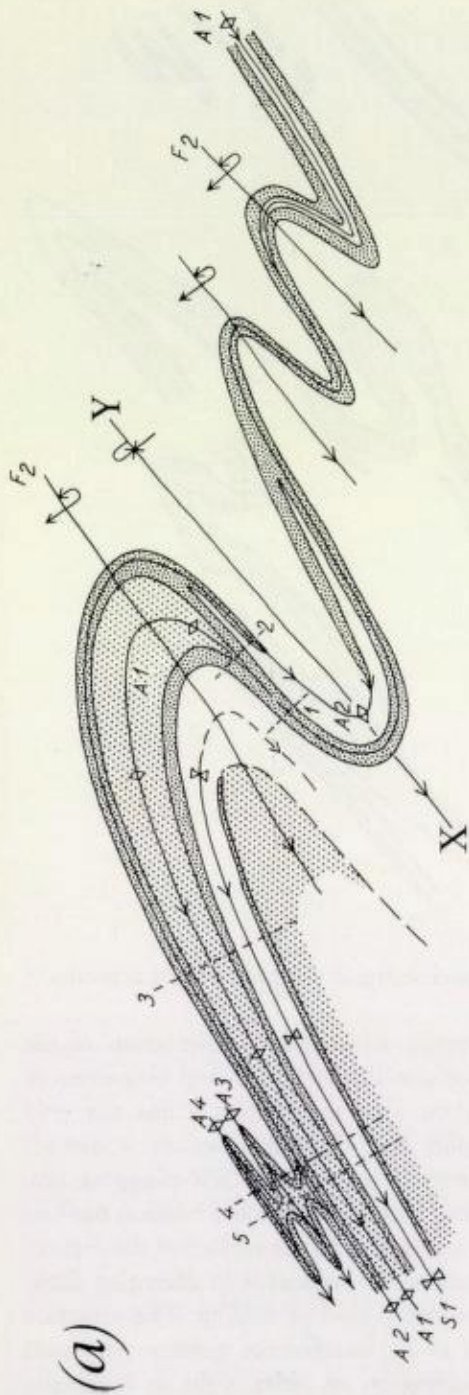
Fig. 3 b.

to produce the present erosion surface, and seeing if the model truly reproduces all the observed features.

The pattern shown in Fig. 4 is a partly schematic representation of the road-section between 90 and 150 m (see also Plates 1 & 2, and Graversen & Hageskov, 1971, Fig. 10), and it is now seen that gneiss forms not only lamellae but also larger cores in amphibolite. One also notices a distinct bilateral symmetry around the northernmost overturned, NW-plunging synform (X-Y); to the north the 'uppermost' garnet amphibolite horizon outlines two isoclinal folds, whose fold axes run subparallel to the surface of the section.

The bilateral symmetry and the occurrence of fold axes in diverging directions suggest the presence of more than one period of folding. The structure outlined in Fig. 4a may be explained as an interference pattern generated through the superimposition of NW folding on an older, tight or isoclinally folded, amphibolite sheet.

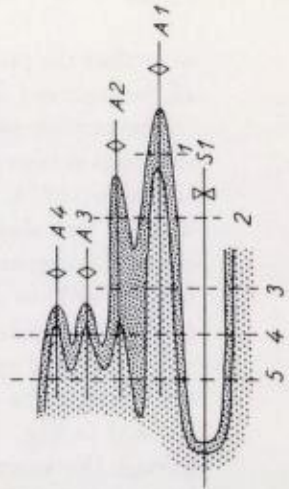
The older folding is now referred to as F_1 and the NW folding as F_2 . The F_2 folding shows overturned tight to isoclinal folds that plunge to the NW at



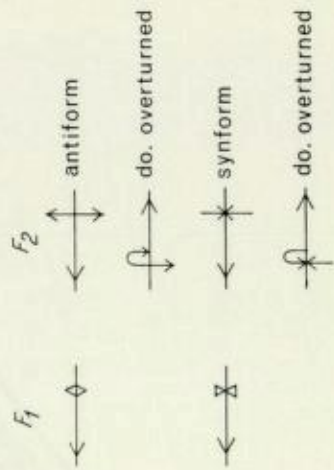
— REPRODUCED IN STRUCTURAL STEREOGRAM (FIG. 5) —

(a)

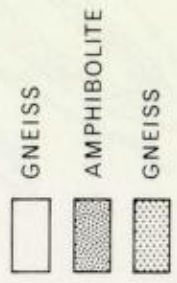
PROFILE $\perp F_1$



TRACE OF AXIAL PLANES



LEGEND



O. G. II - 70

Fig. 4. (a) Schematic representation and correlation of the amphibolite horizons from the road-section between 90 and 150 m (cf. Plates 1 & 2). (b) Profile normal to the F_1 fold axis, looking south.

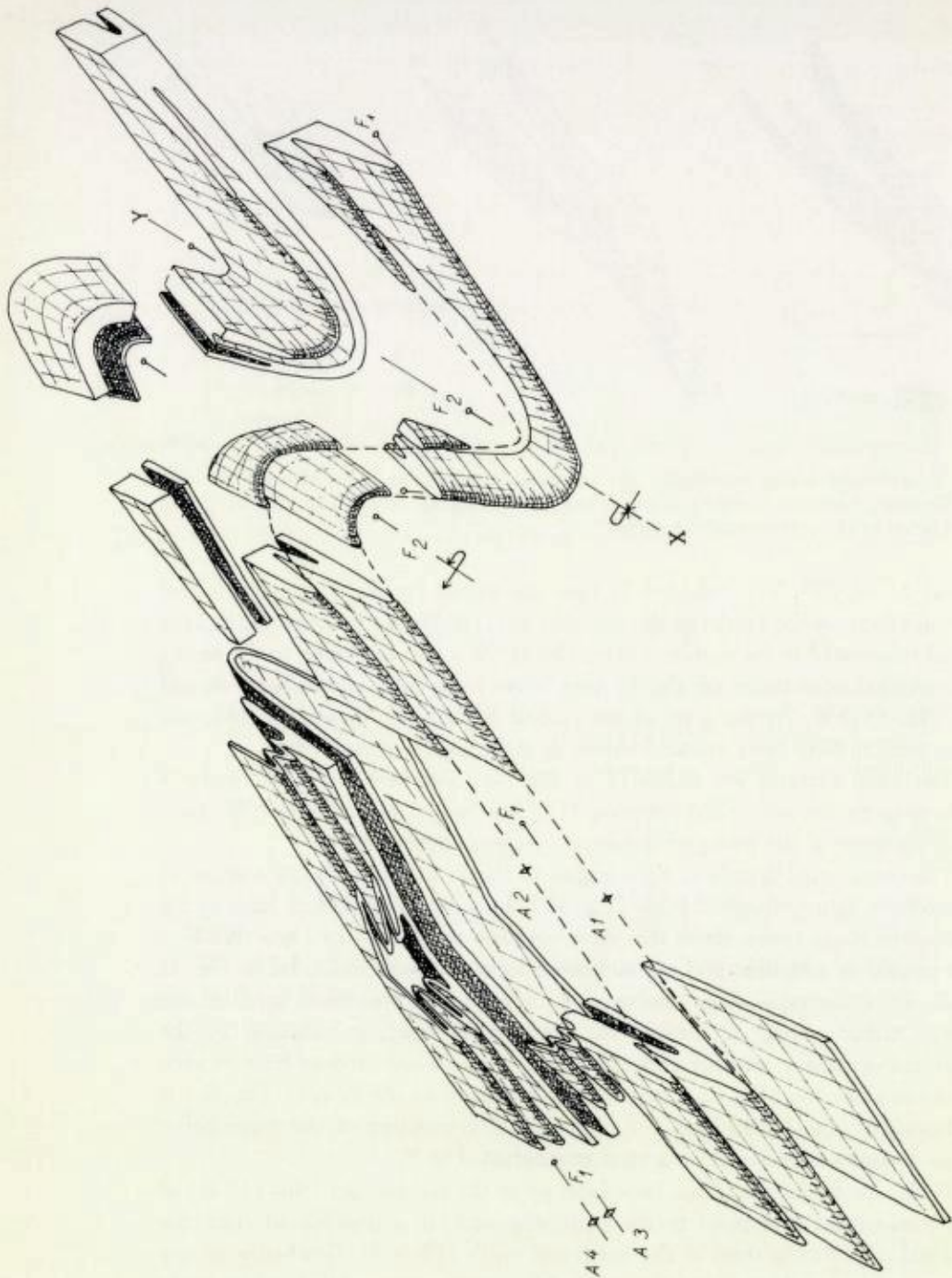
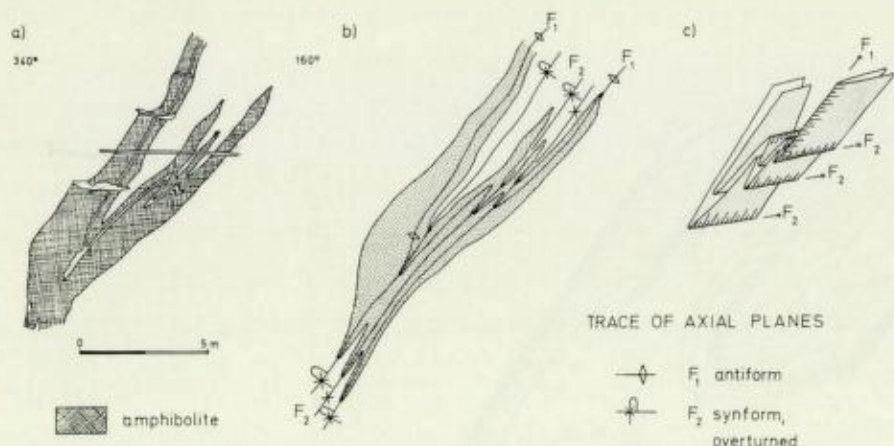


Fig. 5. Structural stereogram based on the structural analysis shown in Fig. 4.



Z-71 00

Fig. 6. (a) Double-folded amphibolite. (b) Structural interpretation of (a) showing the trace of the axial planes. (c) Tentative sketch where the orientations of the fold axes are shown in relation to the present road-cut surface.

about 5° to 25° . The refolded F_1 axes are shown by the isoclinally folded amphibolites on the flanks of the second ($=F_2$) folds. At present the F_1 axes trend subparallel to the section surface ($N 20^\circ W$), but according to the model the original orientation of the F_1 axes must have been somewhere around (N)NE-(S)SW. At the start of the second folding the F_1 and F_2 fold axes thus seem to have been oriented almost at right angles to each other.

The axial surfaces are indicated in Fig. 4a, and here the axial surfaces belonging to the oldest deformation (F_1) are folded around the NW axes, whereas those of the youngest deformation are undeformed.

The constructed profile at right angles to the F_1 fold axis shows a series of recumbent tight to isoclinal folds (Fig. 4b). In order to be able to refer to the individual hinge zones, those that close towards the road - i.e., face WSW - are treated as anticlines and are numbered successively as indicated in Fig. 4; there are a corresponding number of synforms. The structural level of the gneiss, either 'above' or 'below' the amphibolite sheet, is indicated by the different ornament, and the correspondence between the erosion level as seen in the road-section (Fig. 4a) and the profile normal to the F_1 axis (Fig. 4b) is indicated by the dashed lines 1-5. The spatial orientation of the amphibolite sheet is represented in the structural stereogram, Fig. 5.

When the model which has been built up in the central part (90-150 m) of the road-section is applied to the remaining part, it is possible to trace the original amphibolite sheet to the north and south (Plate 2). Gradually, as one moves to the north, more of the original F_1 structure is revealed, and a more complete picture of this structure can be obtained. The gneiss from 155-175 m is structurally 'below' the amphibolite sheet folded during the first deformation, and this means that the garnet amphibolite lenses A 6-7-8, Plate 2, must lie at a 'lower' level compared to the rest of the amphibolites. These amphib-

olite lenses are therefore interpreted as the closures of folds in a new, separate amphibolite sheet (see profile perpendicular to the F_1 axis in Plate 2).

If the correlation between the northernmost amphibolite bands shown in Plate 2 is correct, all these bands (with the exception of those in the lenses mentioned above) belong to one and the same sheet, which is most probably the same sheet as that forming the more centrally situated amphibolite bands.

The northernmost structure in the road-section (Plate 1, 195 m, and Fig. 6) appears to fit well into the model built up so far, in which the centrally placed gneiss lamellae is a gneiss core formed during the first isoclinal folding, F_1 , and refolded during the F_2 folding (Fig. 6b & c). The F_1 axis must trend parallel to the section surface, since the gneiss core has a constant thickness, and by unfolding the folds of the latest deformation the original orientation of the F_1 axis in the NE-SW quadrants is confirmed. That the structure is a refolded F_1 anticline (i.e., the amphibolite sheet closes towards the road) is seen from the fact that the gneiss core disappears in the southern limb whereas it continues throughout the northern one. (With the given axial directions, the reverse relations would appear in a refolded synclinal structure.) This structure is therefore naturally linked to the same sheet as the rest of the amphibolites, and does not reflect a primary intrusive feature of the amphibolite.

The structure outlined by the amphibolites in the southern part of the road-section (Plate 1, 0-90 m) can be explained as an interference pattern similar to those in the central and northern parts of the section, although only a part of the F_1 structure, S 1-A 6, is observed to the south (see Plate 2). This correlation also implies that only one generation of amphibolite is present.

It seems reasonable now to conclude that the structure pictured in Fig. 3 was also generated through two successive stages of folding. The central gneiss core disappears to the left, but fragments are seen at two other positions; this is due to the present orientation of the F_1 axis subparallel to the section surface. To the lower right the amphibolite sheet is quite thin (Fig. 3), and here the road-cut surface must be close to the outer part of the amphibolite fold closure formed during the F_1 folding.

Style and type of folding

The NW folding, F_2 , generally shows a more open style than does the first folding, F_1 (Plate 2), wherein a considerable compression seems to have taken place, and this has led to a minor variation in the orientation of the F_1 axis.

Buckling is observed in the concave part of the hinge zones at several locations in the F_2 folds (see for example Fig. 3), and this together with the general style indicates that buckle folding played a major role in the second deformation. In contrast to this, a 'fork' can be observed in the hinge zone to the lower right in Fig. 3, and the formation of this is referred to a shear movement (F_2') parallel to the axial plane of the F_2 folds that occurred during or shortly after this folding.

Summary

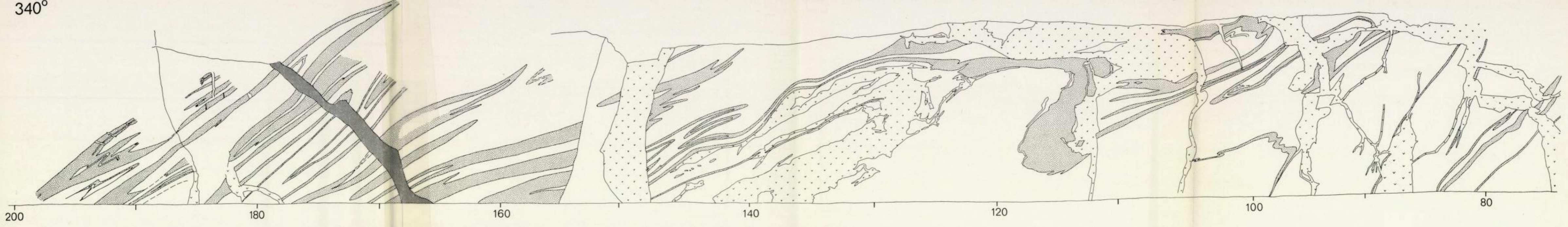
From the detailed structural analysis of the gneiss-amphibolite sequence it has been possible to distinguish two periods of folding. It is only the presence of marker horizons that has permitted this interpretation; F_1 folds are impossible to observe in the strongly foliated gneiss alone, and even the second folds are often difficult to distinguish. On the other hand, when the amphibolite bands were used in the analysis, problems arose concerning the distinction between primary and secondary structures, together with the problem whether one or more generations of amphibolites were involved. These problems were solved through the structural analysis, which showed that the observed structures are not of intrusive origin, and that only one major sheet of amphibolite is present.

Acknowledgements. - The author thanks Professor A. Berthelsen and Dr. T. C. R. Pulvertaft for their critical interest in the work. Dr. Pulvertaft has kindly improved the English.

REFERENCE

- Graversen, O. & Hageskov, B. 1971: Basic magma tectonics contrasted to folding of basic rocks. *Geol. Rdsch.* 60, 1442-1455.

340°



160°

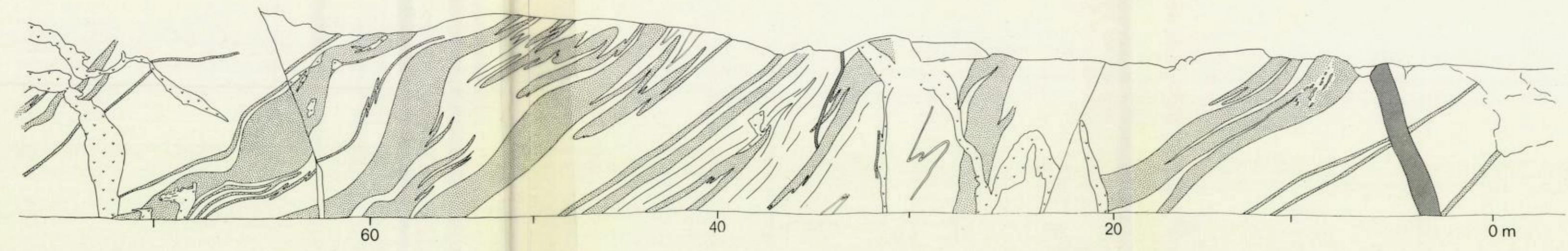


PLATE 1

LEGEND





- | | |
|--|--|
|  Gneiss |  Pegmatite |
|  Garnet amphibolite |  Permian dolerite |

Plate 1. Outcrop-pattern of gneiss/amphibolite from road-section along the eastern side of E 6 (location is given in Fig. 1).

Rb-Sr Isochron Age of Caledonian Acid Volcanics from Stord, Western Norway

HARRY N. A. PRIEM AND TORE TORSKE

Priem, H. N. A. & Torske, T. 1973: Rb-Sr isochron age of Caledonian acid volcanics at Stord, western Norway. *Norges geol. Unders.* 300, 83-85.

An eight-point Rb-Sr whole-rock isochron from Caledonian rhyolites at Stord in western Norway defines an age of 455 ± 5 m.y. and an initial $^{87}\text{Sr}/^{86}\text{Sr}$ of 0.7071 ± 0.0018 ($\lambda^{87}\text{Rb} = 1.39 \times 10^{-11}/\text{a}$; errors with 95 percent confidence limits). This places the volcanism in the Upper Ordovician, close to the Ordovician/Silurian boundary.

H. N. A. Priem, ZWO Laboratorium voor Isotopen-Geologie, De Boelelaan 1085, Amsterdam-11, The Netherlands

T. Torske, Norges geologiske undersøkelse, P.O. Box 3006, N-7001 Trondheim, Norway

The island of Stord, some 45 km south of Bergen in western Norway, lies at the southwestern extremity of the Norwegian Caledonides. Geologically, the island is divided by a NW dipping thrust zone into two tectonic units, a sequence of folded metasediments with interbedded spilitic metavolcanics in the southeast and an igneous complex in the west (Fig. 1). The igneous complex is mainly composed of saussurite gabbro and metavolcanics (basic and acid lavas and pyroclastics) intruded by granodiorite and microcline granite (Kvale 1937). It is believed that this complex is allochthonous, forming part of a large Caledonian nappe (Strand 1972). The metasedimentary sequence to the southeast consists of greywackes, argillites, conglomerates, and limestones; in its youngest part it contains fossiliferous horizons which can be placed in the Ashgill and Lower Llandovery (Skordal 1948).

A Rb-Sr isochron study has been made on eight whole-rock samples of acid volcanics from Kattnakken in the igneous complex. All rocks are of rhyolitic composition and have been only slightly affected by low-grade metamorphism, approximately in the lower greenschist facies. The Rb and Sr contents and Rb/Sr ratios have been determined by X-ray fluorescence spectrometry. Strontium isotope ratios were normalized to $^{88}\text{Sr}/^{86}\text{Sr} = 8.3752$ and adjusted to $^{87}\text{Sr}/^{86}\text{Sr} = 0.7085$ in the Eimer & Amend $\text{Sr}(\text{CO}_3)_2$ standard. The maximum relative errors in the Rb/Sr and $^{87}\text{Sr}/^{86}\text{Sr}$ ratios are estimated at 2.0 and 0.5 per cent, respectively. The analytical techniques follow those described by Priem et al. (1973). In the map of Fig. 1 the sampling sites are shown, while the analytical results are plotted in the isochron diagram and listed in Table I. All Rb-Sr ages mentioned in this paper are based upon the ^{87}Rb decay constant of $1.39 \times 10^{-11}/\text{a}$.

The Rb-Sr data of the eight samples are very well linearly correlated, defining an age of 455 ± 5 m.y. with initial $^{87}\text{Sr}/^{86}\text{Sr} = 0.7071 \pm 0.0018$ (least-squares regression analysis according to York 1966, 1967). Both errors

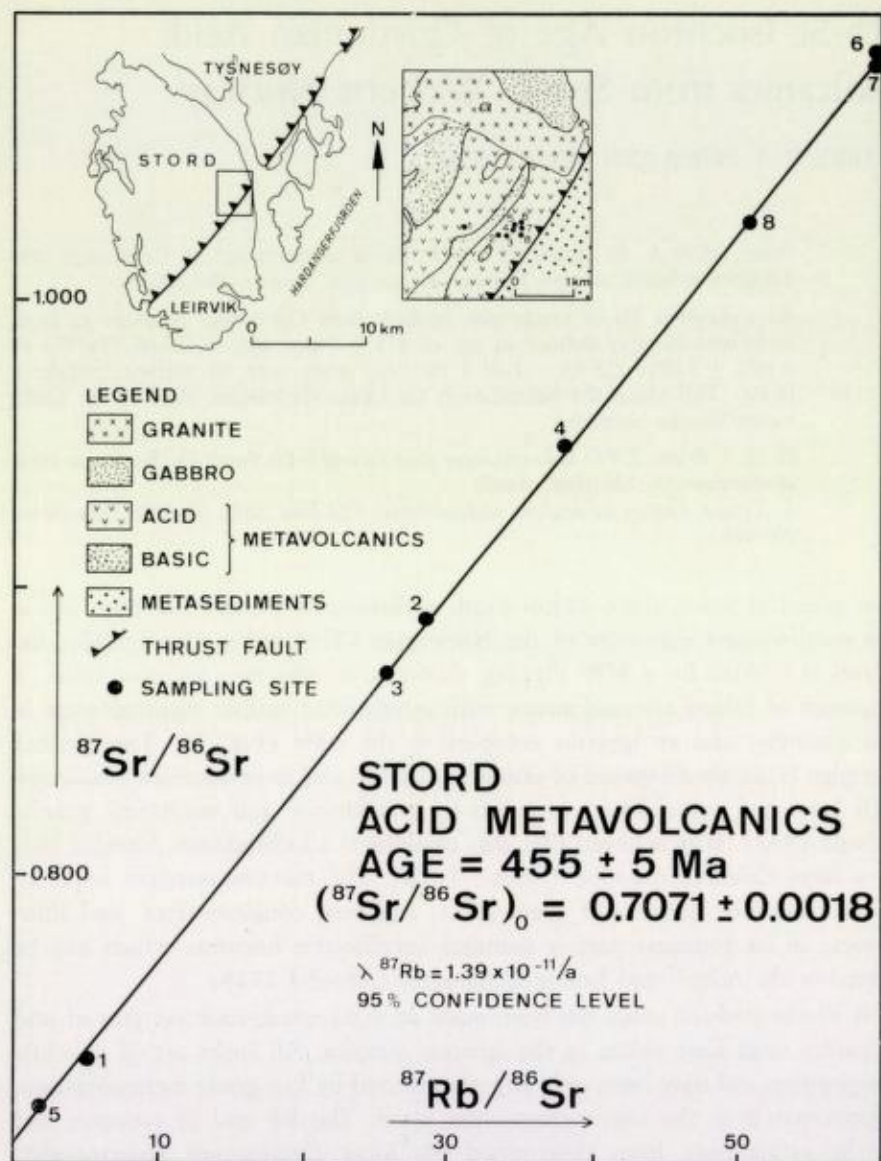


Fig. 1. Isochron plot of eight whole-rock samples from the Caledonian acid volcanics at Stord, western Norway. The inset gives a geological sketch map of the area (simplified after Kvale 1937, and Skordal 1948), showing the locations of the investigated samples. The numbers 1 to 8 correspond to the samples 72 Sto 1 to 8 in Table 1.

are given with the 95 percent confidence limits as calculated from the analytical data.

It is difficult to fit this date in the Ordovician–Silurian time-scale, as very few reliable dates critical to the stratigraphic horizons are available (Lambert 1971). Of particular importance to the present investigation is the Rb–Sr isochron age of 438 ± 4 m.y. measured by Bofinger et al. (1970) on volcanics in the Canberra area, Australia, which overlie sediments accurately placed as

Table 1. Rb-Sr data of acid volcanics from Stord

Sample No.	$^{87}\text{Sr}/^{86}\text{Sr}$	Rb/Sr (Wt/Wt)	Rb (ppm Wt)	Sr (ppm Wt)	$^{87}\text{Rb}/^{86}\text{Sr}$
72 Sto 1	0.7372	1.721	220	128	5.00
72 Sto 2	0.8890	9.683	207	21.3	28.5
72 Sto 3	0.8705	8.754	181	20.6	25.8
72 Sto 4	0.9493	12.85	246	19.1	38.1
72 Sto 5	0.7202	0.6624	156	235	1.92
72 Sto 6	1.081	19.84	260	13.1	59.6
72 Sto 7	1.086	19.86	287	14.4	59.7
72 Sto 8	1.027	17.04	238	13.9	50.9

Lower Ludlovian on fossil evidence and may well be of Lower Ludlovian age themselves. The same authors estimate the age of the Upper Llandovery as 445 ± 7 m.y., fixing the Ordovician/Silurian boundary at around 450 m.y. Concerning the lower boundary of the Ordovician, reference may be made to the Rb-Sr isochron date of 502 ± 5 m.y. recently obtained from volcanics overlain by Tremadoc sediments in the Krivoklát-Rokycany zone in Bohemia (Vidal et al. 1973). The Cambrian/Ordovician boundary can thus be dated at around 500 m.y., leaving some 50 million years for the duration of the Ordovician Period.

It can thus be concluded that the acid volcanics of the overthrust igneous complex on Stord have been extruded close to the Ordovician/Silurian boundary, in Upper Ordovician time (probably Ashgill).

Acknowledgements. - We would like to thank Drs. N. A. I. M. Boelrijk, E. H. Hebeda, E. A. Th. Verdurmen and R. H. Verschure, all of the ZWO Laboratorium voor Isotopen-Geologie, for their cooperation and helpful suggestions. This work forms part of the research programme of the 'Stichting voor Isotopen-Geologisch Onderzoek', supported by the Netherlands Organization for the Advancement of Pure Research (ZWO).

REFERENCES

- Bofinger, V. M., Compston, W. & Gulson, B. L. 1970: A Rb-Sr study of the Lower Silurian Stage Circle Shale, Canberra, Australia. *Geochim. Cosmochim. Acta* 34, 433-445.
- Kvale, A. 1937: Et kaledonisk intrusiv- og effusivfelt på Stord. *Bergens Mus. Arbok* 1937, *Naturvidensk. rekke Nr. 1*, 138 pp.
- Lambert, R. St. J. 1971: The pre-Pleistocene Phanerozoic time-scale, a review. In: The Phanerozoic time-scale, a supplement. *Geol. Soc. London special publ. No. 5*, 9-32.
- Priem, H. N. A., Boelrijk, N. A. I. M., Hebeda, E. H., Verdurmen, E. A. Th., & Verschure, R. H. 1973: Rb-Sr investigations on Precambrian granites, granitic gneisses and acidic metavolcanics in central Telemark (Norway): metamorphic resetting of Rb-Sr whole-rock systems. *Norges geol. Unders.* 289, 37-53.
- Skordal, A. J. 1948: Vulkaniter og sedimenter på den sørøstre del av Stord. *Univ. Bergen Arbok* 1948, *Naturvidensk. rekke Nr. 2*, 58 pp.
- Strand, T. 1972: The Norwegian Caledonides, VI, areas with Cambro-Silurian deposits along the west coast of south Norway. pp. 67-71 in *Scandinavian Caledonides, Interscience Publishers*.
- Vidal, Ph., Auvray, B., Charlot, R., & Fediuk, F. 1973: Contribution to the age of the Cambrian-Ordovician boundary: radiometric age of volcanics of the Krivoklát-Rokycany zone (Bohemian Massif). Paper presented at the 3rd European Colloquium of Geochronology, Cosmochronology and Isotope Geology, Oxford, 4-8 September 1973.
- York, D. 1966: Least-squares fitting of a straight line. *Can. J. Phys.* 44, 1079-1086.
- York, D. 1967: The best isochron. *Earth Planet. Sci. Lett* 2, 479-482.